Final Report on the Project

Bio-Inspired Sensing and Display of Polarization Imagery

Proposed Duration: March 1, 2002-December 31, 2004

submitted to

Air Force Office of Scientific Research (AFOSR)
Bio-Inspired Concept Theme
Life Sciences Directorate
4015 Wilson Blvd
Arlington, VA 22203-1954

By

PI: Nader Engheta (ESE Dept.)
Co-PI: Edward N. Pugh, Jr. (Ophth. Dept.)
University of Pennsylvania
Philadelphia, Pennsylvania 19104

Bio-Inspired Sensing and Display of Polarization Imagery

Abstract

Polarization is an important feature of electromagnetic waves, and it can be affected by surface shapes, materials, local curvature and features, and relative location of sources and objects, and thus it can provide useful information about the observed scene and objects. Of the several characteristics of visible light, only two – intensity and wavelength – are encoded by the human eye and subsequently mapped by the visual system into perceptual qualities. Intensity is mapped to brightness and wavelength information is mapped to perceived color. In contrast, without appropriate instruments human eyes cannot effectively utilize light's polarization. However, it is well known that eyes of certain animal species are sensitive to the polarization of light. Polarization sensing has mostly been shown to provide information for navigation, as originally discovered by the Nobel laureate Karl von Frisch in his work with honeybees. In addition, it has been hypothesized that some species may have evolved polarization sensitivity as a mechanism of enhancing the contrast of targets in media that scatter light (e.g., under water). Indeed, in our earlier work, we have shown that an optical imaging system utilizing such contrast enhancement through polarization differencing can increase the distance over which targets can be detected, and their critical features discriminated. Thus, "polarization imagery" is a naturally occurring and demonstrably successful strategy for enhancing vision.

Since the human eye is effectively polarization-blind, in mapping polarization information into visual displays, the output should be exhibited in a way compatible with the biology of the human visual system. In our group's earlier work, we have shown one such bio-inspired mapping, in which polarization information was pseudo color-coded, based on the opponent-colors model of human vision. The results established several promising imaging strategies for making available in a natural way the contrast enhancement of polarization imagery of objects in scattering media.

During our research efforts in the period of March 1, 2002 till December 31, 2004, we have explored and investigated various bio-inspired display methodologies for mapping polarization information into visual information that can be readily perceived by the human visual system, and we have studied those mappings most suitable for specific applications for object detection, scene classifications, and visibility enhancement. We have introduced and developed various imaging algorithms, sensing schemes and visualization and display methodologies inspired and informed by biological consideration. Our research efforts have demonstrated that these bio-inspired polarization sensing and imaging techniques enable us to achieve better target detection, enhanced visibility in otherwise low-contrast conditions, longer detection range in optically scattering media, man-made polarization-sensing adaptation based on changing environments, surface deformation/variation detection (e.g., detection of finger prints on a smooth surface using polarization-based vision), "shadow removal" by displaying polarization information instead of conventional intensity information, and many more novel outcomes. These results have shown the numerous possibilities and potential applications of these bio-inspired methods in various sensing, imaging, and display technologies. We have also explored several ideas for mapping polarization information, including using pseudocolor mapping, static and dynamic textures with varying in orientations, flickering, modulating luminance and/or color contrast of scenes in terms of certain aspects of polarization values, and fusing polarization information into optical imagery. Our efforts have shown that the *polarization* can bring another "dimension of information" into the domain of imaging and sensing for detection, visibility enhancement, and display methodologies. These techniques have the potentials to bring novel advances in various areas of Air Force needs such as imaging systems for navigation in low-visibility conditions.

Background and Introduction

Polarization is an important feature of electromagnetic waves, and can be affected by various factors in the scene such as surface shapes, surface curvatures and materials, and position of objects with respect to the source(s) and the observer [1], and therefore it can provide useful information about the observed scene and objects – information which otherwise would be lost. Two characteristics of visible light, i.e., intensity and wavelength, can be detected and encoded by the human visual system and interpreted as perceptual qualities of brightness and color. Another important characteristic of light, namely, polarization, however, cannot be effectively exploited by unaided human eyes. The imaging system of the human eye is effectively "polarization-blind", and cannot utilize the polarization of light without the aid of an artificial, polarization-sensitive instrument. The eyes of some animal species (e.g., honeybees, desert ants, backswimmer flying water bug, salmon, cuttlefish), however, can sense the polarization of light (see e.g., [2-23]), and it has been shown by biologists and zoologists that such polarization vision in certain species may facilitate their navigation (see e.g., [4-7]). Moreover, it has been suggested that some species may utilize the polarization sensitivity to enhance the contrast of targets in scattering media (see e.g., [18]).

It is known that the function of man-made sensing, imaging, detection, and navigational systems can be severely limited and constrained by the scattering of optical waves in media surrounding the targets [1], which leads to major challenges in the wave-based direction finding and navigation, imaging and target detection, and reduction of contrast in such media. Any strategies to alleviate such contrast-degrading effects of scattering, and thus to enhance the imaging, information gathering, and detection and navigation under such scattering conditions are clearly welcome additions to the repertoire of imaging and sensing techniques. It is believed that the biology of visual systems of some animal species that possess polarization vision may provide novel solutions to such challenging problems of imaging and navigation in scattering media. As an excellent example, the underwater environment is a domain where scatterers are present, and thus the performance of imaging systems is limited. Therefore, the aquatic species may have adaptations for improving the quality of vision in scattering media, and much insight and inspiration can be gained by learning from what biologists and zoologists have found about such polarization-sensitive visual systems.

The biophysical basis of polarization detection in invertebrates with polarization vision is an inherent dichroism, the alignment of chromophores (the molecules of visual pigments) along the photoreceptor microvilli (see e.g., [3-8], [14]). Furthermore, in some vertebrates, for which there is behavioral evidence for polarization sensitivity, such dichroism is not present since the chromophores are free to rotate in the plane of the disc membrane of the outer segment of photoreceptors. However, many teleosts have interesting double-cone mosaic in their retinas [35-36], and there have been exciting ideas to explain the functions of such double-cone mosaic in the context of polarization sensitivity [10, 21]. Moreover, it has been shown by Labhart and his colleagues that some insects with polarization vision possess polarization-opponent interneurons to allow the two polarization components of received signals interact antagonistically leading to enhanced polarization sensitivity [6]. This is indeed the concept of *polarization opponency*, analogous to *color opponency* in human visual system, and in fact such opponent coding is the neurophysiological equivalence of a common-mode rejection and differential amplification in circuit domains. The opponent coding of the polarization signal may yield a polarization difference image in which the visibility and the contrast are enhanced significantly.

Motivated and inspired by the visual systems of some of these animal species with polarization vision and particularly by the concept of polarization opponency, we have been investigating novel imaging methodologies based on the concept of polarization-difference signals [24-34]. In our earlier work, we have shown that biologically inspired *polarization-difference imaging* (PDI) can extend the distance over which objects can be reliably detected in scattering media up to 2-3 fold, even under conditions when the fractional polarization reaching the detector is less than 1% [24-29]. Extending the distance for detection and classification of objects near the limit of visibility increases the time for critical, survival-relevant decisions, and is thus a major advantage in many real-time applications.

In our efforts during the period March 1, 2002 till December 31, 2004, we have developed a series of bio-inspired algorithms and schemes for enhancing sensing and imaging of polarization information in various conditions [30-34]. Here, we review some of our findings under this program. Further details can be found in some of our publications, which either have appeared in print, have been submitted for publication or are in preparation for submission for publication. These can be found in the appendix.

A Sample of our Findings during the period March 1, 2002 till December 31, 2004.

During this period, we have accomplished a variety of different tasks regarding the bio-inspired sensing and mapping of optical polarization information. These investigations are ongoing, and here we present some of our results and works in progress. In the appendix, more information is provided in our publications.

1.Target Detection, Visibility Enhancement, and Detection-Range Increase in Scattering Media

We have continued our efforts in this area by developing and improving various bio-inspired algorithms using polarization information in imaging and sensing targets in scattering media. These include improving the polarization-opponent techniques using different thresholds in the distribution of polarization-difference (PD) signals in an image. Fig. 1 shows a sample of our results using the PD technique with two different threshold levels in the histograms of the PD signals of the image. Here we show the image of an aluminum disk, specifically made for our experiments. This disk is 5.1-cm in diameter with its surface sandblasted, except for 6 patch areas each with 1-cm^2 square. There are 7 patches, six of which are abraded with the emory paper in various specific directions, and the 7th patch in the center is also sandblasted. The sandblasting caused the surface to be Lambertian. The patches were raised a few mills. The abrasions (i.e., scratches) on these six patches form three pairs. Each pair has two orthogonal orientations for the scratches. Specifically, the orientations of the scratches on these six patches are 0°, 30°, 60°, 90°, 120°, and 150° (with respect to the vertical axis.), where the patch pairs with orthogonal orientations, i.e., the pairs with $(0^\circ, 90^\circ)$, $(30^\circ, 120^\circ)$, and $(60^\circ, 150^\circ)$ are located diametrically on the disk. The polarization-sum (PS) and the polarization-difference (PD) images of this target, when front illuminated in a tank of water with a small amount of milk added, are presented in Figs. 1A and 1B, where the PS and PD image intensities were scaled using an affine transformation to utilize the full dynamic range of the 8-bit display. In Figs. 1C and 1D we present the PD images of the same target, but in these images, we have used two different threshold cuts in the histogram of the PD signals. Specifically, after computing the histogram of the image, the brightest and darkest intensity bins with pixel population less than a certain percentage (e.g., T = 1% for Fig. 1C and T = 10% for Fig. 1D) of the population of the largest bin are deemed as outliers and assigned the brightest and darkest display intensity values (0 or 255 for a common 8-bit display). The rest of the image has been

linearly scaled to cover the full dynamic range of the display. As we can see from these figures, the patches and particularly the difference between their various directions of abraded lines can be easily detected in the PD images -- much more efficiently than in the PS image. These PD techniques can remarkably increase the target feature visibility and enhance the contrast. In our efforts here, we have clearly demonstrated that bio-inspired polarization techniques can be instrumental in target feature detection and visibility enhancements.[1]

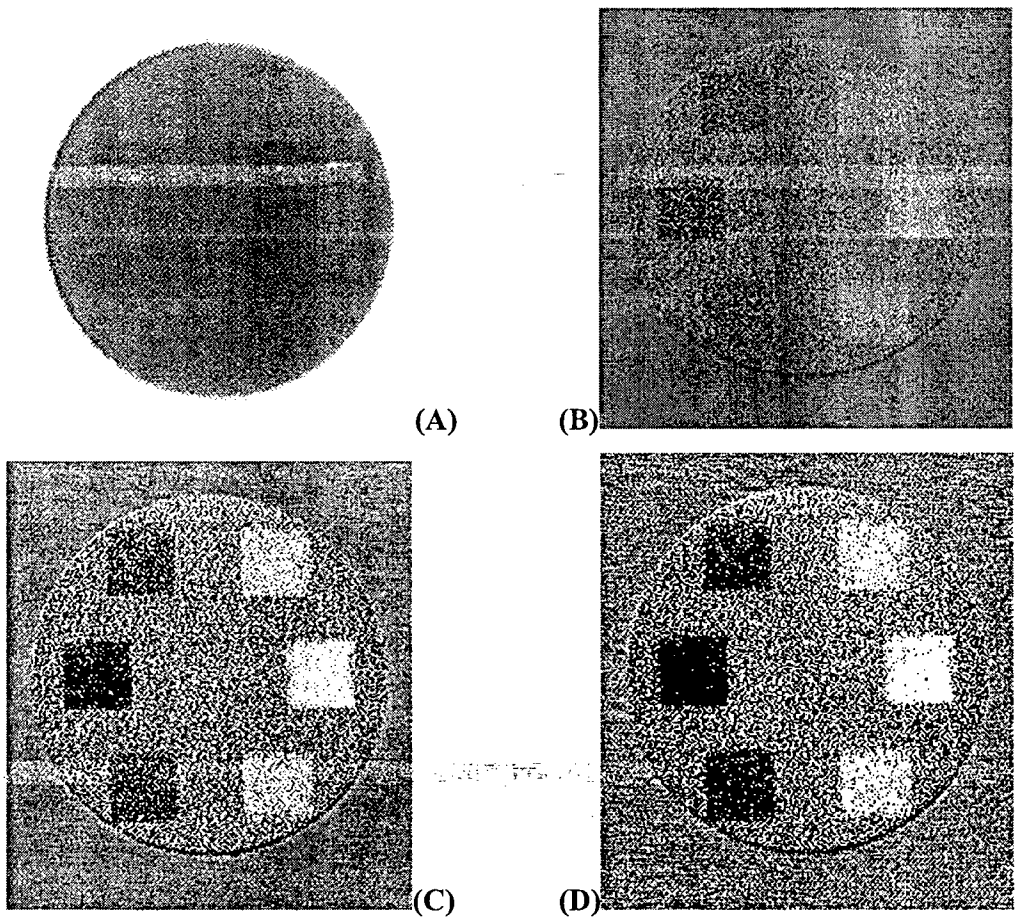

Fig. 1. Affine-transformed Polarization-Sum (PS) and Polarization-Difference (PD) images of a 7-patch aluminum disk, front-illuminated in a tank of water to which a small amount of milk is added. Panel A shows the affine-transformed of PS image, which is effectively equivalent to a conventional image, whereas Panels (B), (C), and (D) present the various PD images, using T = 0 %, T = 1%, and T = 10% thresholding in the PD histograms.

In our earlier work, we had also shown that the PD technique can increase the distance over which a target can be detected in scattering media [24]. Using the statistical-analytical

[1] This target was specifically constructed in order to make the light scattered from the patch areas partially polarized (with the major axis of the partial polarization parallel to the direction of abrasion), while the light scattered from the sandblasted areas (including the 7th patch) is largely unpolarized. (As a result, in the PD image of this 7-patch target, Figs 1B, 1C, and 1D, the centered 7th patch is

methods of signal detection theory, we analyzed the intrinsic detectibility of targets in scattering media when polarization-difference imaging is utilized [24]. Figure 2 shows the spatial sensitivity index computed at each

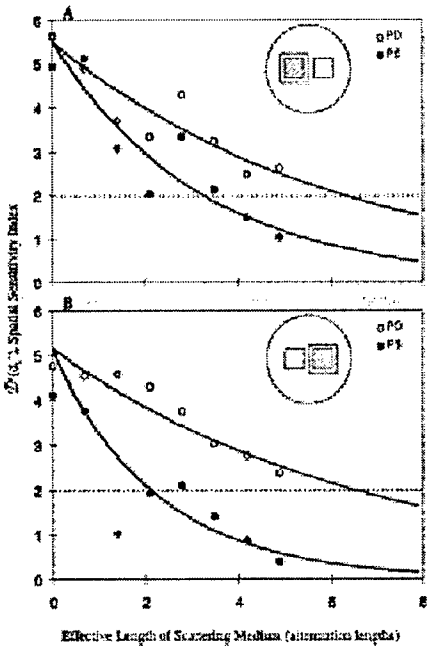

Fig. 2. Spatial sensitivity index of the variable d'_a, computed at each effective distance for both types of images [24]. This quantity reveals how well one can distinguish the patch from its surrounding. Panel A presents the data from the left target patch; panel B presents the data from the right target patch. At all times, PDI performs as well or better than the conventional (PS) system. In addition, the PS images degrade faster as a function of the attenuation length (proportional to the scatterer concentration). The exponential curves fitted to the data indicate that if any particular value of spatial sensitivity index is chosen as the threshold of detectibility, then the PD system will reach this level at distances at least double that of conventional (PS) systems.

effective distance for both types of images (PS and PD images) of the right and left patches. This index is a measure of how well the patch can be reliably distinguished/detected from its surrounding in these images by an "ideal observer". Figure 2 clearly shows that at low effective target distances the statistical distributions of sensitivity index of the patches and the surrounding frames are at least as separated in the PD images as they are in the PS images. However, the separation of these distributions decays more slowly in the PD case than in the PS case as effective distance is increased. If any of the value of the spatial sensitivity index is chosen as a threshold of detectibility, this value is reached in the PD images at effective lengths 2-3 times greater than in the PS images. This reveals the enhanced intrinsic detectibility of PD images, and offers great potential for enhancement of underwater observation, seeing through fog, and sensing

indistinguishable from the sandblasted surface of the disk, and thus only six abraded patches can be seen.) For detailed description of

in other scattering environments. More results can be found in our manuscripts shown in the appendix.

2.Bio-Inspired Adaptive Algorithms in Polarization Sensing and Imaging

One of the important issues in polarization imaging is how to process the polarization information after (or while) it is collected by the imaging system. As one possible processing technique, as shown in the previous section we have worked on the methods of "polarization-difference imaging" (PDI), inspired by polarization vision in certain species, and we demonstrated that optical imaging systems utilizing PDI techniques may facilitate the detection of targets in scattering media, even when the targets produce only very weak polarization. In that work, we showed that in the PDI technique, the intensities of the two orthogonal polarization components of imaging-forming light for each pixel at (x,y), i.e., $I_{\parallel}(x,y)$ and $I_{\perp}(x,y)$, were captured and then the "polarization-sum" (PS) $I_{PS}(x,y)=I_{\parallel}(x,y)+I_{\perp}(x,y)$ and "polarization-difference" (PD) $I_{PD}(x,y)=I_{\parallel}(x,y)-I_{\perp}(x,y)$ intensities were formed. It had also been shown by one of the alumni of our research team, Scott Tyo [28], that the optimum linear combination of $I_{\parallel}(x,y)$ and $I_{\perp}(x,y)$ channels for a scene, in which the polarization angle is assumed to be a random variable with a uniform probability density function over the image pixels, are indeed PS and PD signals, utilizing the analogy and parallelism with the biology of color vision in the human visual system and related principal component analysis done by Buchsbaum and Gottschalk [37]. Therefore, in that scenario the PS and PD channels were optimum in the information theoretic sense, i.e., their contents were statistically uncorrelated, requiring minimum bandwidth for encoding [28]. However, the situation is different when the scene has a polarization distribution with a non-uniform probability density for the state of polarization, such as occurs in shallow water where mostly the sunlight penetrating the water is partially horizontally polarized as viewed by the polarization-sensitive marine species. What would then be the optimum linear combination for polarization channels in this general case? We have been investigating techniques to adaptively form the optimum linear combination for polarization channels. Specifically, the two linear channels in general can be expressed as

$$PC_1^{adaptive}(x,y)=\alpha\, I_{\parallel}(x,y)+\beta\, I_{\perp}(x,y) \quad (1)$$

$$PC_2^{adaptive}(x,y)=\gamma\, I_{\parallel}(x,y)+\zeta\, I_{\perp}(x,y) \quad (2)$$

---

the experimental setup, see Ref [24].

with unequal weighting coefficients α, β, γ, and ζ, which should be determined based on the statistics of the polarization distribution in any given scene. Utilizing the technique of principal components analysis for non-uniform distributions of polarization state in an image, we can determine the appropriate values for these coefficients, which will depend on the polarization statistics of the scene. Moreover, once an algorithm for determining and applying them is in place, the coefficients can be adaptively adjusted as the environment observed by the imaging system changes (for example, due to the transit of the sun in the sky) or as the imaging system is moved to different environments. Such optimum combinations for polarization channels with unequal weighting coefficients suitable for environment with non-uniform polarization distribution (such as under water) may point to an interesting processing in the polarization vision in certain aquatic species, and can lead to images with higher contrast and better target detection for man-made imaging systems. We have been working on the theoretical and experimental aspects of such adaptive algorithms [34]. Figure 4 shows a preliminary sample of the results of our work in this bio-inspired adaptive algorithm. The experimental setup is shown in Fig. 3. In this case, the 7-patch disk is immersed in a tank of water with a small amount of milk added, and the tank is illuminated from the left side and the images are taken by a digital camera located on top of the tank looking into the tank from the above. Since the light is coming from the side of the tank, the background light scattered from the milky water and propagating towards the camera is partially polarized, with orientation of polarization along the up-down direction in the scene viewed by the camera. Images are then collected at three orientations, $\theta = 0^\circ, 45^\circ, 90^\circ$ of the linear polarization analyzer in front of the camera, and then the polarization information at each pixel is evaluated. We then analyzed all possible combinations for the two-channel polarization imaging systems as a function of channel orientations θ_1 and θ_2 (not shown here), and then for each pair of two channels, using the principal component analysis we calculated the weighting coefficients $\alpha(\theta_1,\theta_2)$, $\beta(\theta_1,\theta_2)$, $\gamma(\theta_1,\theta_2)$, $\zeta(\theta_1,\theta_2)$ to form the principal component (PC) outputs as $PC1 = \alpha(\theta_1,\theta_2) I_1(\theta_1) + \beta(\theta_1,\theta_2) I_2(\theta_2)$ and $PC2 = \gamma(\theta_1,\theta_2) I_1(\theta_1) + \zeta(\theta_1,\theta_2) I_2(\theta_2)$. Since the background light coming from the water around the target is not unpolarized, we have found from our analysis that the coefficients $\alpha(\theta_1,\theta_2)$, $\beta(\theta_1,\theta_2)$, $\gamma(\theta_1,\theta_2)$, $\zeta(\theta_1,\theta_2)$, which are determined from eigenvectors of the covariance matrix of two-channel polarization signals, are not identical, (i.e., $\alpha \neq \beta$ and $\gamma \neq -\zeta$, but they follow the relations $\gamma = \beta$ and $\zeta = -\alpha$) and thus the $PC1$ and $PC2$ are different from "regular" polarization-sum and polarization-difference signals. Figure 4A and 4B show the "regular" PS and PD images of the scene, obtained using the

expressions $PS = I_1(90^\circ) + I_2(0^\circ)$ and $PS = I_1(90^\circ) - I_2(0^\circ)$, after they are affine transformed with 1% thresholding, whereas Figs. 4C and 4D present the same scene but with the adaptive PC signals (i.e., *PC1* and *PC2*, respectively) obtained using the adaptive analysis we described above. If we compare Fig. 4B and 4D, we can see that in the PC2 image (i.e., 4D) the effect of partially polarized background is reduced, resulting in a better contrast and visibility for the target features [34]. This suggests various interesting possibilities for polarization imaging in changing environments where the optimal linear combinations of the two-channel (or three-channel) polarization should be adaptively adjusted for better target detection. This is a promising technique, and we are currently developing and expanding this technique. More results can be found in our manuscripts shown in the appendix.

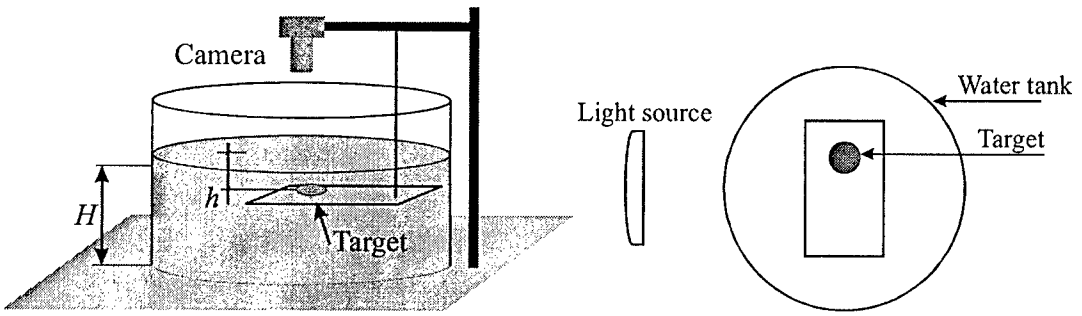

Fig. 3. Schematic of the experimental setup for the sample results shown in Fig. 4 for the study of adaptive polarization imaging.

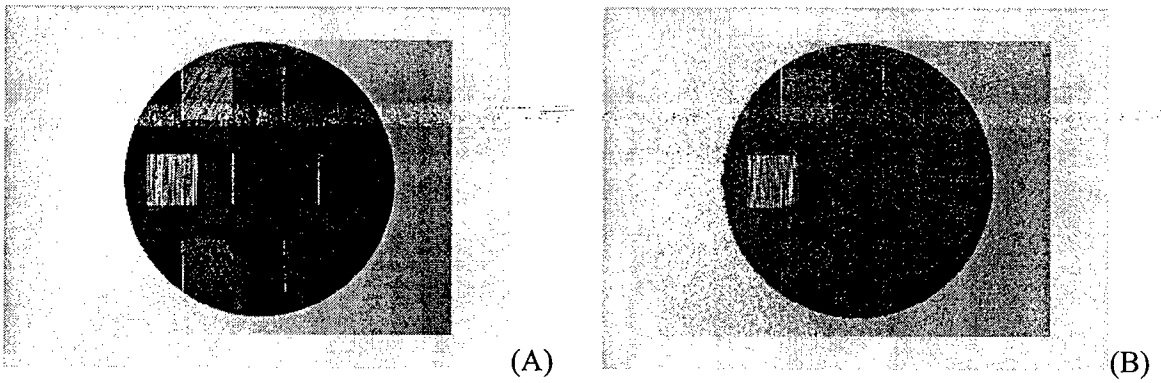

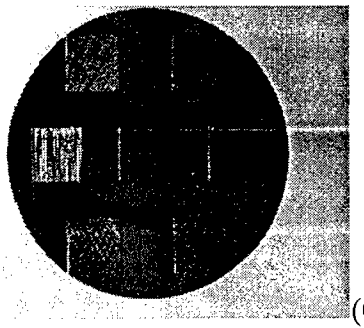
(C)

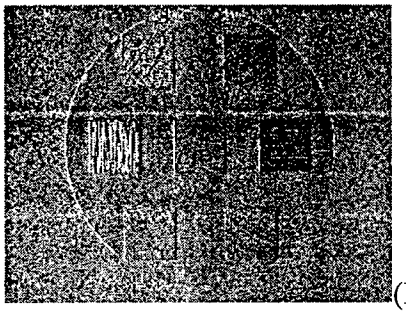
(D)

Fig. 4. Panels A and B show the "regular" PS and PD images of the 7-patch disk as a target in Fig. 3, after they are affine transformed with 1% thresholding. Panel C and D present the principal components 1 and 2, PC1 and PC2, for the "optimal" choice of the channel orientations and weighting coefficients in this example. Panel 4D clearly shows a better visibility, feature extraction, and lesser effect from the background light as compared with Panel 4B. More detailed results can be found in our manuscript that is being prepared for submission for publication. See the appendix for a draft of this manuscript.

3.Bio-Inspired Ideas for Non-Invasive Detection and Imaging of Latent Finger Prints and Skin Surface

One of the interesting species with polarization vision is backswimmer flying water bug, *Notonecta glauca*. It has been found by Schwind [11-13] that in the ventral region of the compound eyes of this species the microvillar directions of the photoreceptors are arranged such that they can pick up horizontally polarized light very well. This ability helps the species to find bodies of water in their habitats, since the light reflected from the surface of the water is mostly horizontally polarized. Furthermore, as discovered by Schwind [11-13], this species lands on the surface of the water at angle of 53° from the normal [5], which is approximately the Brewster's angle of water, therefore optimizing the horizontal polarization coming to its visual system [11, 5]. (See Fig. 5). So this species can "see" the surface of the water efficiently and thus can land on it. Fig. 6 shows the polarimetric images of a body of water and a tree, obtained using a digital camera equipped with a polarization analyzer, after having been processed in order to find the pixel intensity distribution (Panel A), degree of linear polarization (Panel B) and the angle of polarization orientation (Panel C) for each pixel. As we can see from Panels B and C, the surface of the water is highly polarized in the horizontal direction.

Inspired by this ability in the backswimmer water bug, we have been motivated to explore how we can take advantage of polarization in detecting other "smooth surfaces" and/or "minute deformation" on smooth surfaces. We decided to explore the possibility of using such bio-inspired techniques in detecting latent finger prints on smooth surfaces. After all, finger prints can be regarded as "deformation" of an otherwise smooth surface.

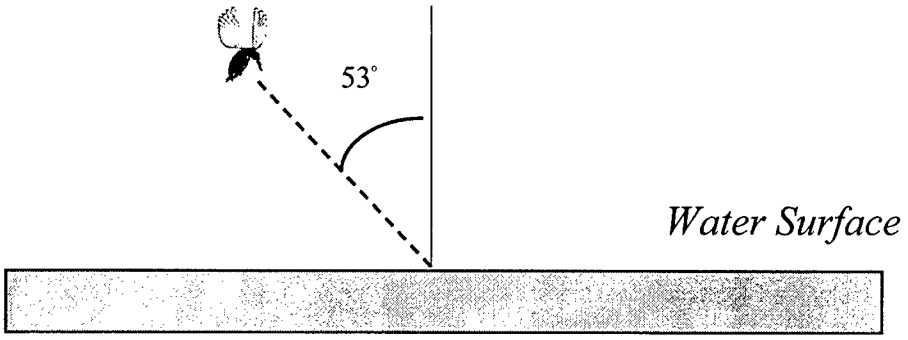

Fig. 5. Backswimmer flying water bug whose visual system is sensitive to the horizontal polarization. Schwind [11-13] discovered that this species lands on the surface of the water at angle 53° from the normal, which is approximately the Brewster angle of water, therefore optimizing the horizontal polarization coming to its visual system.

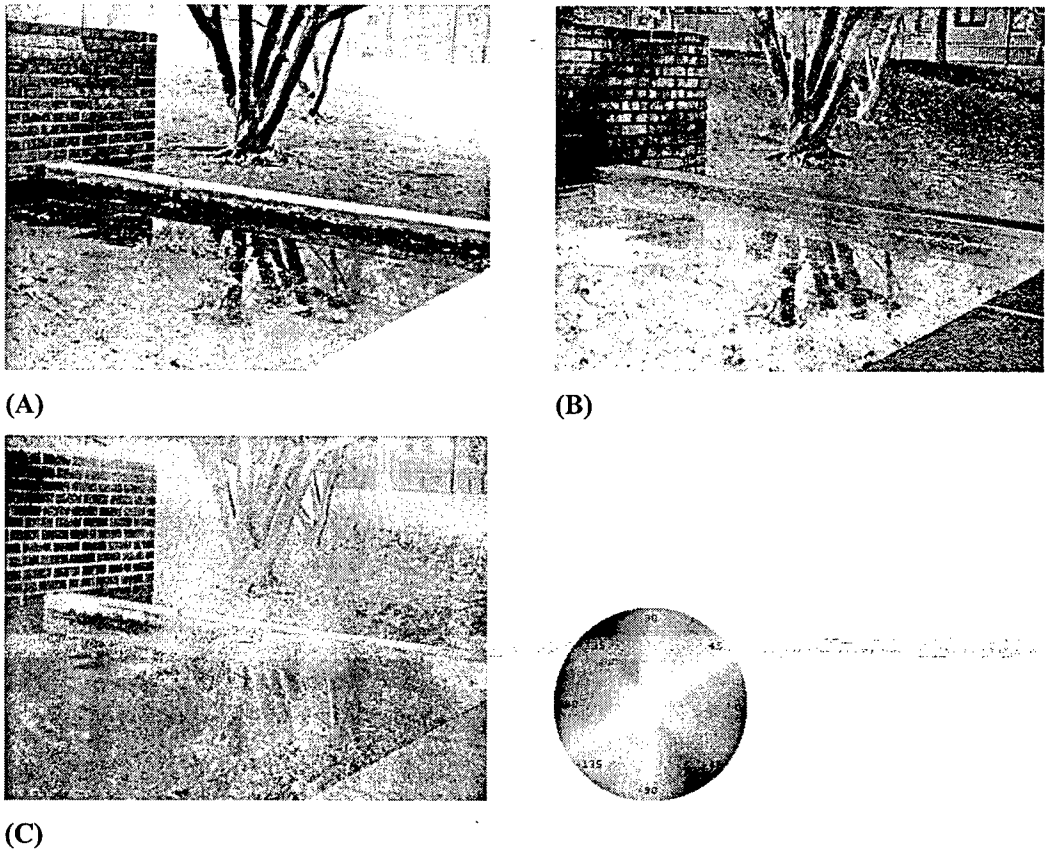

Fig. 6. (A) A processed image of a body of water and a tree after the histogram equalization of its V channel; (B) Degree of linear polarization $p(x,y)$ image after it is histogram equalized; (C) Angle of polarization ellipse, $\varphi_o(x,y)$, shown in pseudo-color scheme. The angle-to-hue color wheel is shown to the right.

Our ongoing efforts in this direction have shown promising results for this bio-inspired technique for finger print detection and other deformation on smooth surfaces. Figure 7 shows the preliminary results of our polarization imaging in enhancing the detection of finger print on a smooth surface. Panel 7A presents a normal image of a soft plastic CD protector with white

cotton cloth lining, taken with the digital camera without any polarization information (the image is auto-level enhanced.) There is a finger print on this CD cover, which is very hard to detect in the regular image shown in Panel 7A. Then a polarization analyzer was added to the digital camera, and then the complete polarization information (i.e., the intensity, the degree of linear polarization, and the angle of polarization orientation for each pixel) was derived. Panel 7B shows the image of the "degree of linear polarization" after histogram-equalization. This image is *not* the pixel intensity image, but rather is the distribution of the degree of linear polarization of pixels. So we can clearly see the presence of the finger print on this cover. Panels C and D present the "cropped" version of Panels A and B, after they are auto-level enhanced and histogram-equalized, respectively. We can see that even after we realize the location of the finger print, the "regular" image in Panel C is less detectable than the one in Panel D, which is from the degree of linear polarization. Panel E represents the segmentation of the degree of linear polarization, and then Panel F shows the extracted segment with the finger print. Finally, Panel G illustrates the application of Canny edge detection [61] to the selected segment in Panel F. This shows reasonably well the lines of the finger prints in our image. We are currently working on various techniques to improve this bio-inspired technique for finger print detection. More results can be found in our manuscript that has been submitted for publication, and is attached in the appendix.

We will also consider applying this technique to detection of other surface deformation and variation.

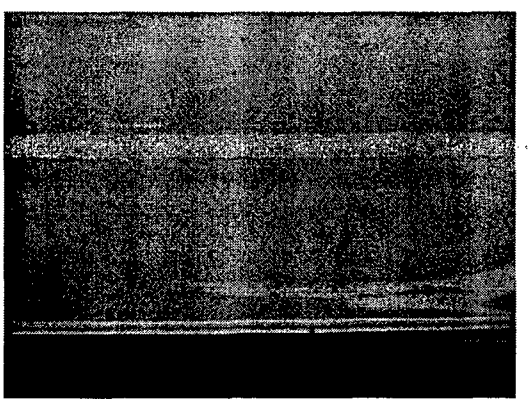

(A)

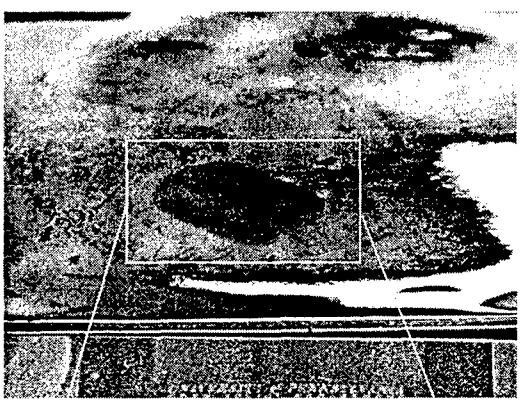

(B)

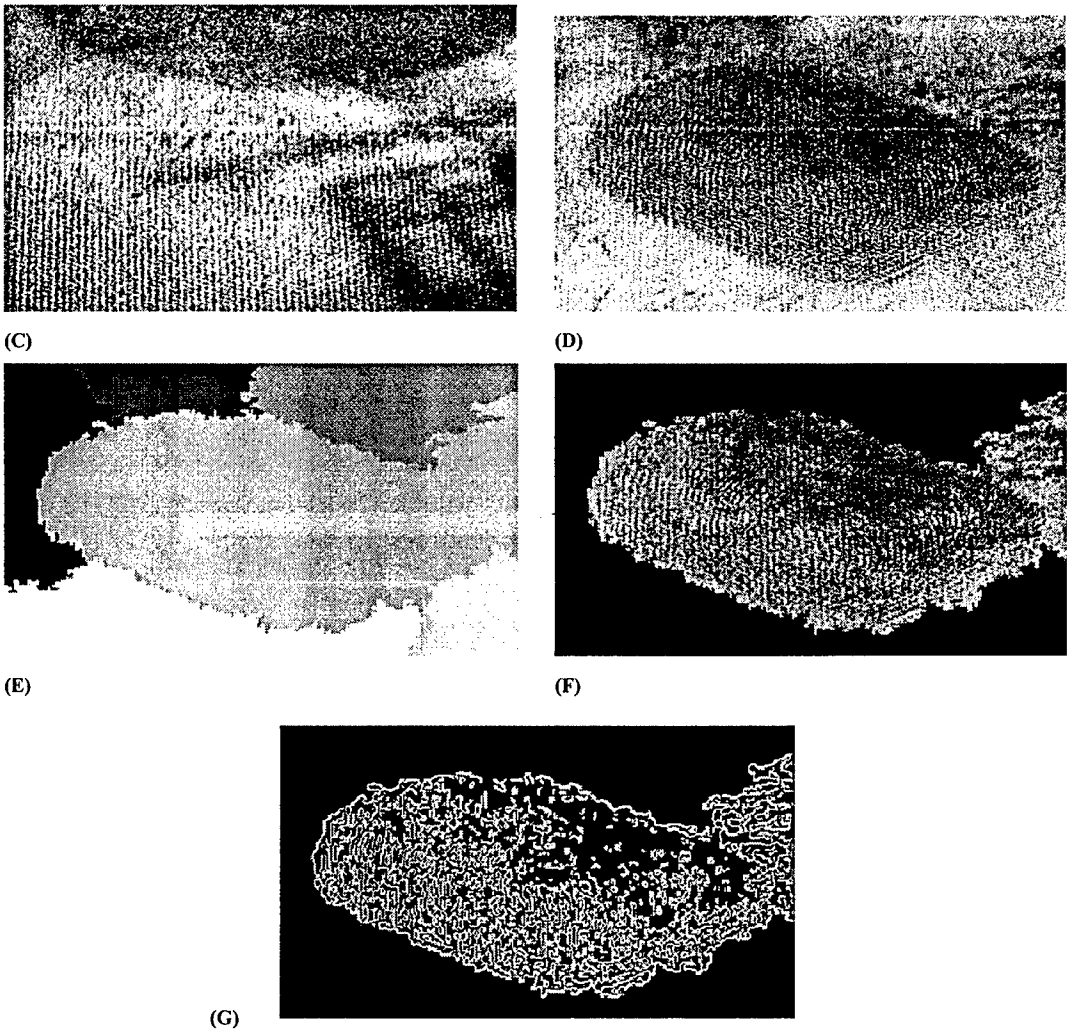

Fig. 7. Preliminary results of a bio-inspired idea for non-invasive imaging of a latent finger print on a smooth surface. Panel A presents a normal (auto-level enhanced) image of a soft plastic CD protector with white cotton cloth lining, taken with the digital camera without any polarization information. Panel B shows the image of the "degree of linear polarization" after it is histogram-equalized. This image is *not* the pixel intensity image, instead it is the distribution of the degree of linear polarization of pixels. The finger print on this cover is clearly visible. Panels C and D present the "cropped" version of Panels A and B, after they are auto-level enhanced and histogram-equalized, respectively. Panel E represents the segmentation of the degree of linear polarization, and Panel F shows the segment extraction with the finger print selected. Panel G illustrates the application of Canny edge detection to the selected segment in Panel F. More detailed results can be found in our manuscript that has been submitted for publication. This is attached in the appendix.

Fig. 8 shows a preliminary result we obtained from polarization imaging from the skin of the back of a hand. Panel B shows the "degree of linear polarization" of the skin (after histogram equalization), which may reveal more information about the surface of the skin. We will investigate a number of specific parameters in such imaging of skin, and explore how the angles of illumination and viewing (and the combination) affect the images.

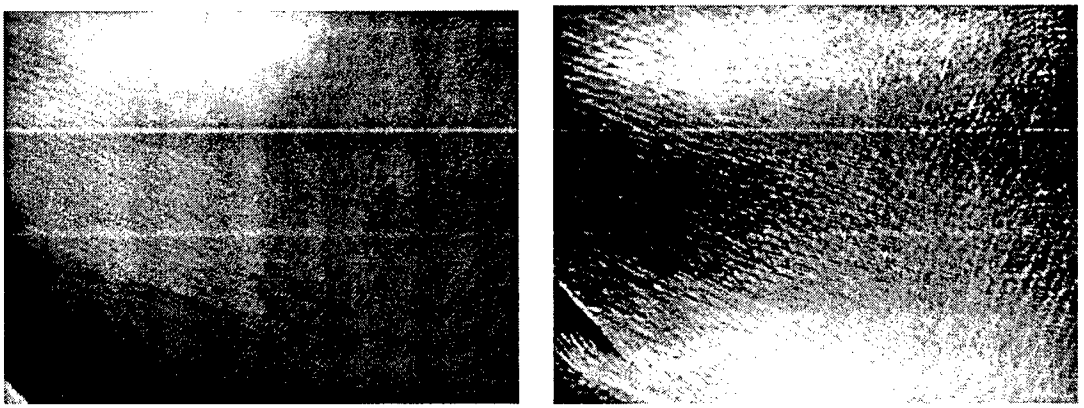

(A) (B)

Fig. 8. Preliminary results of polarization imaging of skin. Panel A shows a "regular" image of the skin of back of a hand without any polarization information. Panel B shows the "degree of linear polarization" of the skin after histogram equalization.

4.Polarization Shadow Removal: Polarization Imaging Techniques for Detection of Objects Hidden in Shadows

In the course of our study of bio-inspired polarization imaging of natural and man-made scenes, we have noticed that when the distribution of the "degree of linear polarization" (instead of regular pixel intensity distributions) at each pixel are shown, certain aspects of the scenes such as "shadows" are presented differently. In fact, we have found that in certain situations, when the image of the degree of polarization is shown, the regular shadows are either disappeared or have been less noticeable. We show our preliminary results of such "shadow removal" by the polarization imaging in Fig. 9. Panel A presents the regular intensity image of a scene on the roof of our building (after histogram equalization), while Panel B shows the distribution of the degree of linear polarization of the same scene (after it is histogram equalized). We notice several interesting features in this image: The shadow in front of the chimney, which is clearly observed in Panel A, is no longer there in Panel B. Likewise, the shadow beneath the edge of the roof is effectively "removed" in Panel B. Therefore, if there is an object hidden in these regions of the image in Panel A, it would become "visible" in Panel B. This can be seen when we look at the details of the "object" to the right of the chimney – such details cannot be seen in Panel A since the shadow makes it dark to see these details, while in Panel B these are clearly more "visible". Moreover, the strings holding the chimney are more visible in Panel B because the light reflected from them is partially polarized. Furthermore, the sky background has one polarization, distinct from the clouds, and the clouds now "pop-out" with much better contrast. If an airplane is flying through the clouds (but not too deep into them), it may also pop out. All these features can offer an exciting possibility for detection of objects hidden in shadow regions using the bio-inspired

polarization imaging techniques. Furthermore, this can alter the perception of object boundaries, if the image is taken and shown using this technique. More results can be found in our manuscript that is being prepared for submission for publication and is attached in the appendix.

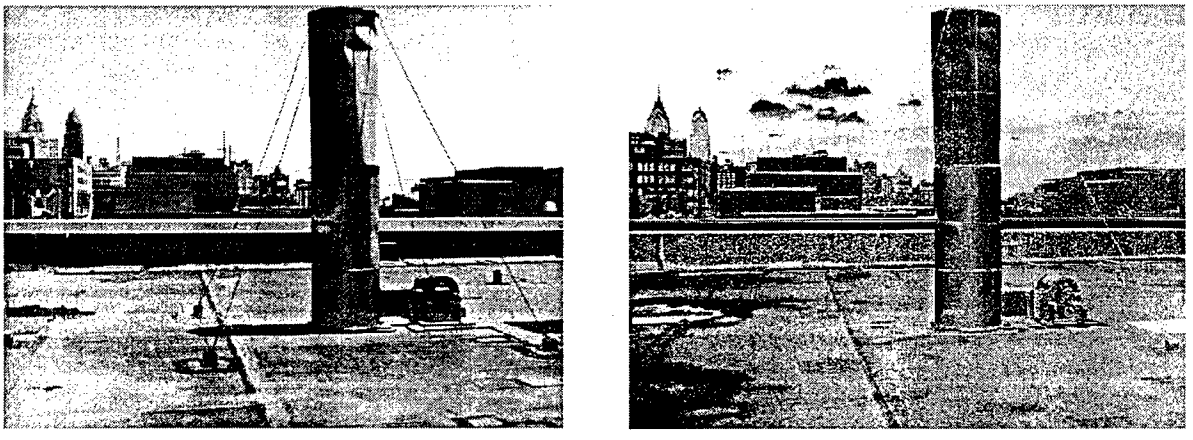

(A) (B)

Fig. 9. Images of a scene on the roof. Panel A shows the "conventional" pixel intensity image (after histogram equalization), while Panel B presents the distribution of the "degree of linear polarization" for pixels in the scene (after it is histogram equalized). Note that some of shadows in Panel A have been effectively "disappeared" in Panel B, and as a result certain details can be "seen" in Panel B. (see the text and the appendix for more detail and other images.)

5.Bio-Inspired Display of Polarization Information Using Selected Visual Cues

As has been shown in the previous parts, it is clear that the polarization of the image-forming light carries important information about the scene that is being imaged. However, an interesting issue arises in dealing with representing the polarization information obtained from a polarimetric imaging system. Since the unaided human eye cannot directly "see" polarization information, how can then such polarization information that is obtained by a polarimetric imaging system be presented to a human observer? After all, the outputs of any imaging system must be presented in such a manner that can be interpretable and recognizable by a human observer. What this implies is that such information should be mapped into visual cues that can be easily detectable by a human observer, hopefully without altering the other information carried by cues such as spectral and luminance information. Effectively, some form of "sensory substitution" is required for presenting polarization "signals" to a "polarization-blind" observer, without affecting other visual information such as color and brightness. In our group's earlier work, we had shown a bio-inspired mapping for the cases where the original spectral information (i.e., the perceived colors) of the scenes was not of interest [26]. In that mapping, polarization-difference information was pseudo-color-coded, based on the opponent-colors model of human

vision, resulting in a contrast enhancement of polarization imagery of objects in scattering media such that the objects became easily detectable by a human observer [26]. However, that mapping ignored the spectral information in the original scene -- information normally mapped into perceived color. In order to preserve the spectral and luminance information in an image, we need to map the polarization into visual cues other than the color and brightness. The human visual system detects and encodes a great variety of visual cues. These include color, intensity, coherent motion, texture, flicker, to name a few. In the first Phase of our efforts, we have been conducting research on a variety of bio-inspired representational schemes as well as certain fusion techniques in order to present polarization information to the human observer in meaningful cues, that is, in a form perceptible to human vision [30-34]. Here, we briefly mention some of our results. The details can be found in our published works [30-32]. These techniques include:

(a) Coherently moving dots: Since human vision is highly sensitive to motion -- including coherent motion detection, form from motion, and biological motion [39-42] --- the sensitivity of coherence detection in human eye can be exploited to display polarization information in an image. We have used coherently moving dots superimposed on images to represent various polarization parameters [30-31]. Fig. 10 illustrates a sample of our results.

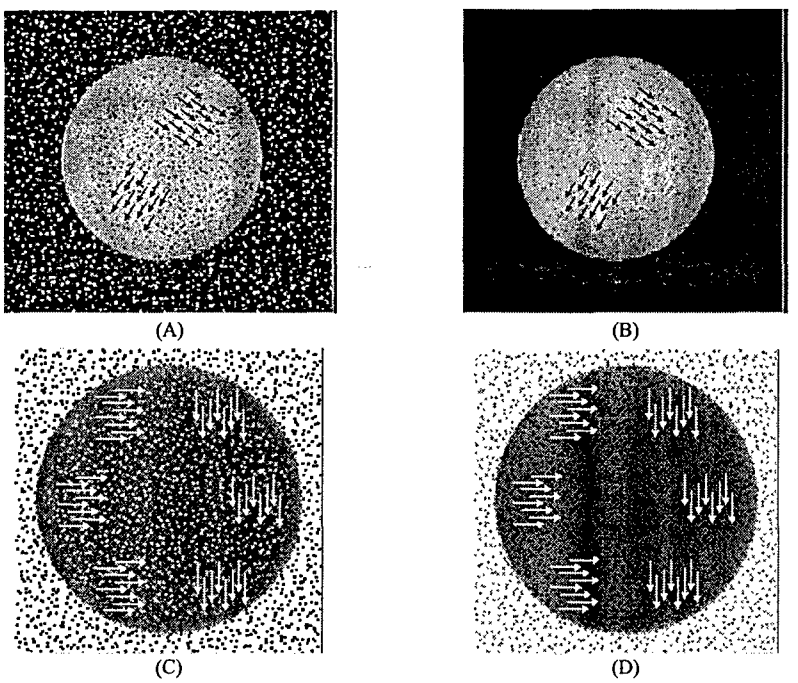

Fig. 10. Panels (A) and (C): Superimposing *moving* dots on the PS images of the 2-patch and 7-patch targets using the contrast scheme [30]. Panels (B) and (D): corresponding images with the percentage scheme [30]. Dot size is 1x1 pixel in Panels (A) and (B), and 2x2 pixels in Panels (C) and (D) Since here we need to show "static image", some "arrows" have been added to give indication of the direction of motion of the coherently moving dots. We have made movie files showing the coherent motion of these dots. Movies are

available in our paper in the online journal *Optics Express* [30].

(b) "Temporal fusion": We utilize the dimension of time, as an additional degree of freedom, to dynamically superimpose polarization-based images with non-polarized images in accordance with the established sensitivity of human eye to temporal variation of brightness and color [31]. A variety of image fusion techniques have been used by many researchers to combine two or more images from different modalities (such as images from the visible band and the IR band) into a single image that ideally contains all the important information of original images (see e.g., [43-47]). In principle, those fusion techniques can also be used to fuse polarization images with non-polarization images (e.g., intensity-only images). We have introduced the concept of "temporal fusion", where the fusing of two different images is achieved in time domain by taking advantage of the biological sensitivity of human visual system to the "fading in and fading out" between two image modalities [31]. As applied to polarization, the image modalities of interest here are an intensity-only image (i.e., PS image) and the polarization-difference (PD) information of the same scene (e.g., this latter image could be a grayscale representation of the PD data, or a pseudo-color representation). A dynamic image (i.e., a movie) consisting of a gradual periodic transition from a PS image to PD image is then created, with the frequency of transition chosen such that the human eye can easily and most sensitively detect this fading in and fading out. In this way, the observer can clearly see and distinguish the PS information and PD information in the same dynamic image. In other words, we take advantage of the dimension of "time" in order to fuse information from two different modalities, i.e., from polarization and non-polarization information. If the PD image is formed as a pseudo-colored image, then we choose the frequency of fading between the PS and PD image in accordance with sensitivity of color channels in the human eye. Figure 11 shows a few snapshots of one of our movies for such temporal fusion.

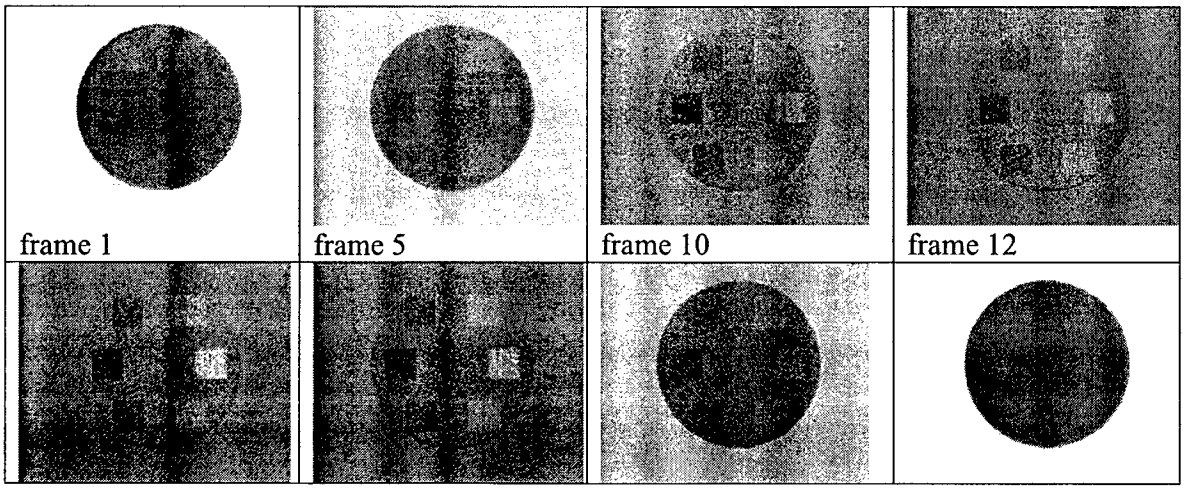

frame 15	frame 18	frame 25	frame 30

Fig. 11. Snapshots of temporal fusion of the grayscale PS and PD images of the back-illuminated 7-patch target using the "sinusoidal" modulation [31]. Every complete cycle of the movie file includes 30 frames, which can be viewed with the rate of 30 frames/sec. In this figure, we only present frames No 1, 5, 10, 12, 15, 18, 25, and 30, from the left to right and the top to bottom. The movie files are available, and we can send them to the interested reader.

We have also studied the temporal fusion of a color image of a natural scene with its pseudo-color polarimetric image. It is well known that for the light coming from every point in a scene, three parameters related to the polarization information detectable by a 2-D imaging sensor, in which the phase information between the two orthogonal polarization components is not available, can be described as the energy intensity (or brightness) I, degree of linear polarization p, and orientation angle φ_o of the polarization ellipse of the polarized portion of the light from that point. The value of p varies between 0 and 1 where $p=0$ presents unpolarized light and $p=1$ corresponds to a completely linearly polarized signal. To find these parameters at every pixel, one needs to collect a minimum of three images of the same scene; each image taken with a different orientation of the polarization analyzer in front of the camera, e.g., with 0°, 45°, and 90° orientation of the polarization analyzer. These three independent "measurements" can provide one with three equations from which the parameters I, p, and φ_o can be evaluated for each pixel. To display these three parameters of a scene in a single image, one can use a variety of mapping strategies. We have investigated several different mapping possibilities. One such mapping is the Bernard and Wehner mapping [48], who suggested the mathematical similarities between a theoretical 3-parameter polarization vision system and the widely used 3-parameter color vision system. They also pointed out that some species may indeed have 3-parameter polarization vision system [48]. The main analogy they draw is the parallelism of the intensity I with the value V, the degree of polarization p with the saturation S, and the angle φ_o with the hue H (in the HSV color space). This parallelism has been used in the past in certain polarization-sensitive imaging systems [49-51]. Here, as an input to our temporal fusion algorithm, we utilize this pseudo-color mapping based on this parallelism to produce a pseudo-color polarimetric image. For display purpose, we incorporate the image enhancement technique "histogram equalization" on the original value V (in the HSV space) of the "true-color" image, and use this equalized V as the V channel, and the contrast enhanced p data for the saturation

channel S. For the angle of polarization φ_o, we map $2\varphi_o$ to the hue angle. As an example, we use a picture of flowers and leaves which we have taken outdoors by taking three images with three orientations of the polarization analyzers as mentioned above. A processed "true-color" image of this scene is shown in Fig. 12A after the histogram equalization has been applied; the distribution of degree of linear polarization $p(x,y)$, after contrast enhancement, is shown in Fig. 12B; and the distribution of the angle of polarization ellipse, $\varphi_o(x,y)$, is depicted in Fig. 12C with the angle-to-hue color wheel shown at its right. Figure 12D illustrates the mapping of (I,p,φ_o) into (V,S,H). We notice that the images with polarization information (Figs. 12B, 12C, and 12D) reveal certain additional information not available in the regular color image in Fig. 12A. For instance, we note that in the distribution of $p(x,y)$ shown in Fig. 12B the leaves in general exhibit higher degree of linear polarization than the flowers (the flowers look "darker" than the leaves in $p(x,y)$). Moreover, we observe that certain parts of the scene with low intensity shown in the conventional image in Fig. 12A, such as the little leaf in the foreground slightly below the three large leaves, may appear more noticeable in the images of $p(x,y)$ and $\varphi_o(x,y)$ shown in Figs. 12B and 12C, since the degree of polarization at a pixel may in general vary independently of intensity of that pixel. We have applied our temporal fusion technique to fuse the image shown in Fig. 12A with that in Fig. 12D and to produce movie files for such fusion. Figure 13 illustrates the snapshots of this temporal fusion with sinusoidal modulation [31].

(A)

(B)

(C) (D)

Fig. 12: (A) A processed "true color" image of a scene after the histogram equalization of its V channel; (B) Degree of linear polarization $p(x,y)$ image after it is contrast enhanced; (C) Angle of polarization ellipse, $\varphi_o(x,y)$, shown in pseudo-color scheme. The angle-to-hue color wheel is shown to the right; and (D) Pseudo-color mapping of three parameter (I,p,φ_o) into (V,S,H).

Fig. 13. Snapshots of temporal fusion of Fig. 12A (color image of the scene) with Fig. 12D (pseudo-color polarimetric image of the same scene) using the sinusoidal function $\alpha(n)$ [31]. Every complete cycle of the movie file includes 30 frames, played back at the rate of 30 frames/sec. The movie files are available upon request.

(c) Flicker: In this method of presenting polarization information, we have exploited the sensitivity of human eye to intensity flicker in an image [52]. After forming the PS and PD images of a scene, we intend to bring the observer's attention to the regions of the image having PD signals with opposite signs. We find these regions by searching for pixels whose raw PD values are greater than $+\delta$ and those that are less than $-\delta$, where δ is a given threshold. These regions we name (+) and (–) regions, respectively. The rest of the image, in which $-\delta < PD < \delta$, is the "PD neutral" region. Then we temporally modulate the intensity of the pixels in PS image belonging to the (+) and (–) regions from frame to frame, forming a movie file. Such temporal modulation can be expressed as: $I^{(+)}(x,y,n) = T_{PS}\left[{}_{PS}I(x,y)\right]\left(1+M_{+}\sin(\Omega t_n)\right)$, $I^{(-)}(x,y,n) = T_{PS}\left[{}_{PS}I(x,y)\right]\left(1+M_{-}\sin(\Omega t_n+\pi)\right)$. Here, x and y are coordinates of the pixels within the image, n is the frame number ranging from 1 to N where N is the number of frames in a complete cycle, t_n corresponds to the time of frame n, M_{+} and M_{-} are the modulation coefficients for the (+) and (–) regions, respectively, $\Omega = 2\pi F$ where F is the frequency of flicker in *Hz*. There is 180° phase difference between the flickers in the (+) and (–) regions. We have applied such a technique in several images obtained using the polarimetric imaging. The

images can be found in our paper [31] and the movies are available upon request.

(d) Textures: In human visual perception, it is known that certain forms of textures can be segregated more easily than others [53-56]. Therefore, textures can be another set of visual cues that can be used to display polarization information. We have been exploring these ideas for polarization visualization. In order to utilize textures for this purpose, we first subdivide the entire image into small cells of $m \times m$ pixels (e.g., $m = 10$), and we evaluate the average PS and PD values in each cell. We then identify the (+) and (–) regions of the image which correspond to pixels with $\langle PD \rangle_{cell} > +\delta$ and $\langle PD \rangle_{cell} < -\delta$, as was described above. Here $\langle PD \rangle_{cell}$ denotes the average value of PD in each cell. We can then superimpose different texture patterns on the original image with each single element of the texture pattern corresponding to a single cell. We use different texture elements/patterns for the PD (+) and PD (–) regions of the image [31]. Here we show one case of such mapping. We have generated some form of texture pattern by having spatial and/or temporal modulation of the intensity of the processed PS image in the regions with the PD (+) and PD (–) values. Such modulation can be written as

$$I^{(+)}(x,y,n) = T_{PS}\left[{}_{PS}I(x,y)\right]\left\{1 + M_{+}\cos\left[\Omega t_n + \kappa x \sin(\varphi) - \kappa y \cos(\varphi)\right]\right\}$$

$$I^{(-)}(x,y,n) = T_{PS}\left[{}_{PS}I(x,y)\right]\left\{1 + M_{-}\cos\left[\Omega t_n + \kappa x \sin\left(\varphi + \frac{\pi}{2}\right) - \kappa y \cos\left(\varphi + \frac{\pi}{2}\right)\right]\right\}$$ where M_{+}, M_{-}, Ω were defined above, $\kappa = 2\pi/\Lambda$ with Λ being the spatial wavelength of spatial modulation, φ is the direction of $\|$ polarization component, and the angle $\frac{\pi}{2}$ is added to φ for modulation in the (–) region to indicate the direction of $\perp$ polarization component. Spatial as well as temporal modulations of intensity of the PS image provide texture patterns that can be easily detected by the human observer, resulting in segregation of the PD (+) and PD (–) regions. Figure 14 illustrates the *static* case of such textures using the spatial modulations for the 2-patch target. (This *static* texture corresponds to $\Omega = 0$ in the above equations.) For the spatial *and* temporal modulations we have made movie files, which are available upon request. One can easily see the presence of the two regions with PD (+) and PD (–) values.

More detailed description of our algorithms can be found in our manuscript is attached in the appendix.

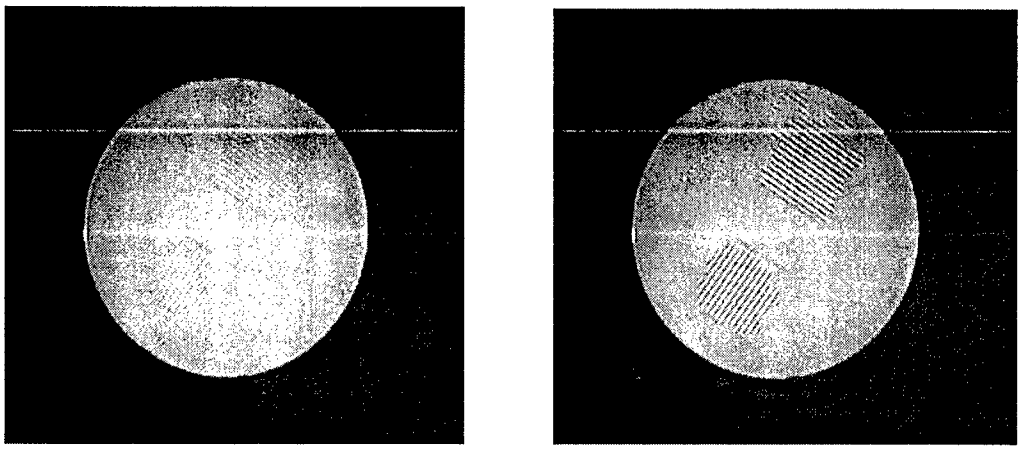

(A) (B)

Fig. 14. Static texture using spatial modulation of the intensity of the processed PS image of the 2-patch target to represent regions with PD $(+)$ and PD $(-)$. (This PS image without modulation was originally taken and used in our work in Ref [26]) Panel (A): $M_+ = M_- = 0.05$, $\kappa = 1$; Panel (B): $M_+ = M_- = 0.25$, $\kappa = 1$.

6.Instrumentation and Camera Systems for Polarimetric Imaging

During our efforts in this period, we have developed various camera and imaging systems capable of collecting images with the polarization information. We have (a) two digital cameras with a polarizing beam splitter, capable of collecting two simultaneous images with orthogonal polarizations (Fig. 15A); (b) a digital camera (one of the cameras in (a)) that can capture images with various polarization using a polarization analyzer in front of it; (c) 4-video-board-camera system that are placed on a platform and can obtain images at 4 different polarization orientations (Fig. 15B); (d) individual video cameras equipped with a ferroelectric liquid crystal rotator; and (e) a six-camera system; two in the visible range, two in the near-infradred (NIR); and two in the far-infrared (FIR) regimes (Fig. 15C). With these imaging systems, we have been collecting useful images for our research in bio-inspired polarimetric sensing.

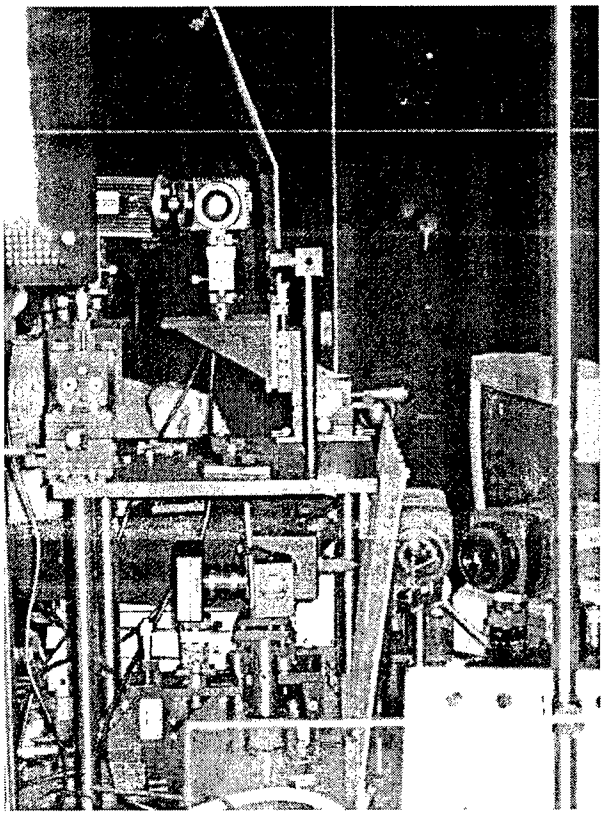

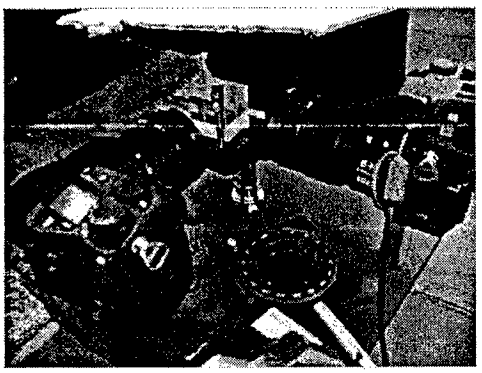

(A)

(B)

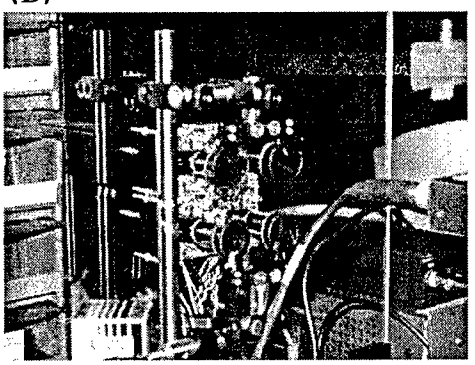

(C)

Fig. 15. Some of the imaging systems used in our research efforts.

References

[1] G. P. Konnen, *Polarized Light in Nature*, Cambridge University Press, New York, 1985.

[2] K. von Frisch, "Die Polarisation des Himmelslichtes als orientierender Faktor bei den Tanzen der Bienen," *Experientia*, vol. 5, pp. 142-148, 1949.

[3] R. Wehner, "Neurobiology of Polarization Vision," *Trends in Neurosciences*, vol. 12, pp. 353-359, 1989.

[4] R. Wehner, "Polarized-light navigation by insects," *Scientific American*, **235**, pp. 106-114, 1976.

[5] R. Wehner, "'Matched filters' – neural models of the external world", J. Comp. Physiol. A, Vol. 161, pp. 511-531, 1987.

[6] T. Labhart, "Polarization Opponent Interneurons in the Insect Visual System, " *Nature*, vol. 331, pp. 435-437, 1988.

[7] T. Labhart and E. P. Meyer, "Detectors for polarized skylight in insects: A survey of ommatidial specializations in the dorsal rim area of the compound eye," Microscopy Research and Technique, Vol. 47, pp. 368-379, 1999.

[8] T. Labhart, "How Polarization-Sensitive Interneurones of Crickets Perform at Low Degrees of Polarization, " *Journal of Experimental Biology*, vol. 199, pp. 1467-1475, 1996.

[9] Hawryshyn, C.W., "Ultraviolet polarization vision in fishes: possible mechanisms for coding e-vector", *Proc. Trans. Roy. Soc. (Lond.)* 335: 1187 – 1190, 2000

[10] Novales Flamarique, I., C.W. Hawryshyn & F.I. Harosi, "Double cone internal reflection as a basis for polarized light detection" *J. Opt. Soc. Am. A.* 15: 349-358, 1998.

[11] R. Schwind, "The plunge reaction of the backswimmer Notonecta glauca," J. Comp. Physiol. A., Vol. 155, pp. 319-321, 1984.

[12] R. Schwind, "Visual system of Notonecta glauca: A neuron sensitive to movement in the binocular field," J. Comp. Physiol. A. Vol. 123, pp. 315-328, 1978.

[13] R. Schwind, "Zonation of the optical environment and zonation in the rhabdom structure within the eye of the backswimmer, Notonecta glauca," Cell and Tissue Research, Vol. 232, pp. 53-63, 1983.

[14] T. H. Waterman, "Polarization Sensitivity" in *The Handbook of Sensory Physiology vol. Vii/6B Vision in Invertebrates*, H. Autrum (ed.), Springer-Verlag, New York, 1981.

[15] N. Shashar and T. W. Cronin, "Polarization Contrast Vision in Octopus," *The Journal of Experimental Biology*, Vol. 199, pp. 999-1004, 1996.

[16] N. Shashar, P. Rutledge, and T. W. Cronin, "Polarization vision in cuttlefish: a concealed communication channel?" J. Exp. Biol., Vol. 199, 2077-2084, 1996.

[17] T. W. Cronin and N. Shashar, "The linearly polarized light field in clear, tropical marine waters: spatial and temporal variation of light intensity, degree of linear polarization, and e-vector angle," J. Exp. Biol., Vol. 204, pp. 2461-2467, 2001.

[18] J. N. Lythgoe and C. C. Hemmings, "Polarized Light and Underwater Vision", *Nature*, vol. 213, pp. 893-894, March 1967.

[19] R. Menzel, "Polarized Light Sensitivity in Arthropods," in *Light as an Ecological Factor II*, Evas, G. C. R. Bainbridge and O. Rackman (eds.), Blackwell Scientific Pub., London, 1975.

[20] W. Saidel, J. Y. Lettvin, and E. F. MacNichol, Jr., "Processing of Polarized Light by Squid Photoreceptors," *Nature*, vol. 304, pp. 534-536, 1983.

[21] M. P. Rowe, N. Engheta, S. S. Easter, and E. N. Pugh, Jr. "Graded Index Model of a Fish Double Cone Exhibits Differential Polarization Sensitivity," *Journal of Optical Society of America, A.*, Vol. 11, No. 1, pp. 55-70, January 1994.

[22] M. P. Rowe, J. M. Corless, N. Engheta, and E. N. Pugh, Jr., "Scanning Interferometry of Sunfish Cones: I. Longitudinal Variation in Single-Cone Refractive Index," *Journal of Optical Society of America A.*, Vol. 13, No. 11, pp. 2141-2150, November 1996.

[23] M. P. Rowe, N. Engheta, J. M. Corless, and E. N. Pugh, Jr., "Refractive Index Gradient in Sunfish Cones," a chapter in *Basic and Clinical Applications of Vision Science, The Professor Jay M. Enoch Festschrift Volume*, (*Documenta Ophthalmologica Proceedings* Series 60), V. Lakshminarayanan (ed.), pp. 51-55, 1997.

[24] J. S. Tyo, M. P. Rowe, E. N. Pugh, Jr., and N. Engheta, "Target Detection in Optically Scattering Media by Polarization-Difference Imaging," in *Applied Optics*. (Information Processing division), Vol. 35, No. 11, pp. 1855-1870, April 10, 1996.

[25] M. P. Rowe, E. N. Pugh, Jr., J. S. Tyo, and N. Engheta, "Polarization-Difference Imaging: A Biologically Inspired Technique for Observation through Scattering Media," *Optics Letters*, Vol. 20, No. 6, pp. 608-610, March 15, 1995.

[26] J. S. Tyo, E. N. Pugh, Jr., and N. Engheta, "Colorimetric Representations for Use with Polarization-Difference Imaging of Objects in Scattering Media," *Journal of Optical Society of America A*, Vol. 15, No. 2, pp. 367-374, February 1998.

[27] J. S. Tyo, *Polarization-Difference Imaging: A means for Seeing through Scattering Media*, Ph.D. Dissertation, Department of Electrical Engineering, University of Pennsylvania, April 1997.

[28] J. S. Tyo, "Optimum Linear Combination Strategy for an N-Channel Polarization-Sensitive Imaging or Vision System," *J. Optical Society of America A*, Vol. 15, pp. 359-366, 1998.

[29] E. N. Pugh, Jr., N. Engheta, M. P. Rowe, and J. S. Tyo, U.S. Patent Number # 5,975,702, "Method of Using Polarization Differencing to Improve Vision", November 2, 1999.

[30] K. M. Yemelyanov, M. A. Lo, E. N. Pugh Jr., N. Engheta, "Display of polarization information by coherently moving dots," *Optics Express*, **11**, No 13, pp. 1577-1584, June 30, 2003. http://www.opticsexpress.org/abstract.cfm?URI=OPEX-11-13-1577

[31] K. M. Yemelyanov, S.-S. Lin, W. Q. Luis, E. N. Pugh, Jr., and N. Engheta, "Bio-Inspired Display of Polarization Information Using Selected Visual Cues," the Polarization Science and Remote Sensing in the *2003 SPIE-The International Society for Optical Engineering, San Diego, California*, August 3-8, 2003, pp. 71-84. (invited).

[32] S.-S. Lin, K. Yemelyanov, E. N. Pugh, Jr., and N. Engheta, "Polarization-Enhanced Visual Surveillance Techniques," to be presented at the the *Special Session on "Visual Surveillance"of the IEEE 2004 International Conference on Networking, Sensing and Control, Taipei, Taiwan,* March 21-23, 2004 (invited).

[33] K. M. Yemelyanov, S.-S. Lin, W. Q. Luis, E. N. Pugh, Jr., and N. Engheta, "Bio-inspired visualization of polarization information using temporal fusion, flicker, coherently moving dots and texture," the *Annual Meeting of the Optical Society of America, Tuscon, Arizona*, October 5-9, 2003, p. WM5 of the CD digest.

[34] S.-S. Lin, K. M. Yemelyanov, W. Q. Luis, E. N. Pugh, Jr., and N. Engheta, "Biomimetic, adaptive, optimum polarization-opponent imaging of scenes with preferential polarization distributions," the *Annual Meeting of the Optical Society of America, Tuscon, Arizona*, October 5-9, 2003, p.. MT32 of CD digest.

[35] K. Engstrom, "Cone Types and Cone Arrangements in Teleost Retinae" *Acta Zoologica,* vol. 44, pp. 179-243, 1963.

[36] M. A. Ali and M. Anctil, *Retinas of Fishes*, Springer-Verlag, New York, 1976.

[37] G. Buchsbaum and A. Gottschalk, "Trichromacy, opponent colours coding and optimum colour information transmission in the retina," *Proceedings of Royal Society of London*, Ser. B vol. 220, pp.. 89-113, 1983.

[38] *Advances in Fingerprint Technology*, vol. III of *CRC Series in Forensic and Police Science,* B. A. J. Fisher, Ed., (CRC Press LLC, Boca Raton, FL, ed. 2, 2001), pp. 1-444.

[39] D. Jokisch, "Biological motion as a cue for the perception of size," *Journal of Vision*, **3**, pp. 252-264, 2003.

[40] W. Curran, O. J. Braddick, "Speed and direction of locally-paired dot patterns," *Vision Research*, **40**, pp. 2115-2124, 2000.

[41] W. A. van de Grind, A. J. van Doorn, J. J. Koenderink, "Detection of coherent motion in peripherally viewed random-dot patterns," *J. Optical Society of America A*, **73**, pp. 1674-1683, 1983.

[42] E. D. Grossman, R. Blake, "Perception of coherent motion, biological motion and form-from-motion under dim-light conditions", *Vision Research*, **39**, No 22, 3721-3727, 1999.

[43] A. Toet, J. K. IJspeert, A. M. Waxman, and M. Aguilar, "Fusion of Visible and Thermal Imagery Improves Situational Awareness," *Diplays*, Vol. 18, pp. 85-95, 1997.

[44] A. M. Waxman, M. Aguilar, D. A. Fay, D. B. Ireland, J. P. Racamato, Jr., W. D. Ross, J. E. carrick, A. N. Gove, M. C. Seibert, E. D. Savoye, R. K. Reich, B. E. Burke, W. H. McGonagle, and D. M. Craig, "Solid-State Color Night Vision: Fusion of Low-Light Visible and Thermal Infrared Imagery," *MIT Lincoln Laboratory Journal*, Vol. 11, No. 1, pp. 41-59, 1998.

[45] M. Aguilar, D. A. Fay, W. D. Ross, A. M. Waxman, D. B. Ireland, and J. P. Racamato, "Real-Time Fusion of Low-Light CCD and Uncooled IR Imagery for Color Night Vision," *Proceedings of SPIE*, Vol. 3364, April 13-14, 1998, Orlando, Florida, pp. 124-135.

[46] D. A. Fay, A. M. Waxman, M. Aguilar, D. B. Ireland, J. P. Racamato, W. D. Ross, W. W. Streilein, and M. I. Braun, "Fusion of 2- /3- /4-Sensor Imagery for Visualization, Target Learning and Search," *Proceedings of SPIE*, Vol. 4023, pp. 1-10, 2000.

[47] D. A. Fay, J. G. Verly, M. I. Braun, C. Frost, J. P. Racamato, and A. M. Waxman, "Fusion of Multi-Sensor Passive and Active 3D Imagery," *Proceedings of SPIE*, Vol. 4363, pp. 1-12, 2001.

[48] G. D. Bernard and R. Wehner, "Functional Similarities between polarization vision and color vision," *Vision Research*, Vol. 17, pp. 1019-1028, 1977.

[49] L. B. Wolff and T. E. Boult, "Constraining object features using a polarization reflectance model," *IEEE Transactions on Pattern. Anal. Mach. Intell.* Vol. 13, pp. 635-657, 1991.

[50] L. B. Wolff and T. A. Mancini, "Liquid crystal polarization camera," in *Proceedings of the IEEE Workshop on Applications of Computer Vision* (IEEE, New York, 1992), pp. 120-127, 1992.

[51] T. W. Cronin, N. Shashar, and L. Wolff, "Imaging technology reveals the polarized light fields that exist in nature," Biophotonics, Vol. 2, No. 2, pp. 38-41, 1995.

[52] D. H. Kelly, "Flicker" in *The Handbook of Sensory Physiology, Vol. VII/4: Visual Psychophysics*, Springer-Verlag, New-York, 1972, pp. 273-302.

[53] H. C. Nothdurft, "Texton segregation by associated differences in global and local luminance distribution," *Proc. Royal Society of London*, B 239, pp. 295-320, 1990.

[54] H. C. Nothdurft, "Different effects from spatial frequency masking in texture segregation and texton detection tasks," *Vision Research*, Vol. 31, No. 2, pp. 299-320, 1991.

[55] B. Julesz, "A Theory of Preattentive Texture Discrimination Based on First-Order Statistics of Textons," *Biol. Cyber.*, vol. 41, pp. 131-138, 1981.

[56] B. Julesz, "Textons, the Elements of Texture Perception, and Their Interactions," *Nature, Lond.* Vol. 290, pp. 91-97, 1981.

[57] R. A. Eatock and W. T. Newsome, "Sensory Systems: Editorial Review", *Current Opinion in Neurobiology*, Vol. 9, pp. 385-388, 1999

[58] A. Menini, "Calcium signaling and regulation in olfactory neurons," *Current Opinion in Neurobiology*, Vol. 9, pp. 419-426, 1999.

[59] R. Fettiplace and A. J. Ricci, "Adaption in auditory hair cell," *Current Opinion in Neurobiology*, Vol. 13, pp. 446-451, 2003.

[60] E. N. Pugh, Jr., S. Nikonov, and T. D. Lamb, "Molecular mechanism of vertebrate photoreceptor light adaptation," *Current Opinion in Neurobiology*, Vol. 9, pp. 410-418, 1999.

Appendix

Manuscripts: published, submitted for publication, and in preparation for submission

Manuscript Entitled:

"Display of polarization information by coherently moving dots"

Konstantin M. Yemelyanov, Matthew A. Lo, Edward N. Pugh Jr., Nader Engheta

Appeared in Optics Express, Vol. 11, No 13, pp. 1577-1584, June 30, 2003. Online at http://www.opticsexpress.org/abstract.cfm?URI=OPEX-11-13-1577

Display of polarization information by coherently moving dots

K. M. Yemelyanov, M. A. Lo[2]

Department of Electrical and Systems Engineering, University of Pennsylvania
Philadelphia, Pennsylvania 19104-6390, USA
kostya@ee.upenn.edu, mwlo@wharton.upenn.edu,

E. N. Pugh, Jr.
F. M. Kirby Center for Molecular Ophthalmology and Institute of Neurological Sciences, University of Pennsylvania
422 Curie Boulevard, Philadelphia, Pennsylvania 19104-6069, USA
pugh@mail.med.upenn.edu

N. Engheta[3]
Department of Electrical and Systems Engineering and Institute of Neurological Sciences, University of Pennsylvania
Philadelphia, Pennsylvania 19104-6390, USA
engheta@ee.upenn.edu

Abstract: It is known that human-eyes are effectively polarization-blind. Therefore, in order to display the polarization information in an image, one may require exhibiting such information using other visual cues that are compatible with the human visual system and can be easily detectable by a human observer. Here, we present a technique for displaying polarization information in an image using coherently moving dots that are superimposed on the image. Our examples show that this technique would allow the image segments with polarization signals to "pop out" easily, which will lead to better target feature detection and visibility enhancement.

OCIS codes: 110.0110 (Imaging systems), 260.5430 (Polarization), 230.5440 (Polarization-Sensitive devices), 330.1880 (Detection)

References and links

1. K. von Frisch, "Die polarisation des himmelslichtes als orientierender faktor bei den tanzen der bienen," *Experientia*, vol. 5, pp. 142-148, 1949.
2. T. Labhart, "Polarization opponent interneurons in the insect visual system," *Nature*, vol. 331, pp. 435-437, 1988
3. R. Wehner, "Neurobiology of polarization vision," *Trends in Neurosciences*, vol. 12, pp. 353-359, 1989
4. T. H. Waterman, "Polarization sensitivity" in *The Handbook of Sensory Physiology vol. Vii/6B Vision in Invertebrates*, H. Autrum (ed.), Springer-Verlag, New York, 1981.
5. R. Wehner, "Polarized-light navigation by insects," Scientific American, Vol. 235, pp. 106-114, 1976.
6. J. N. Lythgoe and C. C. Hemmings, "Polarized Light and Underwater Vision", *Nature*, vol. 213, pp. 893-894, March 1967.
7. M. P. Rowe and E. N. Pugh, Jr., J. S. Tyo, N. Engheta, "Polarization-difference imaging: a biologically inspired technique for observation through scattering media", *Optics Letters*, Vol. 20, No. 6, pp. 608-610, 1995.
8. J. S. Tyo, M. P. Rowe, E. N. Pugh, Jr., N. Engheta, "Target detection in optically scattered media by polarization-difference imaging", *Applied Optics*, Vol. 35, No 11, pp. 1855-1870, 1996.
9. J. S. Tyo, E. N. Pugh, Jr., N. Engheta, "Colorimetric representation for use with polarization-difference imaging of objects in scattering media", *J. Opt. Soc. Am. A*, Vol. 15, No 2, pp. 367-374, 1998.
10. W. Curran and O. J. Braddick, "Speed and direction of locally-paired dot patterns," Vision research, Vol. 40, pp. 2115-2124, 2000.
11. W. A. van de Grind, A. J. van Doorn, and J. J. Koenderink, "Detection of coherent motion in peripherally viewed random-dot patterns," Journal of the Optical Society of America, Vol. 73, pp. 1674-1683, 1983.
12. E. D. Grossman, R. Blake, "Perception of coherent motion, biological motion and form-from-motion under dim-light conditions", *Vision Research*, 1999, vol. 39, No 22, pp. 3721-3727.
13. J. S. Tyo, ""Optimum linear combination strategy for an N-channel polarization-sensitive imaging or vision system," *J. Opt. Soc. Am. A.*, 1998, Vol. 15, No. 2, pp. 359-366.

1. Introduction

Polarization is an important feature of electromagnetic waves, and it can be affected by surface shapes, materials, local curvature and features, and relative location of sources and objects, and thus it can provide

[2] Present address: AIG Global Investment Group, New York, New York 10038, mwlo2000@yahoo.com

[3] The author to whom correspondence should be addressed.

useful information about the observed scene and objects. Of the several characteristics of visible light, only two – intensity and wavelength – are received and encoded by the human eye and mapped by the visual system into perceptual qualities of brightness and color. In contrast, without appropriate instruments human eyes cannot effectively utilize light's polarization. However, it is well known that eyes of some animal species are sensitive to the polarization of light (see e.g., [1]-[5]). Polarization sensing by some of these species has mostly been shown to provide information for navigation [5], as originally discovered by the Nobel laureate Karl von Frisch in his work with honeybees [1], and it has been suggested that some species may have evolved polarization sensitivity as a mechanism of enhancing the contrast of targets in scattering media [6]. In our previous work, we have shown that an optical imaging system utilizing such contrast enhancement through polarization differencing can increase the distance over which targets can be detected, and their critical features discriminated [7]-[9]. Thus, "polarization imagery" is a naturally occurring and demonstrably successful strategy for enhancing vision.

However, since the human eye cannot "see" the polarization information, when this information is captured by a polarimetric imaging system, it has to be displayed into some form of visual cues/information that can be detectable by a human observer. In other words, some form of "sensory substitution" should be exploited for representing polarization "signals". In our group's earlier work, we have shown one such bio-inspired mapping, in which polarization information was pseudo color-coded, based on the opponent-colors model of human vision [9]. The results established several promising imaging strategies for displaying in a natural way the contrast enhancement of polarization imagery of objects in scattering media. Such mapping of polarization information into pseudo-colors ignores the "true" colors of the scene, namely, the spectral information contained in the scene. So if one wants to preserve the spectral and luminance information in an image, one will need to map the polarization into visual cues other than the color and brightness.

We are interested to explore and investigate certain bio-inspired display methodologies for mapping polarization information into visual information that can be readily perceived by the human visual system. In this Letter, we describe one such mapping, namely representation of polarization information by a set of coherently moving dots superimposed on an image. It is known that human vision is capable of motion perception, which includes coherent motion detection, form from motion, and biological motion (e.g., [10]-[12]). We exploit the sensitivity of coherence detection in human eye in displaying polarization information in an image. One of the motivations behind using coherently moving dots in such mapping is to preserve, by and large, various features of the image, such as color and luminance, while "displaying" the polarization information.

2. Mapping of Polarization-Difference (PD) Signal into Coherently Moving Dots

In our earlier work, we introduced the concept of polarization-difference imaging [7]. In this technique, at every pixel of the image, the intensities of the two orthogonal polarization components of the light reaching the camera, $I_{\parallel}(x,y)$ and $I_{\perp}(x,y)$, are obtained, and then the sum and difference of these two quantities are evaluated

$$_{PS}I(x,y) = I_{\parallel}(x,y) + I_{\perp}(x,y), \qquad (1)$$

$$_{PD}I(x,y) = I_{\parallel}(x,y) - I_{\perp}(x,y), \qquad (2)$$

where (x,y) identifies the pixel position in the image, $\parallel$ and $\perp$ indicate two orthogonal linear polarizations, *PD* stands for the "polarization-difference" signal, and *PS* for the "polarization-sum" signal. If an ideal linear polarization analyzer is used to capture orthogonal polarization components, the PS image will be equivalent to a conventional intensity image.

In order to use moving dots to represent the polarization information in a scene, we first obtain the two orthogonal polarization components at every pixel, and then form the PS image of the scene following Eq. (1). We then superimpose dots on this PS image. The original locations of dots are chosen as follows: The

entire PS image is divided into small identical square-shape cells each having $m \times m$ pixels, e.g., 10×10 pixels. In each cell, a single square dot is placed at a random location within the cell. The size of the dot is $n \times n$ pixels, with $n << m$, and can be properly chosen to make the dots small enough so that the original image would be practically undistorted by the presence of these dots and large enough so the dots can be detected by an observer. In the results presented in this Letter, the dot size is taken to be 2×2 pixels for an observer comfortably seated in front of a computer while viewing the image on the computer monitor at viewing distance of about 50 cm. So in each cell, the 2×2-pixel dot replaces a randomly chosen 2×2-pixel set in the cell. The density of the dot depends on the cell density. The brightness of the dot is chosen according to one of the two algorithms described later. To produce dot motion, we make sequence of several frames of the same image, but in each frame the location of the single dot in each cell is changed with respect to its location in the previous frame as follows. (1) if the averaged PD signal, i.e., the average of ${}_{PD}I(x,y)$, in that cell is greater than certain "threshold" value δ, the direction of change of location of the dot, which becomes the direction of perceived motion of dot in that cell will be chosen along a vector parallel with $\|$ polarization component; (2) if the averaged PD signal in that cell is less than $-\delta$, the direction of dot motion will be selected along the $\perp$ polarization component; and finally (3) if the averaged PD value is between $-\delta$ and δ within that cell, the sequence of location of the dot in that cell will be picked randomly, leading to a random motion of dots in this case (or the dot location can be fixed resulting in dots with no movement). So when these frames are played sequentially, the dots in all the cells with average PD signals greater than δ appear to be moving coherently in the direction parallel with the $\|$ polarization component, while the dots in cells with average PD signals less than $-\delta$ move coherently along the orthogonal direction. The dots in cells with average PD signal between $-\delta$ and δ move randomly (or they do not move at all). Since the human visual system can detect and perceive coherent motion, the two regions with dots moving coherently in two orthogonal directions can be pre-attentively segregated and "popped out" against the rest of the image where the dots are moving randomly (or they are fixed). Thus, in this technique, the observer views the PS image with its details as a conventional image, while detecting three regions in the image representing areas with $PD > \delta$, $PD < -\delta$, and $-\delta < PD < \delta$ signals.

The brightness/intensity of the dots must be chosen such that they are easily detectable against the background image. Here we suggest two different recipes; (1) the intensity of each pixel of a dot in each cell is selected to be in "contrast" with the PS signals of the pixels the dot is replacing. Specifically, if ${}_{PS}I(x,y)$ of each of the pixels which are being replaced by the $m \times m$-pixel dot is greater than 128 pixel intensity in an 8-bit display system, the intensity of each pixel of the dot in that cell will be assigned as $I_{dot}(x,y) = {}_{PS}I(x,y) - 128$. However, if ${}_{PS}I(x,y) < 128$, then we will choose $I_{dot}(x,y) = {}_{PS}I(x,y) + 128$. In this scheme, which we call the "contrast scheme", the dot intensity is "complemented" against the background intensity in each cell; (2) in this method, the intensity of each pixel in a dot in each cell is chosen to be M% less than the PS signal in the image pixel which it is replacing. So $I_{dot}(x,y) = (1 - M/100)\,{}_{PS}I(x,y)$. This approach, we call "percentage scheme".

3. Results

To demonstrate this mapping strategy, we develop the above algorithm in the MATLAB® environment. The frame sequences generated using this algorithm are presented as movies with 20 frames/second in the .avi format. These movies can be viewed by any player, e.g., Microsoft Windows Media™ Player, Apple QuickTime™ Player, or the likes.

First, in a dark background with no target, we show how a region with coherently moving dots can be easily segregated against the rest of the image with randomly moving dot. Figure 1 shows a collection of randomly located white dots on a dark background. When one clicks on the link to the movie file of this Figure, a movie appears, and one can see that dots in certain rectangular region move coherently while the dots in the rest of the image move randomly. The coherent motion of dots can be easily detected, and the region containing these dots is readily noticed by the observer.

We now apply this algorithm to the images of a target that was previously used by our group in the study of polarization-difference imaging [7]-[9]. We use the same PS and PD images used in (Fig. 1 in [9]) in order to allow the fair comparison between mapping of polarization using the new algorithm described in this Letter with that of the colorimetric PDI algorithm we employed in [9]. The target was an aluminum disk with 3.8-cm diameter. The surface of this disk, except for two 1-cm^2 square patch areas, was sandblasted to make it Lambertian. The patches were raised a few mills and were abraded with the emory paper in orthogonal directions. This target was specifically constructed as such in order to have a surface that may give rise to scattered light with partial polarization from the patch areas (each with partial polarization parallel with the direction of abrasion), and scattered light with essentially no polarization from the sandblasted surface. Figure 2 shows the PS and PD images of this target when in our previous study it was immersed in a 40-L plexiglas tank of water to which 5mL of milk was added, and it was front-illuminated [9]. The PD image was scaled using a "symmetric" affine transformation [9] to utilize the full dynamic range of the 8-bit display. In other words, if for instance the range of PD values is between $-a$ and $+b$ (with $b > a$), the zero value of PD signal is mapped to pixel intensity 128, while $+b$ and $-b$ are mapped to 255 and 0, respectively. These images were originally obtained and used in our study of colorimetric PDI by Tyo, Pugh, and Engheta [9].

Figure 3 presents implementation of the current mapping scheme on the image of our target. The threshold value is taken to be $\delta = 32$ in the affine transformed PD image (which is effectively a threshold intensity value of $\delta = 2$ in the raw PD image with PD value range between ± 8.) The cell size is 10×10 pixels and the dot size is 2×2 pixels. Dot intensity is assigned using the "contrast scheme" in Fig. 3A and the "percentage scheme" with $M = 30\%$ in Fig. 3B. (Click on appropriate links to the movie file of each Figure to start the movie.) Observing these movies, one is able to distinguish between the regions with $PD > \delta$ and $PD < -\delta$ signals (which is equivalently $PD > \delta + 128$ and $PD < -\delta + 128$ in the affine transformed PD image), and the region with $-\delta < PD < \delta$ signal (or equivalently $-\delta + 128 < PD < \delta + 128$ in the affine transformed PD image), while the original information contents of the PS image is essentially intact. With regard to the two schemes for dot intensity, we notice that the "contrast scheme" may work better in images where the PS intensity distribution may be somewhat uniform over certain segment of the image (such as the disk face in our example). The "percentage scheme", on the other hand, may be better for situations in which unimportant segments of an image possess the PS intensity near zero (for example, the dark background in the images shown here). In this way, the dots in such regions have low intensity, and thus do not distract the observer from noticing the dots with higher intensity in regions of importance.

Figure 4 shows the corresponding results when the threshold value is chosen to be $\delta = 48$ in the affine transformed PD image (i.e., effectively threshold value of 3 in the raw PD image.) (Click on appropriate links to the movie file of each Figure to start the movies.) Here we notice that smaller regions of the image possess coherently moving dots, which represent patch areas where PD signals have higher absolute values. So the choice of threshold value is important is segregating regions of the image with specific values of PD signals.

Finally, Fig. 5, when clicked on appropriate links, illustrates a similar mapping of polarization into moving dots. The difference here, however, is that the dots form short lines with time-varying lengths as they move, providing additional cues for perception of polarization direction. This mapping, of course, results in higher number of pixels to be replaced with dots and lines, but it may provide stronger cues for polarization representation.

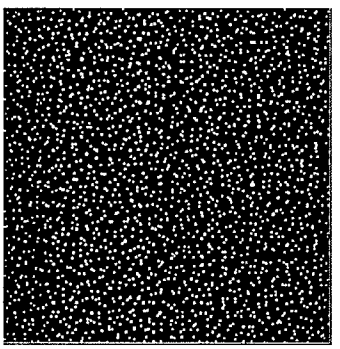

Fig. 1. (2.5 MB) A collection of randomly located dots on a dark background. Click here to start the movie. One can see that the region with coherently moving dots can be easily "popped out" against the background having randomly moving dots. Other information: image size: 316x316 pixels, cell size: 7x7, dot's pixel intensity: 255, frame rate: 20frames/sec, dot's speed in the region with coherently moving dots: 20 pixels/sec. (12.5 MB version)

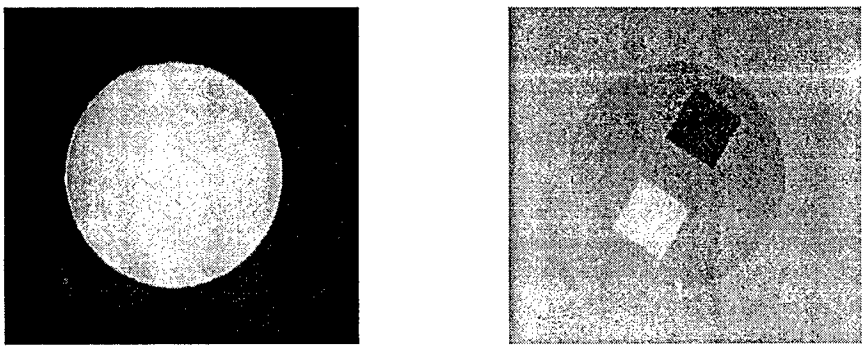

(A) (B)

Fig. 2. (A) PS image and (B) PD image of the target to which we apply the polarization-to-moving-dots mapping strategy introduced here. These target images were originally obtained and used in our previous study of polarization difference imaging (PDI) reported in (Fig. 1 in [9]). The light scattered from the two square patch areas are slightly partially polarized parallel to the direction of abrasion on these patches. The goal here is to map the polarization information contained in the PD image into the PS image by using coherently moving dots. Image size: 512 x 479 pixels.

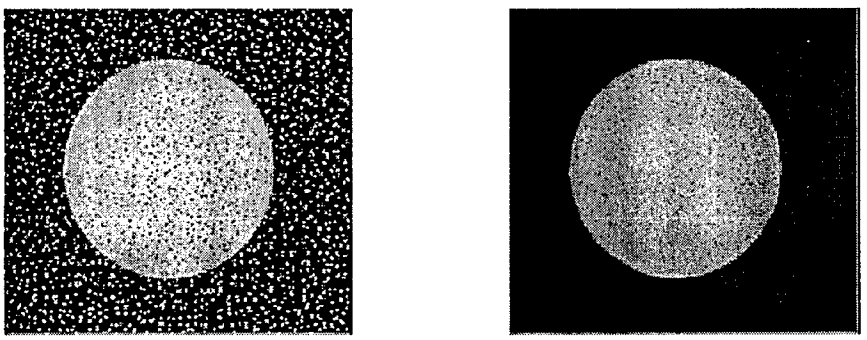

(A) (B)

Fig. 3. (Click on A and B to see the movies.) Implementation of the mapping technique described here on the image of target shown in Fig. 2. Polarization information from the affine transformed PD image (Fig. 2B) is mapped as moving dots onto the PS image (Fig. 2A). Here the threshold value is chosen to be $\delta = 32$ for the affine transformed PD values. In (A), the dot intensity is prescribed using the "contrast scheme", while in (B) it is chosen using the "percentage scheme" with $M = 30\%$. Viewing the moving dots, our visual system can distinguish among the regions with $PD > \delta$, $PD < -\delta$, and $-\delta < PD < \delta$ PD signals. Other information: Image size: 340 x 316 pixels, cell size: 7x7 pixels, frame rate: 20frames/sec. (A-14.9 MB version, B-10.3 MB version).

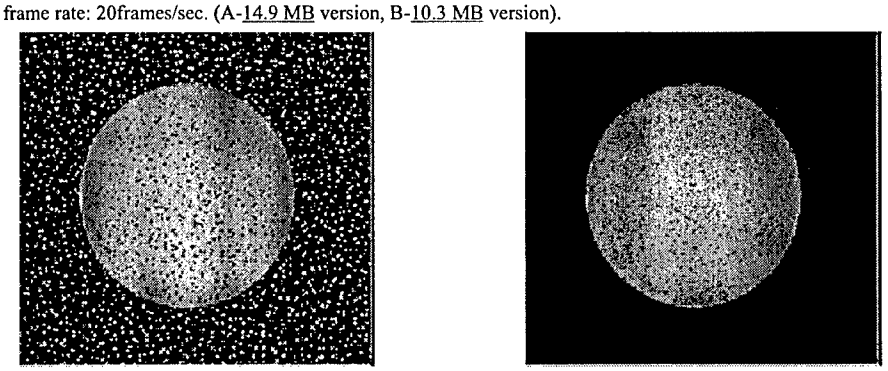

(A) (2.54 MB) (B) (1.51 MB)

Fig. 4. (Click on A and B to see the movies.) Similar to Fig. 3, except here the threshold value is chosen to be $\delta = 48$ for the affine transformed PD values. We note that the higher threshold value results in having smaller regions with coherently moving dots, thus highlighting the patch areas where the PD signal has higher absolute values. Other information: Image size: 340 x 316 pixels, cell size: 7x7 pixels, frame rate: 20 frames/sec. (A-12.7 MB version, B-10.4 MB version).

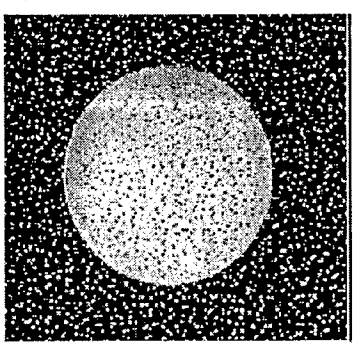

(A) (2.58 MB)

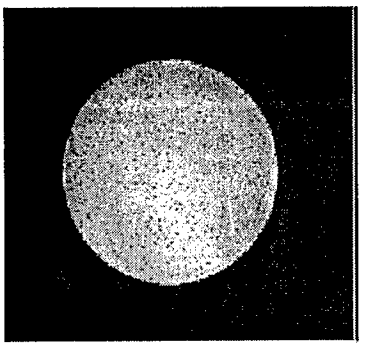

(B) (1.2 MB)

Fig. 5. (Click on A and B to see the movies.) Similar description as Fig. 3, except here the moving dots form short line with time-varying lengths, resulting in additional cues to visualize polarization information from the PD image given in Fig. 2B. Other information: Image size: 340 x 316 pixels, cell size: 7x7 pixels, frame rate: 20 frames/sec. (A-12.9 MB version, B-6.15 MB version).

The above examples clearly demonstrate the possibility of exploiting the sensitivity of human visual systems to coherent motion as one possible representational mechanism for visualization of polarization information in an image. This provides the observer with additional information about the scene with little or no distortion to the other non-polarization-related information, such as color and luminance, in the image. This mapping represents one possible "sensory substitution" for displaying polarization information to human observers while retaining the conventional image information.

Polarization is a manifestation of the vectorial nature of optical waves, and the display method employed here is designed to visualize the polarization information in an image. However, it is important to point out that the same display technique can be used to represent other vector quantities in images. Applied to optical polarization,, we have specifically used this technique to map the "polarization-difference (PD)" signal, since it was shown by Tyo [13] that the PD signal is indeed uncorrelated or "orthogonal", in the information theoretic sense, to the "polarization-sum (PS)" signal, i.e., to the conventional intensity signals. Thus, , PD and PS channels constitute together an optimum basis of the polarization components. Since we want to superimpose PD information on a PS (i.e., intensity) image, we use coherently moving dots to represent the PD information arising in optical polarization. In this context it bears emphasis that for a circularly-polarized light, the PD value is zero and thus no coherently moving dots are associated with it. Such neglect of circular polarization is justifiable, since in any optical imaging system in which the phase information between the two orthogonal polarization components is not available, a circularly-polarized light would be "equivalent" to an unpolarized light, thus resulting in a zero PD value. Were circular polarization information available, one could conceivably employ a set of dots that are coherently moving in a circular pattern to represent the local circular polarization. This requires further investigation.

5. Conclusions

We have introduced a visualization technique for mapping polarization information into an image without essentially altering the information contents of the original image. Dots have been superimposed on the image, and the motion of such dots has been implemented. Regions with $PD > \delta$ and $PD < -\delta$ signals are given dots that move coherently in two orthogonal directions representing main directions of partial polarization, and the regions with $-\delta < PD < \delta$ signals are assigned randomly moving dots. Since human vision can sense and perceive coherent motion, segments of the image with coherently moving dots can be readily detected and distinguished against the region with random motion. In this way, the segments with various ranges of PD signals "pop out". Such polarization representation can lead to visibility enhancement, better target detection and feature extraction.

Acknowledgements

This work was supported in part by the U.S. Air Force Office of Scientific Research (AFOSR), through grants F49620-01-1-0470 and F49620-02-1-0140. We thank Dr. J. S. Tyo currently of the University of New Mexico for his effort in gathering the target image originally shown in Fig. 1 of [9], now in Fig. 2 here, while he was in our research group at the University of Pennsylvania working on the colorimetric polarization-difference imaging reported in [9].

Manuscript Entitled:

"Bio-inspired display of polarization information using selected visual cues"

Konstantin M. Yemelyanov, Shih-Schön Lin, William Q. Luis, Edward N. Pugh, Jr., and Nader Engheta

Invited paper, appeared in the Polarization Science and Remote Sensing in the 2003 SPIE-The International Society for Optical Engineering, San Diego, California, August 3-8, 2003, pp. 71-84

Bio-inspired display of polarization information using selected visual cues

Konstantin M. Yemelyanov[a], Shih-Schön Lin[a], William Q. Luis[a], Edward N. Pugh, Jr. [b], and
Nader Engheta[c*]
[a]Dept. of Electrical and Systems Engineering, University of Pennsylvania, Philadelphia, PA USA 19104-6390
[b]F. M. Kirby Center for Molecular Ophthalmology and the Institute for Neurological Sciences, University of Pennsylvania, Philadelphia, PA USA 19104-6069
[c]Dept. of Electrical and Systems Engineering and the Institute for Neurological Sciences, University of Pennsylvania, Philadelphia, PA USA 19104-6390

ABSTRACT

For imaging systems the polarization of electromagnetic waves carries much potentially useful information about such features of the world as the surface shape, material contents, local curvature of objects, as well as about the relative locations of the source, object and imaging system. The imaging system of the human eye however, is "polarization-blind", and cannot utilize the polarization of light without the aid of an artificial, polarization-sensitive instrument. Therefore, polarization information captured by a man-made polarimetric imaging system must be displayed to a human observer in the form of visual cues that are naturally processed by the human visual system, while essentially preserving the other important non-polarization information (such as spectral and intensity information) in an image. In other words, some forms of sensory substitution are needed for representing polarization "signals" without affecting other visual information such as color and brightness. We are investigating several bio-inspired representational methodologies for mapping polarization information into visual cues readily perceived by the human visual system, and determining which mappings are most suitable for specific applications such as object detection, navigation, sensing, scene classifications, and surface deformation. The visual cues and strategies we are exploring are the use of coherently moving dots superimposed on image to represent various range of polarization signals, overlaying textures with spatial and/or temporal signatures to segregate regions of image with differing polarization, modulating luminance and/or color contrast of scenes in terms of certain aspects of polarization values, and fusing polarization images into intensity-only images. In this talk, we will present samples of our findings in this area.

Keywords: imaging systems, display, polarization vision, motion, texture, image fusion, temporal fusion, flicker

1. INTRODUCTION

1.1. Motivation and objectives

Polarization is an important feature of electromagnetic waves, and can be affected by various factors in the scene such as surface shapes, surface curvatures and materials, and position of objects with respect to the source(s) and the observer, and therefore it can provide useful information about the observed scene and objects – information which otherwise would be lost. Two characteristics of visible light, i.e., intensity and wavelength, can be detected and encoded by the human visual system and interpreted as perceptual qualities of brightness and color. Another important characteristics of light, namely, polarization, however, cannot be effectively exploited by unaided human eyes. The eyes of some animal species (e.g., honeybees, desert ants), however, can sense the polarization of light (see e.g., [1-0]). Such polarization vision in those species has often been shown to facilitate their navigation[0]. Moreover, it has been suggested that some species may utilize the polarization sensitivity to enhance the contrast of targets in scattering media.[6]

*engheta@ee.upenn.edu; phone: +1-215-898-9777; fax +1-215-573-2068;

Motivated and inspired by the visual systems of some of those animal species with polarization vision and particularly by the concept of polarization opponency (analogous to color opponency), we have been investigating novel imaging methodologies based on the concept of polarization "difference" signals. In our previous work, we have shown that an optical imaging system utilizing contrast enhancement through polarization differencing can increase the distance over which targets can be reliably detected[7-9], and have demonstrated that polarization-difference imaging (PDI) is indeed a useful tool for enhancing vision. However, an interesting issue arises in dealing with representing the polarization information in a polarimetric imaging system. Since the human eye cannot directly "see" polarization information, how can then such polarization information that is obtained by a polarimetric imaging system be presented to a human observer? After all, the outputs of any imaging system must be presented in such a manner that can be interpretable and recognizable by a human observer. What this implies is that such information should be mapped into visual cues that can be easily detectable by a human observer, hopefully without altering the other information carried by cues such as spectral and luminance information. In our group's earlier work, we have shown one such bio-inspired mapping for the cases where the original spectral information (i.e., the perceived colors) of the scenes were not of interest. In this mapping, polarization-difference information was pseudo-color-coded, based on the opponent-colors model of human vision[9], resulting in a contrast enhancement of polarization imagery of objects in scattering media such the objects became easily detectable by a human observer. However, that mapping ignored the spectral information in the original scene, information normally mapped into perceived color. In order to preserve the spectral and luminance information in an image, we need to map the polarization into visual cues other than the color and brightness.

There are a great variety of visual cues that are detectable by the human visual system. These include color, intensity, coherent motion, texture, flicker, to name a few. In this paper, we use several visual cues as well as certain image fusion techniques in order to present polarization information in a form perceptible to human vision.

1.2. Review of the Concept of Polarization-Difference Imaging

In this subsection, we give a brief overview of the Polarization Difference Imaging (PDI) technique. This algorithm was first introduced in Ref [7] and was further enhanced and developed in Refs. [8-9]. In this technique, the intensities of the two orthogonal polarization components of the light detected at each pixel (x,y) of the image are obtained, and then the sum and the difference of these two quantities, $I_{\parallel}(x,y)$ and $I_{\perp}(x,y)$, are evaluated. These sum and difference signals are given as follows:

$$_{PS}I(x,y) = I_{\parallel}(x,y) + I_{\perp}(x,y), \tag{3}$$

$$_{PD}I(x,y) = I_{\parallel}(x,y) - I_{\perp}(x,y), \tag{4}$$

where $\parallel$ and $\perp$ indicate parallel and perpendicular components of the polarizations (the "parallel" and "perpendicular" directions are with respect to a given orientation of the polarization analyzer), *PD* stands for the "polarization-difference" signal, and *PS* for the "polarization-sum" signal. Obviously, for an ideal linear polarization analyzer the PS image will be equivalent to a conventional intensity image.

In this paper, we apply our visualization techniques to several different man-made, as well as, natural targets. The first man-made target, already used in our previous study[9, 0] is an aluminum disk of 3.8-cm diameter with its surface sandblasted, except for two 1-cm^2 square regions or patches. The sandblasting caused the surface to be Lambertian. The patches were raised a few mills and were abraded with emory paper in orthogonal directions. PS and PD images of this target, when front illuminated, are presented in Figs. 1A and 1B, respectively, where the PD image intensities were scaled using a "symmetric" affine transformation[9] to utilize the full dynamic range of the 8-bit display.

For instance, if the range of PD values is between $-a$ and $+b$ (with $b > a > 0$), the zero value of PD signal is mapped to pixel intensity 128, while $+b$ and $-b$ are mapped to 255 and 0, respectively. (These Figures 1A and 1B were originally obtained and used in our study of colorimetric PDI.[9]) The second specially designed target was another aluminum disk with 5.1-cm diameter created in a similar way as in the first one; however, this disk has seven patches, six of which are abraded with the emory paper in various specific directions. The abrasions (i.e., scratches) on these six patches form three pairs. Each pair has two orthogonal orientations for the scratches. More specifically, the orientations of the scratches on these six patches are 0°, 30°, 60°, 90°, 120°, and 150° (with respect to the vertical axis.), where the patch pairs with orthogonal orientations, i.e., the pairs with $(0^\circ, 90^\circ)$, $(30^\circ, 120^\circ)$, and $(60^\circ, 150^\circ)$ are located diametrically on the disk. The surface of the seventh patch, located at the center of the disk, is sandblasted and thus is Lambertian. The affine transformed PS and PD images of this target, in the back-illuminated condition, are presented in Figs. 1C and 1D, respectively. These targets were specifically constructed in order to make the light scattered from the patch areas partially polarized (with the major axis of the partial polarization parallel to the direction of abrasion), while the light scattered from the sandblasted areas (including the 7^{th} patch) is largely unpolarized. (As a result, in the PD image of this 7-patch target, Fig. 1D, the centered 7^{th} patch is indistinguishable from the sandblasted surface of the disk, and thus only six abraded patches can be seen.) For detailed description of the experimental setup, see Ref [8]. In addition to these specially manufactured targets, we also use here some natural targets which will be discussed later.

2. DISPLAY OF POLARIZATION INFORMATION USING COHERENTLY MOVING DOTS

The first visualization scheme we present here is the representation of polarization information by a set of coherently moving dots superimposed on the image. We exploit the sensitivity of the human eye to coherent motion in order to display polarization information in an image. It is known that human visual system is capable of various forms of motion perception (e.g., Refs [11-14]). One of the motivations behind using coherently moving dots in such mapping is to preserve the original non-moving features of the image, such as color and luminance, while "displaying" the polarization information. The details of this technique are described in our recent paper[10]. Here we give a brief review of this technique.

In this method, many dots are randomly superimposed on the entire PS image, and then these dots are made to move coherently in orthogonal directions according to the value of the PD signal at the location of the dots. The directions of dots motion are chosen in the following way: dots in the region with associated PD greater than a certain threshold δ are made to move in the direction parallel with $\parallel$ polarization component; dots in the regions with associated PD signal less than $-\delta$ are made to move in the direction along the $\perp$ polarization component; dots outside the above-mentioned regions, i.e., in the regions with PD value between $-\delta$ and $+\delta$ are made to move randomly. The size of the dot is properly chosen to make the dots small enough so that the original image would be practically undistorted by the presence of these dots and large enough so that the dots can be detected by an observer. The brightness/intensity of the dots must be chosen such that they are easily detectable against the original image. Here we use two different methods:

1) The intensity of each pixel of a dot is selected to be in "contrast" with the PS signals of the pixels the dot is replacing. In this scheme, which we call the "contrast scheme", the dot intensity is "complemented" against the background intensity in each cell
2) In the second method, the intensity of each pixel in a dot is chosen to be M percent less than the PS signal in the image pixel which it is replacing. In other words,

$I_{dot}(x,y) = (1 - M/100)_{PS} I(x,y)$. We call this approach "percentage scheme". Detailed analysis of this algorithm can be found in Ref [10].

The representation of polarization information using this algorithm was implemented in the MATLAB® environment. To illustrate the visualization concept of coherently moving dots, we use PS and PD images of the 2-patch target presented in Figs. 1A and 1B (which was originally given in Fig. 1 of Ref [9]) and PS and PD images of the 7-patch target shown in Figs. 1C and 1D. We have developed movie files for these images with coherently moving dots superimposed (to be shown in the presentation). Here in this paper, we present only static images with superimposed dots (i.e., a single frame of the movie) corresponding to the contrast scheme (Figs. 2A and 2C) and percentage scheme (Figs. 2B and 2D). In Figs. 3A and 3B, we also show the same images but with "arrows" added to give indication of the direction of coherently moving dots. (The reader interested in receiving the movie files can send e-mail to: engheta@ee.upenn.edu. The movie files of moving dots on the 2-patch target can also be found in Ref [10], which is published in the online journal *Optics Express* with multimedia files included.) For the percentage scheme, we have chosen parameter $M = 30\%$. When these movies are viewed, the human observer can easily and pre-attentively segregate the region containing coherently moving dots from the regions with randomly moving dots. The significance of this result is that polarization-difference information has been superimposed on the image in a manner that allows visualization of target regions having similar polarization signatures, without the loss of the luminance information.

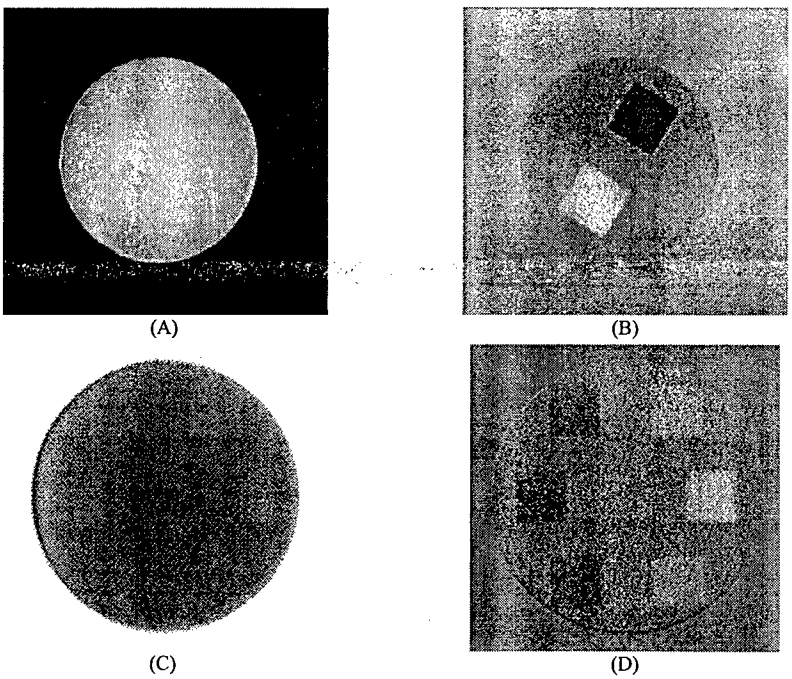

Figure 1: PS images of the 2-patch target front illuminated (A) and the 7-patch target back illuminated (C). Panels (B) and (D) are the PD images of the same targets, respectively, to which we apply the polarization-to-moving-dots mapping strategy. Image (B) has been "symmetrically" affine transformed[9], while image (D) is simply affine transformed. Images (A), (B) were originally obtained and used in our previous study of polarization difference imaging (PDI) reported in Ref [9] (Fig. 1 in Ref [9]).

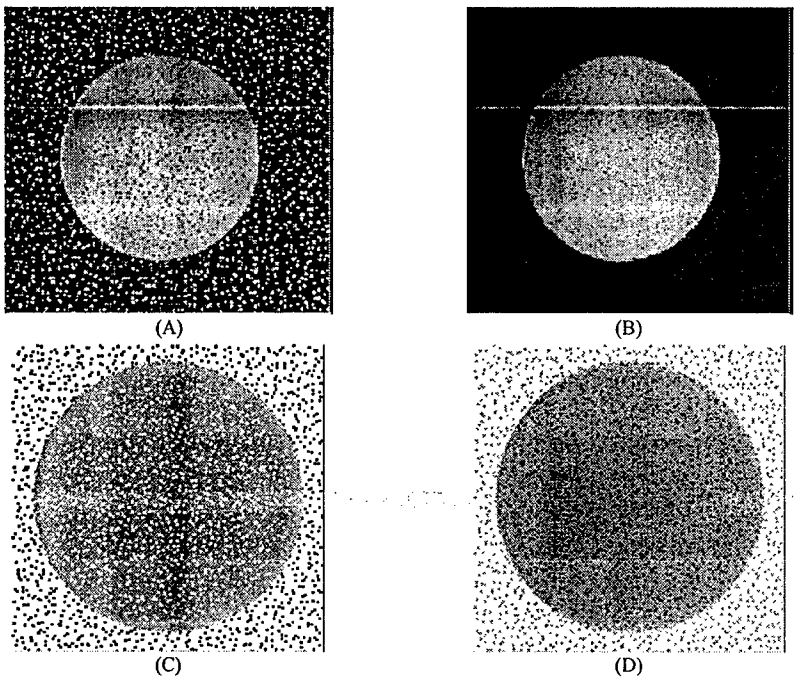

Figure 2: Panels (A) and (C): Superimposing dots on the PS images of the 2-patch and 7-patch targets using the contrast scheme. Panels (B) and (D): corresponding images with the percentage scheme. Dot size is 1x1 pixel in Panels (A) and (B), and 2x2 pixels in Panels (C) and (D). Images in Panels (A) and (B) were originally presented in Ref [10]

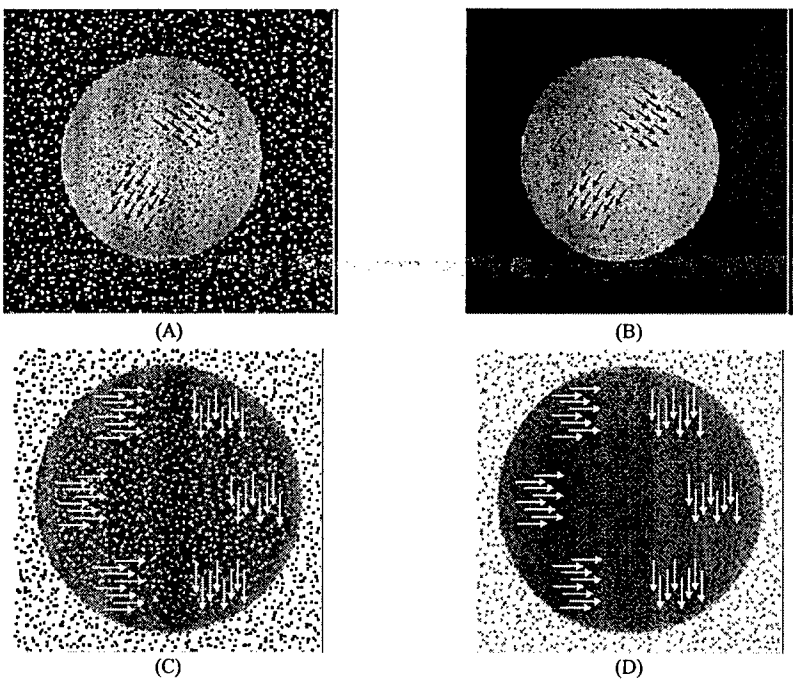

Figure 3: The same as in Fig. 2, except that some "arrows" have been added to give indication of the direction of motion of the coherently moving dots. We have made movie files showing the coherent motion of these dots. Movies will be shown in the presentation. Interest readers can contact the corresponding author to get copies of the movie files.

3. REPRESENTATION OF POLARIZATION INFORMATION USING TEMPORAL FUSION TECHNIQUE

A variety of image fusion techniques have been used by many researchers to combine two or more images from different modalities (such as images from the visible band and the IR band) into a single image that ideally contains all the important information of original images.[15] In principle, those fusion techniques can also be used to fuse polarization images with non-polarization images (e.g., intensity-only images). Our colorimetric polarization-difference imaging technique, developed earlier, is indeed a fusion technique in representing polarization information with a pseudo-color mapping.[9] Here, we introduce the concept of "temporal fusion", where the fusing of two different images is achieved in time domain by taking advantage of the biological sensitivity of human visual system to the "fading in and fading out" between two image modalities. As applied to polarization, the image modalities of interest here are an intensity-only image (i.e., PS image) and the polarization-difference (PD) information of the same scene (e.g., this latter image could be a grayscale representation of the PD data, or a pseudo-color representation). A dynamic image (i.e., a movie) consisting of a gradual periodic transition from a PS image to PD image is then created, with the frequency of transition chosen such that the human eye can easily and most sensitively detect this fading in and fading out. In this way, the observer can clearly see and distinguish the PS information and PD information in the same dynamic image. In other words, we take advantage of the dimension of "time" in order to fuse information from two different modalities, i.e., from polarization and non-polarization information. If the PD image is formed as a pseudo-colored image, as will be discussed below, then we choose the frequency of fading between the PS and PD image in accordance with sensitivity of color channels in the human eye.

In our temporal fusion technique, one image (e.g., PS image) "fades" into the other (e.g., PD image) via a sequence of intermediate image frames, each of which combines information from PS and PD images with different weights. The period of one complete cycle is selected in accordance with the sensitivity of the human visual system to flicker (see e.g., Ref [18]). Our algorithm can be described in the following way:

The first and the last frames, i.e., frame numbers $n=1$ and $n=N$, of each complete cycle of the movie are chosen as PS images. The "intermediate frames" are computed pixel-by-pixel from PS and PD images using the following expression:

$$I(x,y,n)=\alpha(n)\,T_{PD}\left[{}_{PD}I(x,y)\right]+[1-\alpha(n)]T_{PS}\left[{}_{PS}I(x,y)\right], \tag{5}$$

where $\alpha(n)$ is a temporal fusion weighting function of the frame number $1\le n\le N$. The value of $\alpha(n)$ varies between 0 and 1 with $\alpha(1)=\alpha(N)=0$, (x,y) represents the pixel location in the image, and the operators $T_{PD}[\cdot]$ and $T_{PS}[\cdot]$ represent transformation (or processing) of the "raw" PD and PS data into some forms for PD and PS image representation. For instance, these operations may include symmetric affine transformation, conventional affine transformation, pseudo-colorimetric (R,G,B) or (H,S,V) mapping, to name a few. According to Eq. (3), every frame in the cycle, between $n=1$ and $n=N$, is

created with certain percentages of PD and PS information. There can be various choices for the function $\alpha(n)$, each producing different visual effects. Here, we consider two cases for $\alpha(n)$, viz., the "Gaussian" and the "sinusoidal" modulation. For the Gaussian modulation, the function $\alpha(n)$ is set to be $\alpha(n) \cong \exp\left(-(n-n_o)^2/2\sigma^2\right)$ for $1 < n < N$ where n is current frame number, n_o is the frame number at which only PD image is shown (e.g., $n_o = N/2$), σ^2 is the variance and $\alpha(1) = \alpha(N) = 0$. For sinusoidal modulation, the function $\alpha(n)$ is considered as $\alpha(n) = \sin\left[\pi(n-1)/(N-1)\right]$. The frame sequences generated using either of these two algorithms have 30 frames in each cycle, and are compiled into movie files with playback rate of 30 frame/sec. We show the snapshots of these movies in the following subsections. (Interested reader may contact the corresponding author to receive these movie files.)

3.1. Temporal fusion of grayscale PS and PD images

In this subsection, we show the fusion of the PS and PD images of the 7-patch target as 8-bit grayscale images. The snapshots of the movies which illustrate temporal fusion using Gaussian and sinusoidal modulations are presented in Fig. 4 and Fig. 5, respectively. As can be seen from these snapshots (and even more clearly from the movie files), we can observe both the polarization-information (from the PD image) and the intensity-only information (from the PS image) in the same set of dynamic images.

3.2. Temporal fusion of grayscale PS and pseudo-colorimetric PD images

In our previous work[9], we developed a technique for mapping polarization information into pseudo-colors using the opponent hues consistent with the opponent-colors model of human vision. It is known that most colors perceptible by the human eye can be described in a 3-dimensional color space using three independent parameters, such as "brightness", "saturation", and "hue" in the HSV (Hue-Saturation-Value) color space. For the pseudo-colorimetric representation of the PD image we have considered several mapping schemes. For our temporal fusion technique between the grayscale PS image and the pseudo-colorimetric PD image, we use the following mapping for the PD image, as done in Ref [9]: The affine transformed value of PS image intensity at any pixel is mapped into the "value" (V) of the HSV map. The sign of PD signal at each pixel is mapped into a pair of opponent hues, i.e., positive PD is mapped into one hue, and negative PD is mapped into the corresponding opponent hue. The magnitude of the PD signal at each pixel, after it is affine transformed, is mapped into "saturation" (S).

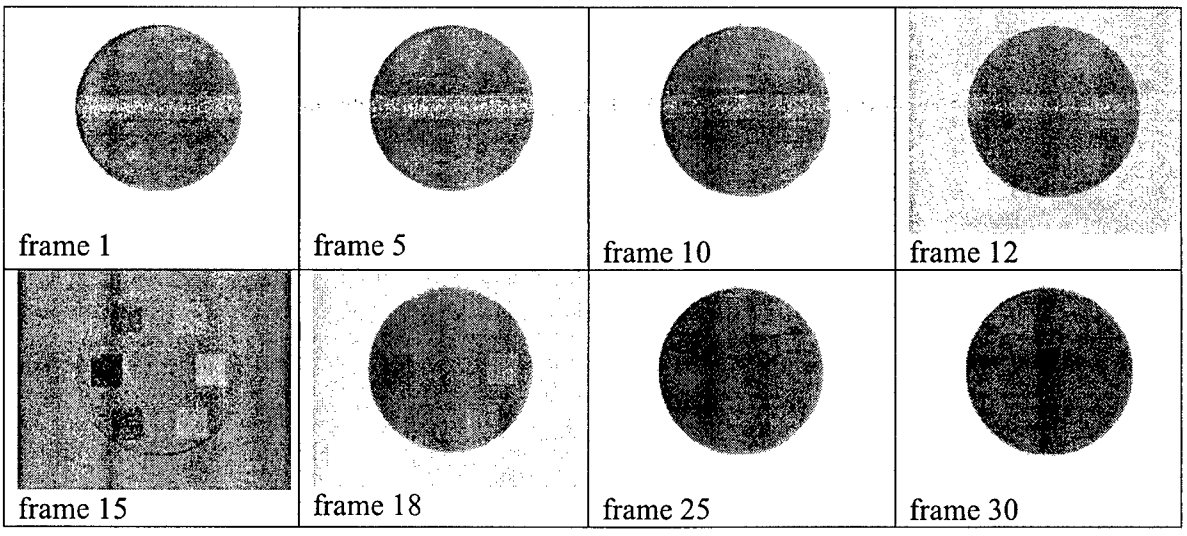

Figure 4: Snapshots of temporal fusion of the grayscale PS and PD images of the back-illuminated 7-patch target using the "Gaussian" modulation with $\sigma = 2$. Every complete cycle of the movie file includes 30 frames, which can be viewed with the rate of 30 frame/sec. In this figure, we only present frames No 1, 5, 10, 12, 15, 18, 25, and 30, from the left to right and the top to bottom.

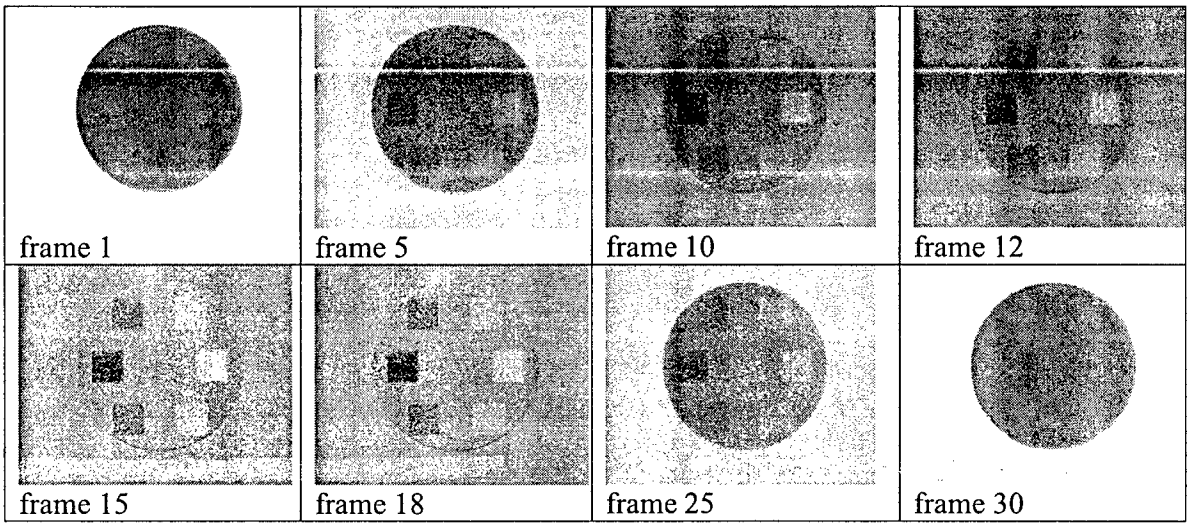

Figure 5: Similar to Fig. 4, except the "sinusoidal" modulation is used in the temporal fusion.

In Figs. 6 and 7 we show the temporal fusion of the pseudo-colorimetric representation of the PD image with the grayscale PS image of the 7-patch target. The equations used here are similar to Eq. (3) as in subsection 3.1 to fuse pseudo-colorimetric PD and grayscale PS images. Snapshots of the resulting movies are given in Fig. 6 (with Gaussian variation for $\alpha(n)$) and Fig. 7 (with the sinusoidal variation). Here the observer can get the information from the grayscale intensity-only image along with the polarization information from the pseudo-color PD image in the same set of dynamic displays.

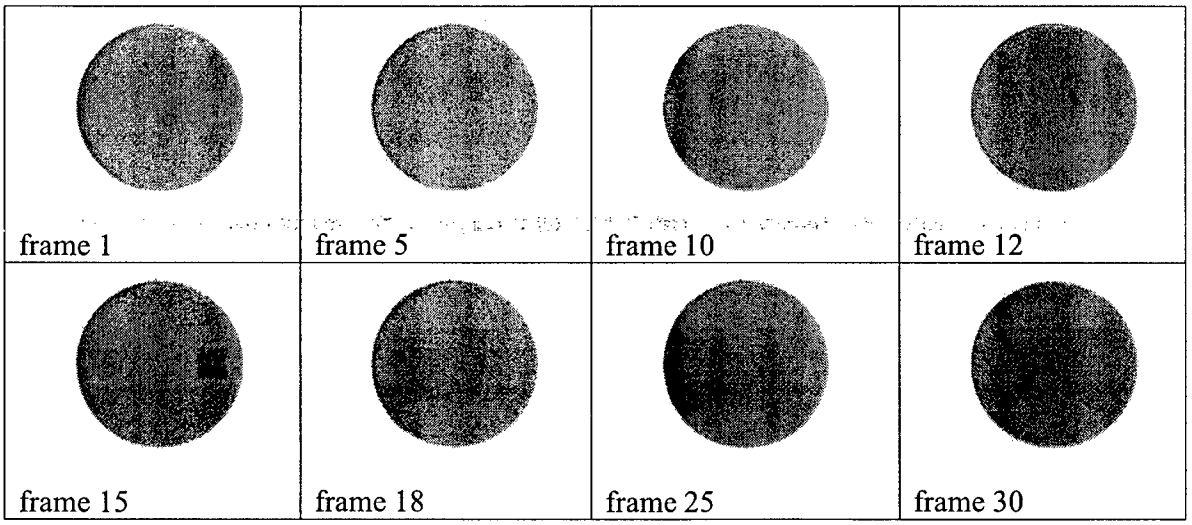

Figure 6: Snapshots of temporal fusion of the grayscale PS with the pseudo-colorimetric PD images of the back-illuminated 7-patch target using the "Gaussian" variation. As in Figs. 4 and 5, every complete cycle of the movie file includes 30 frames, which can be viewed with the rate of 30 frame/sec. (The movie files can be obtained from the corresponding author)

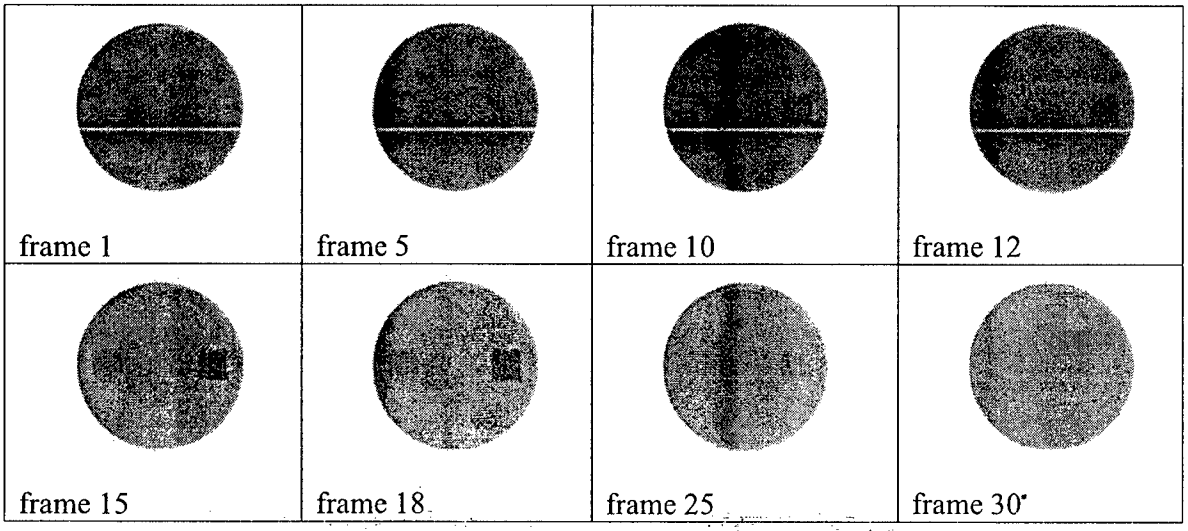

Figure 7: Same as Fig. 6, except the "sinusoidal" variation is used.

3.3. Temporal fusion of a color image with its pseudo-color polarimetric image

In this subsection we consider the temporal fusion of a color image of a natural scene with its pseudo-color polarimetric image. It is well known that for the light coming from every point in a scene, three parameters related to the polarization information detectable by a 2-D imaging sensor, in which the phase information between the two orthogonal polarization components is not available, can be described as the energy intensity (or brightness) I, degree of linear polarization p, and orientation angle φ_o of the polarization ellipse of the polarized portion of the light from that point. The value of p varies between 0 and 1 where $p=0$ presents unpolarized light and $p=1$ corresponds to a completely polarized signal. To find these parameters at every pixel, one needs to collect a minimum of three images of the same scene; each image taken with a different orientation of the polarization analyzer in front of the camera, e.g., with 0°, 45°, and 90° orientation of the polarization analyzer. These three independent "measurements" can provide one with three equations from which the parameters I, p, and φ_o can be evaluated for each pixel. To display these three parameters of a scene in a single image, one can use a variety of mapping strategies. We have investigated several different mapping possibilities. One such mapping is the Bernard and Wehner mapping.[16] Bernard and Wehner suggested the mathematical similarities between a theoretical 3-parameter polarization vision system and the widely used 3-parameter color vision system. They also pointed out that some species may indeed have 3-parameter polarization vision system.[16] The main analogy they draw is the parallelism of the intensity I with the value V, the degree of polarization p with the saturation S, and the angle φ_o with the hue H (in the HSV color space). This parallelism has been used in the past in certain polarization-sensitive imaging systems.[17] Here, as an input to our temporal fusion algorithm, we utilize this pseudo-color mapping based on this parallelism to produce a pseudo-color polarimetric image. For display purpose, we incorporate the image enhancement technique "histogram equalization" on the original value V (in the HSV space) of the "true-color" image, and use this equalized V as the V channel, and the contrast enhanced p data for the saturation channel S. For the angle of polarization φ_o, we map $2\varphi_o$ to the hue angle. As an example, we use a picture of flowers and leaves which we have taken outdoors by taking three images with three orientations of the polarization analyzers as mentioned above. A processed "true-color" image of this scene is shown in Fig. 8A after histogram equalization has been applied; the distribution of degree of linear polarization $p(x,y)$, after contrast enhancement, is shown in Fig. 8B; and the distribution of the angle of polarization ellipse, $\varphi_o(x,y)$, is depicted in Fig. 8C with the angle-to-hue color wheel shown at its right. Figure 8D illustrates the mapping of (I,p,φ_o) into (V,S,H). We notice that the images with polarization information (Figs. 8B, 8C, and 8D) reveal certain additional information not available in the regular color image in Fig. 8A. For instance, we note that in the distribution of $p(x,y)$

shown in Fig. 8B the leaves in general exhibit higher degree of linear polarization than the flowers (the flowers look darker than the leaves in $p(x,y)$). Moreover, we observe that certain parts of the scene with low intensity shown in the conventional image in Fig. 8A, such as the little leaf in the foreground slightly below the three large leaves, may appear more noticeable in the images of $p(x,y)$ and $\varphi_o(x,y)$ shown in Figs. 8B and 8C, since the degree of polarization at a pixel may in general vary independently of intensity of that pixel.

We have applied our temporal fusion technique to fuse image shown in Fig. 8A with that in Fig. 8D and to produce movie files for such fusion. Figure 9 illustrates the snapshots of this temporal fusion using the sinusoidal function for $\alpha(n)$.

4. VISUALIZATION OF POLARIZATION INFORMATION BY TEMPORAL FLICKER

In this method of presenting polarization information, we exploit the sensitivity of human eye to intensity flicker in an image[17]. After forming the PS and PD images of a scene, we intend to bring the observer's attention to the regions of the image having PD signals with opposite signs. We find these regions by searching for pixels whose raw PD values are greater than $+\delta$ and those that are less than $-\delta$, where δ is a given threshold. These regions we name (+) and (–) regions, respectively. The rest of the image, in which $-\delta < PD < \delta$, is the "PD neutral" region. Then we temporally modulate the intensity of the pixels in PS image belonging to the (+) and (–) regions from frame to frame, forming a movie file. Such temporal modulation can be expressed as:

$$I^{(+)}(x,y,n) = T_{PS}\left[{}_{PS}I(x,y)\right]\left(1+M_{+}\sin(\Omega t_n)\right) \tag{4}$$

$$I^{(-)}(x,y,n) = T_{PS}\left[{}_{PS}I(x,y)\right]\left(1+M_{-}\sin(\Omega t_n+\pi)\right) \tag{5}$$

Here, x and y are coordinates of the pixels within the image, n is the frame number ranging from 1 to N where N is the number of frames in a complete cycle, t_n corresponds to the time of frame n, M_{+} and M_{-} are the modulation coefficients for the (+) and (–) regions, respectively, $\Omega = 2\pi F$ where F is the frequency of flicker in *Hz*. There is 180° phase difference between the flickers in the (+) and (–) regions.

In the following example, this visualization technique is illustrated with $M_{+} = M_{-} = 25\%$ and $N = 30$. The flicker frequency is selected to be $F = 1$, 10, and 15 Hz. The movies will be demonstrated in the presentation. The snapshots of the flicker for $F = 1$ Hz are shown here in Fig. 10.

(A)

(B)

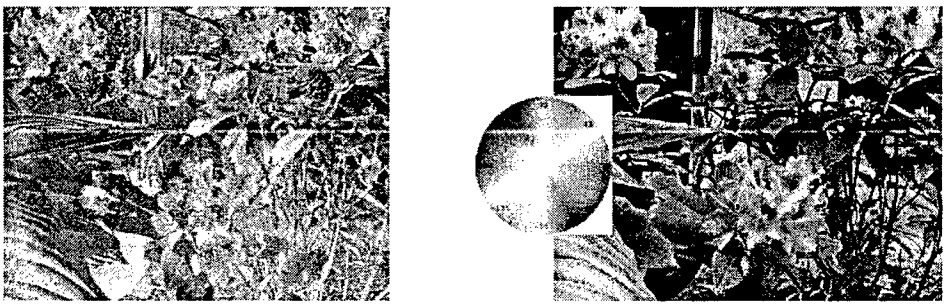

Figure 8: (A) A processed "true color" image of a scene after the histogram equalization of its V channel; (B) Degree of linear polarization $p(x,y)$ image after it is contrast enhanced; (C) Angle of polarization ellipse, $\varphi_o(x,y)$, shown in pseudo-color scheme. The angle-to-hue color wheel is shown to the right; and (D) Pseudo-color mapping of three parameter (I,p,φ_o) into (V,S,H).

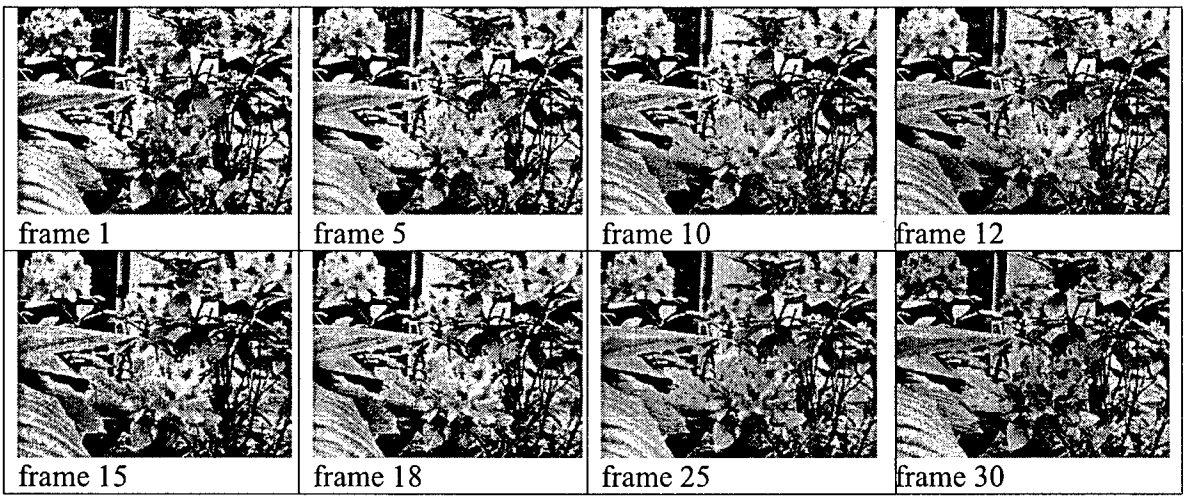

Figure 9: Snapshots of temporal fusion of Fig. 8A (color image of the scene) with Fig. 8D (pseudo-color polarimetric image of the same scene) using the sinusoidal function $\alpha(n)$. Every complete cycle of the movie file includes 30 frames, played back at the rate of 30 frame/sec.

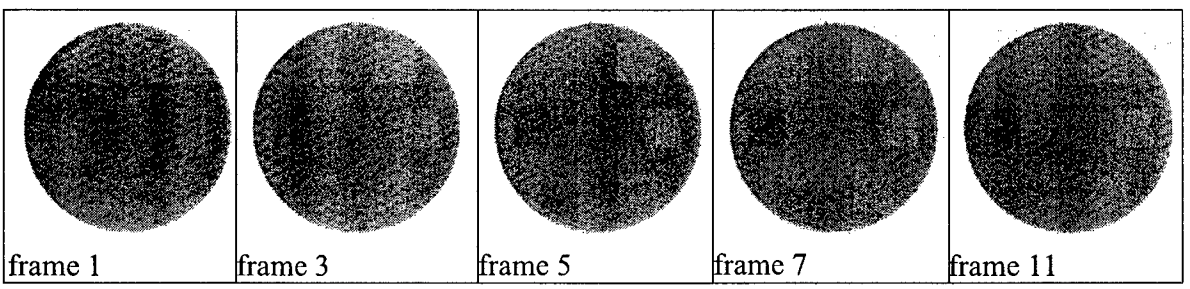

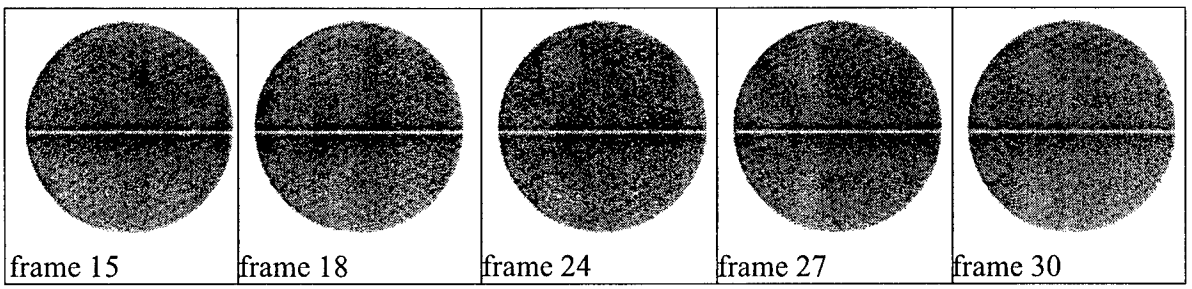

Figure 10: Snapshots of flickering technique as a method to visualize regions with "opponent PD signals". Here $M_+ = M_- = 25\%$, $N = 30$, and frames 1, 3, 5, 7, 11, 15, 18, 24, 27, and 30. (The movie files can be obtained from the corresponding author.)

5. USE OF STATIC AND DYNAMIC TEXTURES TO DISPLAY POLARIZATION INFORMATION

In this subsection, we display polarization information using another visual cue, namely, texture. It is known that certain forms of textures can be segregated by the human visual perception (see e.g., Ref [19-21]). We have been exploring how some textures can be used to visualize the polarization information.

In order to utilize textures for this purpose, we first subdivide the entire image into small cells of $m \times m$ pixels (e.g., $m = 10$), and we evaluate the average PS and PD values in each cell. We then identify the (+) and (−) regions of the image which correspond to pixels with $\langle PD \rangle_{cell} > +\delta$ and $\langle PD \rangle_{cell} < -\delta$, as was described in Section 4. Here $\langle PD \rangle_{cell}$ denotes the average value of PD in each cell. We can then superimpose different texture patterns on the original image with each single element of the texture pattern corresponding to a single cell. We use different texture elements/patterns for the PD (+) and PD (−) regions of the image. For instance, texture patterns with circles "∘" and asterisks "*" can be used for the (+) and (−) regions, respectively. Cells with $-\delta < \langle PD \rangle_{cell} < \delta$ have no texture patterns. Fig. 11A shows a PS image of a leaf we took under indoor fluorescent lighting (this image is histogram equalized). Image in Fig. 11B presents the superimposed texture patterns for threshold $\delta = 0.03$ (with respect to the raw PD data between −1 and +1. One can recognize these two texture patterns, which indicates that the surface of the leaf has positive PD values. (Here the || direction is horizontal.)

Another form of texture pattern can be generated by having spatial and/or temporal modulation of the intensity of the processed PS image in the regions with the PD (+) and PD (−) values. Such modulation can be written as

$$I^{(+)}(x,y,n) = T_{PS}\left[{}_{PS}I(x,y)\right]\left\{1 + M_+ \cos\left[\Omega t_n + \kappa x \sin(\varphi) - \kappa y \cos(\varphi)\right]\right\} \tag{6}$$

$$I^{(-)}(x,y,n) = T_{PS}\left[{}_{PS}I(x,y)\right]\left\{1 + M_- \cos\left[\Omega t_n + \kappa x \sin\left(\varphi + \frac{\pi}{2}\right) - \kappa y \cos\left(\varphi + \frac{\pi}{2}\right)\right]\right\} \tag{7}$$

where M_+, M_-, Ω were defined in Section 4, $\kappa = 2\pi/\Lambda$ with Λ being the spatial wavelength of spatial modulation, φ is the direction of || polarization component, and the angle $\frac{\pi}{2}$ is added to φ for modulation in the (−) region to indicate the direction of ⊥ polarization component. Spatial as well as temporal modulations of intensity of the PS image provide texture patterns that can be easily detected by the human observer, resulting in segregation of the PD (+) and PD (−) regions. Figure 12 illustrates the *static* case of such textures using the spatial modulations for the 2-patch target. (This *static* texture

corresponds to $\Omega = 0$ in Eqs. (6) and (7).) For the spatial *and* temporal modulations we have made movie files, which can be obtained from the corresponding author. One can easily see the presence of the two regions with PD (+) and PD (−) values.

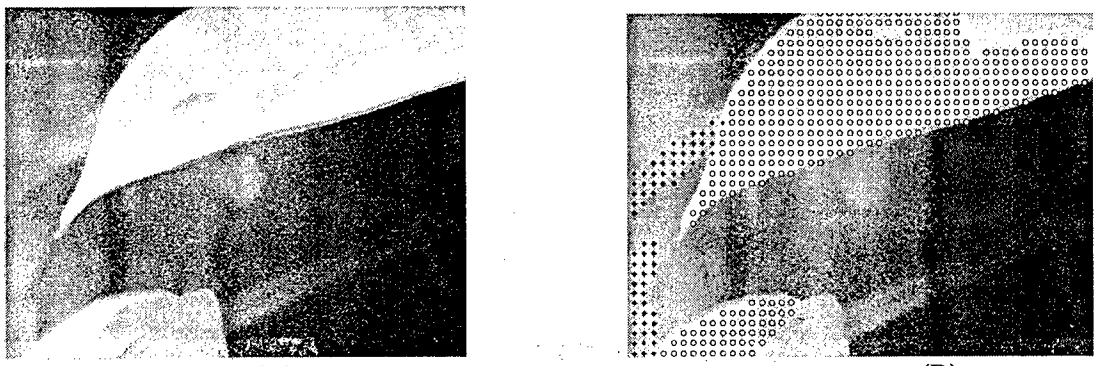

Figure 11: Using textures to display polarization information. Here the texture patterns with circles "o" and asterisks "*" are superimposed in the PD (+) and PD (−) regions. (A) Processed PS image (with histogram equalization), (B) superimposed textures with $\delta = 0.03$.

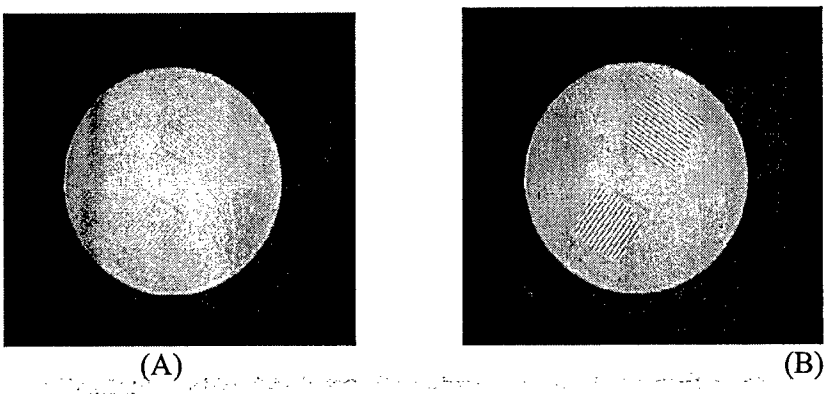

Figure 12: Static texture using spatial modulation of the intensity of the processed PS image of the 2-patch target to represent regions with PD (+) and PD (−). (This PS image without modulation was originally taken and used in our work in Ref [9]) Panel (A): $M_+ = M_- = 0.05$, $\kappa = 1$; Panel (B): $M_+ = M_- = 0.25$, $\kappa = 1$.

CONCLUSIONS

In this paper we have discussed several different visualization techniques for representing polarization information using visual cues detectable and recognizable by the polarization-blind human eyes. These include using coherently moving dots, temporal fusion and flickering, and texture patterns and static and dynamic textures by spatial and/or temporal modulations. These display techniques for visualizing polarization information in an image provide the segments of image with various ranges of PD signals to be segregated and "pop out" and thus allow the polarization-blind human observers to easily "see" polarization information. Such polarization representation can provide visibility enhancement, better target detection and feature extraction, without loss of the information that is present in the image that would be

collected by a system not sensitive to polarization.

ACKNOWLEDGEMENTS

This work was supported by the U.S. Air Force Office of Scientific Research (AFOSR), through grants F49620-01-1-0470, F49620-02-1-0140, and the DURIP grant F49620-02-1-0241.

REFERENCES

1. K. von Frisch, "Die polarisation des himmelslichtes als orientierender faktor bei den tanzen der bienen," *Experientia*, **5**, pp. 142-148, 1949.
2. T. Labhart, "Polarization opponent interneurons in the insect visual system," *Nature*, **331**, pp. 435-437, 1988
3. R. Wehner, "Neurobiology of polarization vision," *Trends in Neurosciences*, **12**, pp. 353-359, 1989
4. T. H. Waterman, "Polarization sensitivity" in *The Handbook of Sensory Physiology vol. VII/6B Vision in Invertebrates*, edited by H. Autrum, Springer-Verlag, New York, 1981.
5. R. Wehner, "Polarized-light navigation by insects," *Scientific American*, **235**, pp. 106-114, 1976.
6. J. N. Lythgoe and C. C. Hemmings, "Polarized Light and Underwater Vision," *Nature*, **213**, pp. 893-894, 1967.
7. M. P. Rowe, E. N. Pugh, Jr., J. S. Tyo, N. Engheta, "Polarization-difference imaging: a biologically inspired technique for observation through scattering media", *Optics Letters*, **20**, No. 6, pp. 608-610, 1995.
8. J. S. Tyo, M. P. Rowe, E. N. Pugh, Jr., N. Engheta, "Target detection in optically scattered media by polarization-difference imaging", *Applied Optics*, **35**, No 11, pp. 1855-1870, 1996.
9. J. S. Tyo, E. N. Pugh, Jr., N. Engheta, "Colorimetric representation for use with polarization-difference imaging of objects in scattering media", *J. Optical Society of America A*, **15**, No 2, pp. 367-374, 1998.
10. K. M. Yemelyanov, M. A. Lo, E. N. Pugh Jr., N. Engheta, "Display of polarization information by coherently moving dots," *Optics Express*, **11**, No 13, pp. 1577-1584, June 30, 2003. http://www.opticsexpress.org/abstract.cfm?URI=OPEX-11-13-1577
11. D. Jokisch, "Biological motion as a cue for the perception of size," *Journal of Vision*, **3**, pp. 252-264, 2003.
12. W. Curran, O. J. Braddick, "Speed and direction of locally-paired dot patterns," *Vision Research*, **40**, pp. 2115-2124, 2000.
13. W. A. van de Grind, A. J. van Doorn, J. J. Koenderink, "Detection of coherent motion in peripherally viewed random-dot patterns," *J. Optical Society of America A*, **73**, pp. 1674-1683, 1983.
14. E. D. Grossman, R. Blake, "Perception of coherent motion, biological motion and form-from-motion under dim-light conditions", *Vision Research*, **39**, No 22, 3721-3727, 1999.
15. A. Toet, J. Walraven, "New false color mapping for image fusion", *Optical Engineering*, **35**, No 3, pp. 650-658, 1996.
16. G. Bernard and R. Wehner, "Functional Similarities between polarization vision and color vision," *Vision Research*, Vol. 17, pp. 1019-1028, 1977.
17. L. B. Wolff and T. A. Mancini, "Liquid crystal polarization camera," in *Proceedings of the IEEE Workshop on Applications of Computer Vision* (IEEE, New York, 1992), pp. 120-127, 1992.
18. D. H. Kelly, "Flicker" in *The Handbook of Sensory Physiology, Vol. VII/4: Visual Psychophysics*, Springer-Verlag, New-York, 1972, pp. 273-302.
19. H. C. Nothdurft, "Texton segregation by associated differences in global and local luminance distribution," *Proc. Royal Society of London B*, **239**, pp. 295-320, 1990.
20. Q. Zaidi, A. Li, "Limitations on shape information provided by texture cues," *Vision Research*, **42**, pp. 815-835, 2002.
21. A. Blake, H. H. Bulthoff, D. Sheinberg, "Shape from texture: ideal observers and human psychophysics," *Vision Research*, **33**, pp. 1723-1737, 1993.

Manuscript Entitled:

"Polarization- and Specular-Reflection-Based, Non-contact Latent Fingerprint Imaging and Lifting"

Shih-Schön Lin, Konstantin M. Yemelyanov, Edward N. Pugh Jr., Nader Engheta

Submitted to Journal of Optical Society of America A

Polarization- and Specular-Reflection-Based, Non-contact Latent Fingerprint Imaging and Lifting

Shih-Schön Lin, Konstantin M. Yemelyanov
Electrical and Systems Engineering Department, University of Pennsylvania, 220 South 33rd Street Moore 203 Philadelphia, PA 19104-6390, USA
Edward N. Pugh, Jr.
F. M. Kirby Center for Molecular Ophthalmology and Institute of Neurological Sciences, University of Pennsylvania 422 Curie Boulevard, Philadelphia, PA 19104-6390, USA
Nader Engheta
Electrical and Systems Engineering Department and Institute of Neurological Sciences, University of Pennsylvania, Philadelphia, PA 19104, USA

In forensic science the finger marks left unintentionally by people at a crime scene is referred to as "latent fingerprints". Most existing techniques to detect and lift latent fingerprints require application of certain material directly onto the exhibit. The chemical and physical processing applied onto the fingerprint potentially degrades or prevents further forensic testing on the same evidence sample. Many existing methods also come with deleterious side effects. We introduce a method to detect and extract latent fingerprint images without applying any powder or chemicals on the object. Our method is based on the optical phenomena of polarization and specular reflection together with the physiology of fingerprint formation. The recovered image quality is comparable to existing methods. In some cases like the sticky side of a tape our method shows unique advantages.

OCIS codes: 150.0150 Machine vision, 110.0110 Imaging systems, 100.0100 Image processing, 260.5430 Polarization.

Introduction

Fingerprinting is one of the most widely used biometric methods for identifying and authenticating individual persons. The modern science of fingerprinting started in the second half of the 19th century. For an interesting historical review see references[1-3]. There are two types of fingerprint data, distinguished by their formation processes. In forensic science finger marks left unintentionally at a crime scene are referred to as "latent fingerprints". Fingerprints acquired directly from human fingers using ink or scanners in controlled environments are referred to as "exemplar fingerprints"[1-4]. Although both types of fingerprints are related to some extent, the recovery of "latent" and "exemplar" fingerprints poses very different technical challenges. There have been considerably more successful optical methods for exemplar fingerprints than for latent fingerprints and sometimes the classification can be confusing. For example, there exist methods using "laser" and "polarization" for extracting fingerprint images directly from

live human fingers[5]; such methods are for "exemplar fingerprints". The purpose and the detailed physical background of that system are both different from those involved in the application of "laser" or "polarization" to "latent fingerprints". Another example is a device that claims to "optically reads a latent fingerprint"[6]. However, the main function of the particular device is to read directly from a human finger (and simultaneously comparing with a known fingerprint pattern) and such device should be classified as an "exemplar fingerprint" reader. Recovery of latent fingerprints are much more difficult than the recovery of exemplar fingerprints because the physical and chemical composition of latent fingerprints and the surfaces on which they are found vary greatly and can often undergone unknown degradation before being examined. In this paper we present a new method for the detection and recovery of "latent fingerprints".

Latent fingerprints differ from exemplar fingerprints in that they are very difficult to detect with unaided human vision under most ordinary viewing conditions (hence their name); they are usually also of lower quality than the exemplar fingerprints, although high quality fingerprint marks can at times also be found at a crime scene. To be precise, non-exemplar fingerprints that can be easily seen by a human observer should be called "patent fingerprints" [1-4]. In practice, however, the term "latent fingerprints" is often used to refer to all fingerprints that are not "exemplar". It is the really "latent" fingerprints that are more common at a crime scene and require greater efforts to render visible. Most techniques employed for this purpose utilize a chemical or physical process that applies some kind of material directly to the surface suspected to bear fingerprints[1-4,7-9]. Once the contrast of the fingerprint mark is sufficiently enhanced by such treatments, the mark is either photographed or "lifted" in order to be permanently archived as evidence. The term "lifting the fingerprint" originates from the oldest, but still widely used fingerprint detection method -- powdering -- in which the powders applied adhere to the fingerprint material, and then are physically lifted out of the original crime scene object by a sticky tape.

Since applying chemicals or powders onto a surface on which fingerprints reside changes the chemical and/or physical composition of the surface, the use of such "invasive" methods can potentially interfere with subsequent forensic testing of different type, and can sometimes inflict deleterious side effects on the surface or the operator. Therefore, in the past 30 years several techniques that can recover latent fingerprints without the need to apply foreign material directly onto the fingerprints have been developed. These methods use specialized light sources(e.g. Laser, UV), filters, and detectors[1-4,7-12]. They are very successful in some cases. However, like all other existing techniques, they do not work in all possible cases and are known to fail completely with certain types of latent fingerprints or object surfaces. As a result chemical enhancers are often reintroduced to aid in the detection of latent fingerprints[1-3,9,12-19]. Further studies show that techniques using special light sources and filters work much better in more cases when combined with the application of certain chemicals on the fingerprint sample first[1,9,12-19]. However the application of chemicals directly onto the fingerprints effectively negates the non-contact advantages and the composite methods reverts back into invasive methods.

It has been known by experienced law-enforcement officers that by varying the angle of a flashlight shining onto a surface suspected to bear latent fingerprint, one can potentially locate latent fingerprints that are otherwise difficult to see[7]. However, in order

to "lift" the latent fingerprints in a form that can be documented and presented as evidence in a court trial, some "invasive" enhancement treatments are usually considered necessary. Pfister[9,20] devised an optical method that uses a semi-transparent mirror that can project light onto a surface at a right angle, while at the same time allowing a camera or observer to view the surface at a right angle. A smooth surface is expected to appear bright due to strong specular reflection, while a fingerprint mark would appear darker due to much less specular reflection. Lennard and Margot[9,21] reported that such method works better when the sample is pretreated with cyanoacrylate. The use of only a right angle in Pfister's method sacrificed quite a bit of flexibility and polarization based techniques can not be applied to further improve the contrast because specular reflection observed at right angle from the surface is not preferentially polarized by the surface. It is widely known that specularly reflected light from dielectrics would be partially polarized at certain range of viewing angles. However, to the best of our knowledge, no known application of polarization has been reported for latent fingerprints, with the exception of using a polarizing filter to remove glare when taking pictures, which is considered a standard photographic technique. Menzel[22] briefly mentioned the possibility of using optical polarization to enhance visibility of latent fingerprints left on glass but it appears that no further development took place.

We propose here a new method which allows the detection and "lifting" of latent fingerprints into clearly identifiable digital images without the application of chemical treatments or indeed, without any physical contact with the surface and fingerprint material. Rather than employing extraneous material, our method takes advantage of the optical properties, particularly those related to specular reflection and polarization, of the latent fingerprint, which usually consists of tiny ridges of skin residue material including sweat (salty water), grease, and lipid[2,3,23], all of which are rather transparent dielectric materials, making them difficult to detect under most viewing conditions. Our method is also applicable to latent fingerprints left on a smooth but pliable dielectric surface. The recovered fingerprint images have comparable or better quality to those obtained by conventional methods. Fig. 1~Fig. 10 illustrate the fingerprint detection and lifting capabilities of our new methods applied to several common items and surfaces. Note that our method is not restricted to viewing the surface at a right angle, and our use of polarization is not restricted to glass, and is not used for removing glare.

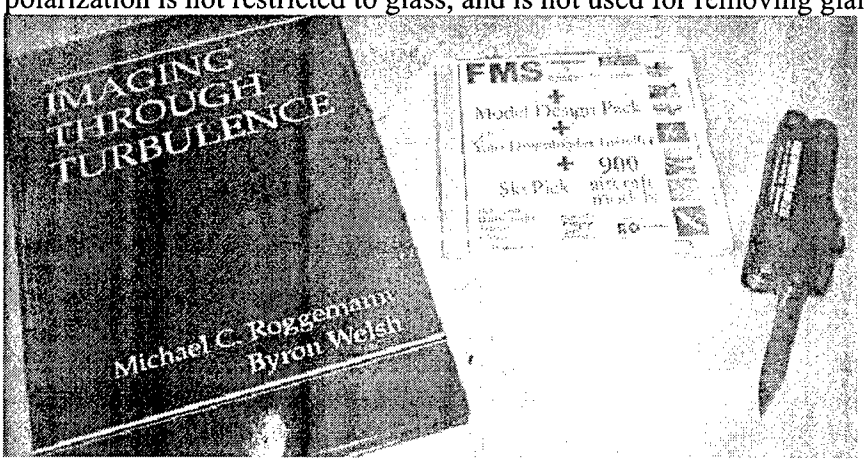

Fig. 1 Picture of the three sample items bearing latent fingerprints: a hard cover book, a plastic CD case with underlying insert patterns, and a stainless steel blade of a Swiss army knife.

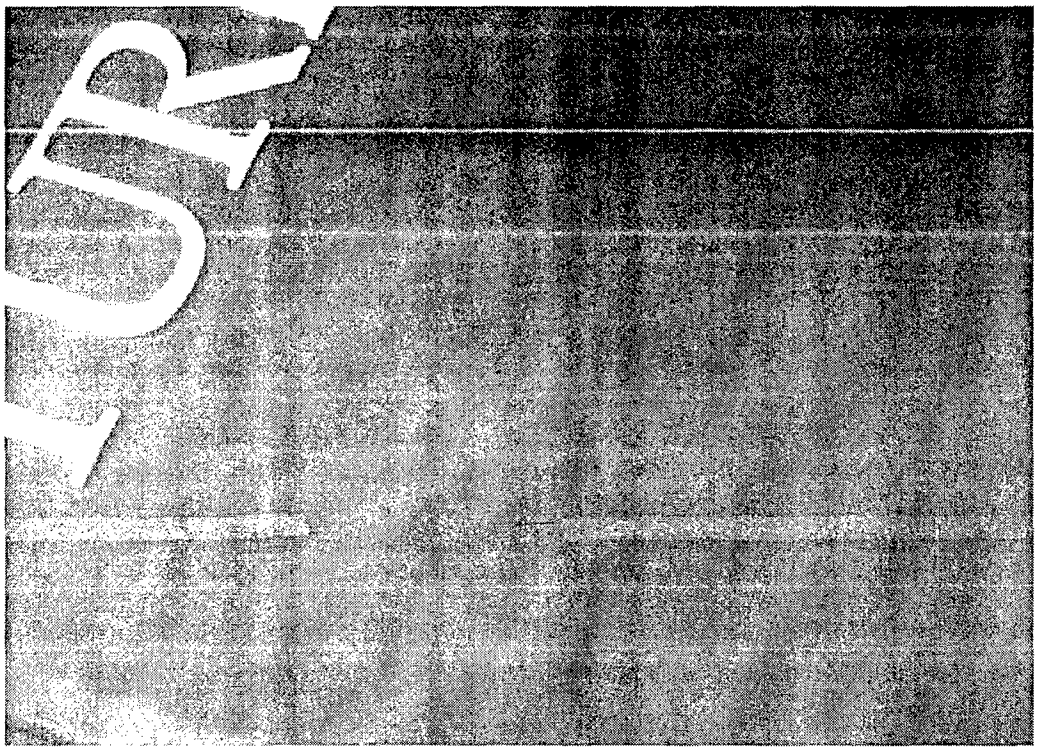

Fig. 2 Close up view of the hard cover book bearing latent fingerprint under normal viewing condition. Note that this image has undergone digital linear contrast enhancement but still the fingerprint mark is not visible.

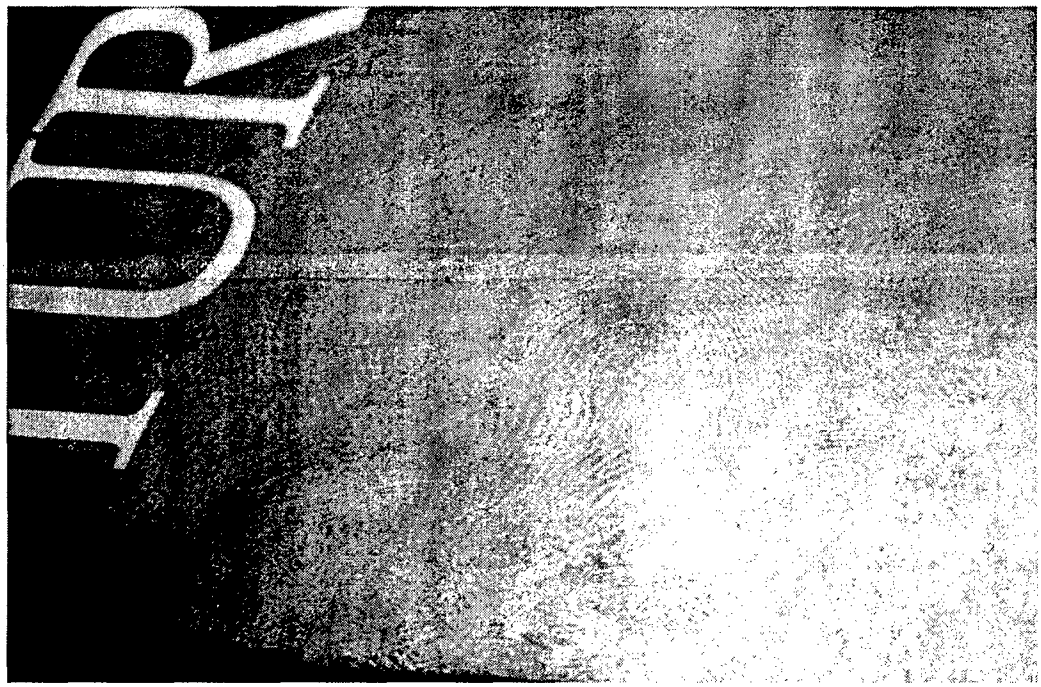

Fig. 3 The same area of the hard cover book as in Fig. 2 but taken with our specially arranged specular lighting condition. The latent fingerprints are revealed.

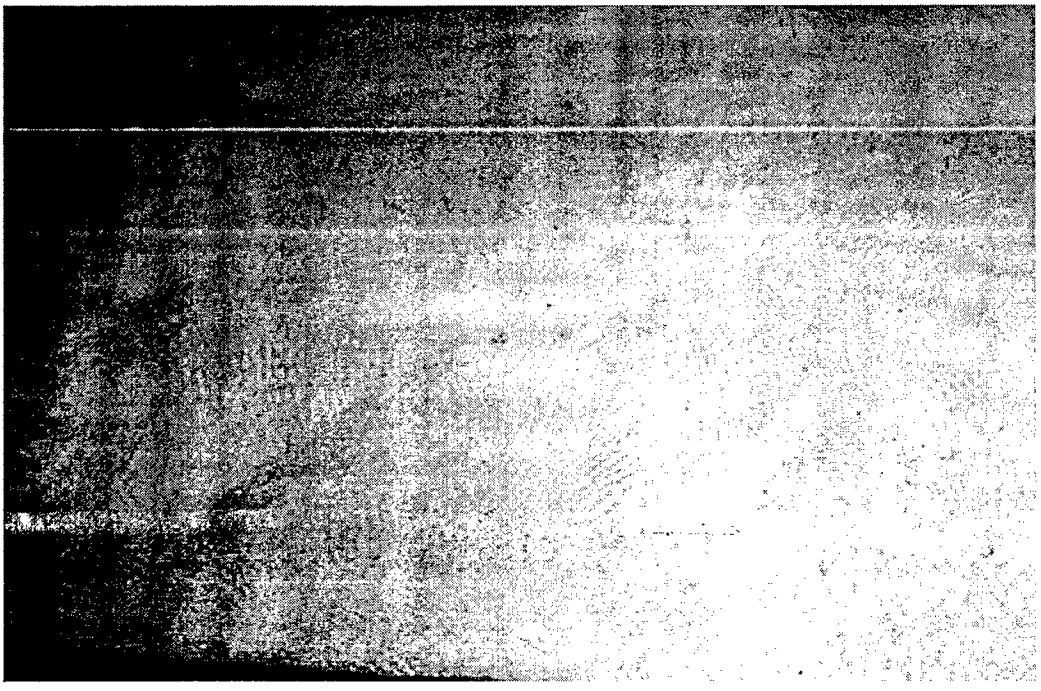

Fig. 4 The same area of the hard cover book as in Fig. 2 but taken with our specially arranged specular lighting condition plus polarization image processing. The latent fingerprints are revealed and at the same time the background pattern from the book title is greatly suppressed.

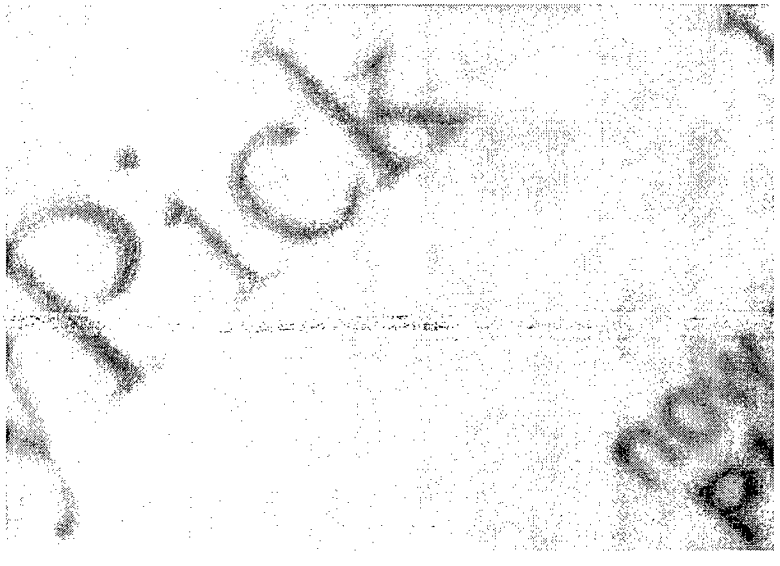

Fig. 5 Close up view of the plastic CD case with insert pattern under normal viewing condition. No fingerprint is visible although the image has undergone digital linear contrast enhancement.

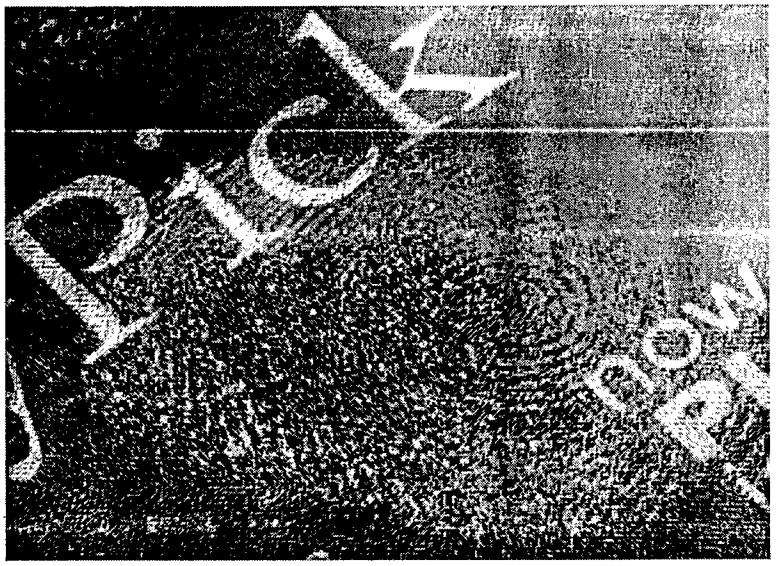

Fig. 6 The same area of the plastic CD cover with insert pattern as in Fig. 5 but taken with our specially arranged specular lighting condition with three different polarizer orientation and then the degree of polarization image computed. The latent fingerprints are revealed.

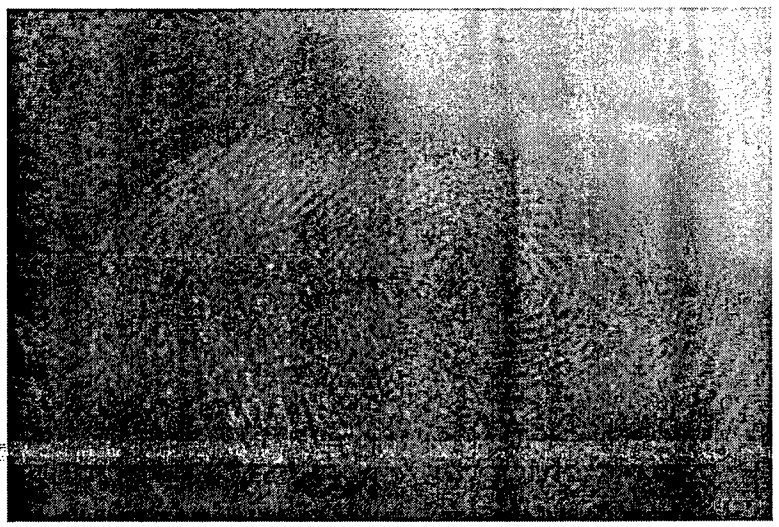

Fig. 7 The same area of the plastic CD cover with insert pattern as in Fig. 5 but taken with our specially arranged specular lighting condition plus polarization image processing. The latent fingerprints are revealed and at the same time the background pattern from the CD insert is greatly suppressed.

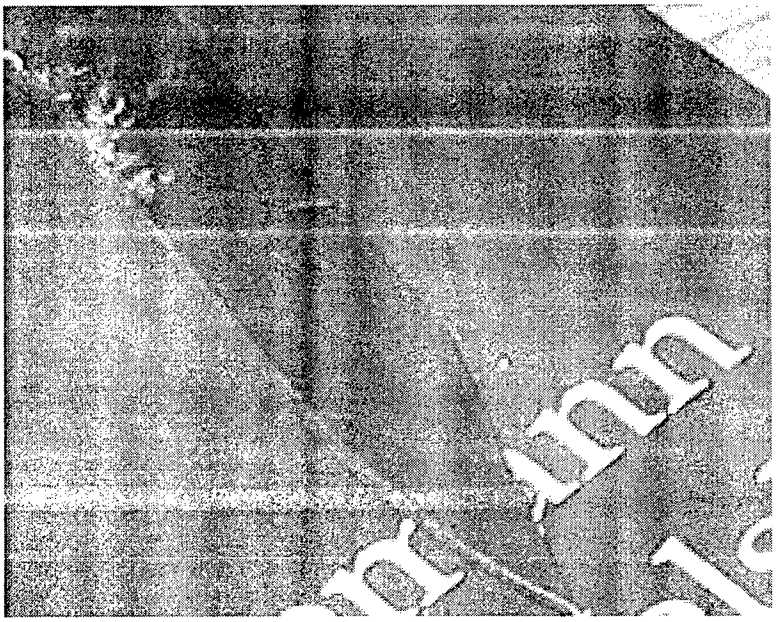

Fig. 8 Close up view of the stainless steel Swiss army knife under normal viewing condition. No fingerprint is visible although the image has undergone digital linear contrast enhancement.

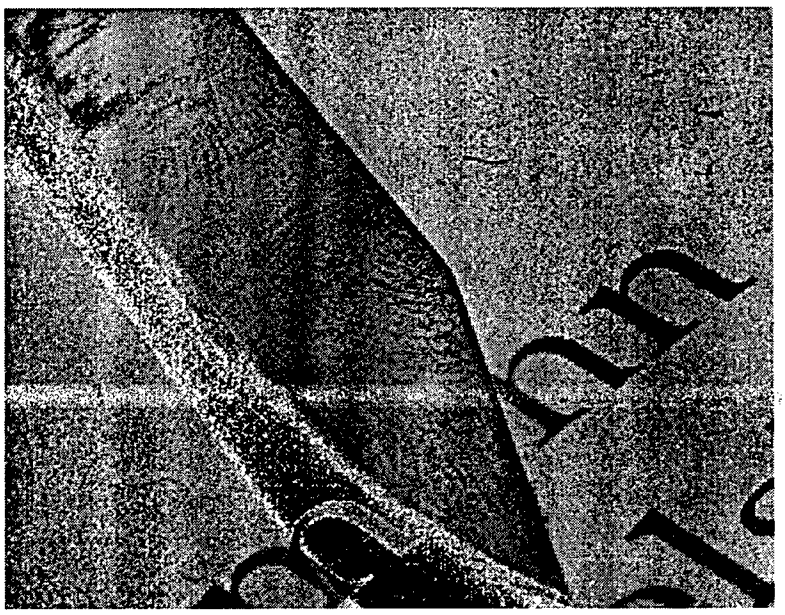

Fig. 9 The same area of the stainless steel Swiss army knife as in Fig. 8 but taken with our specially arranged specular lighting condition plus polarization processing. The latent fingerprints are revealed in the degree of polarization image.

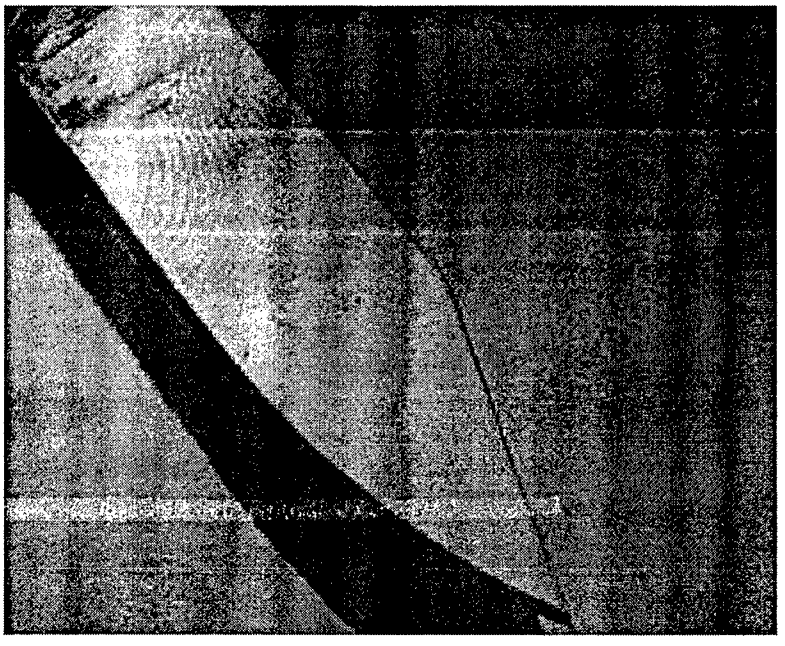

Fig. 10 The same area of the stainless steel Swiss army knife as in Fig. 8 but taken with our specially arranged specular lighting condition plus polarization image processing. The latent fingerprints are revealed and at the same time the background pattern from the book cover is greatly suppressed.

Non-contact optical latent fingerprint enhancement and lifting

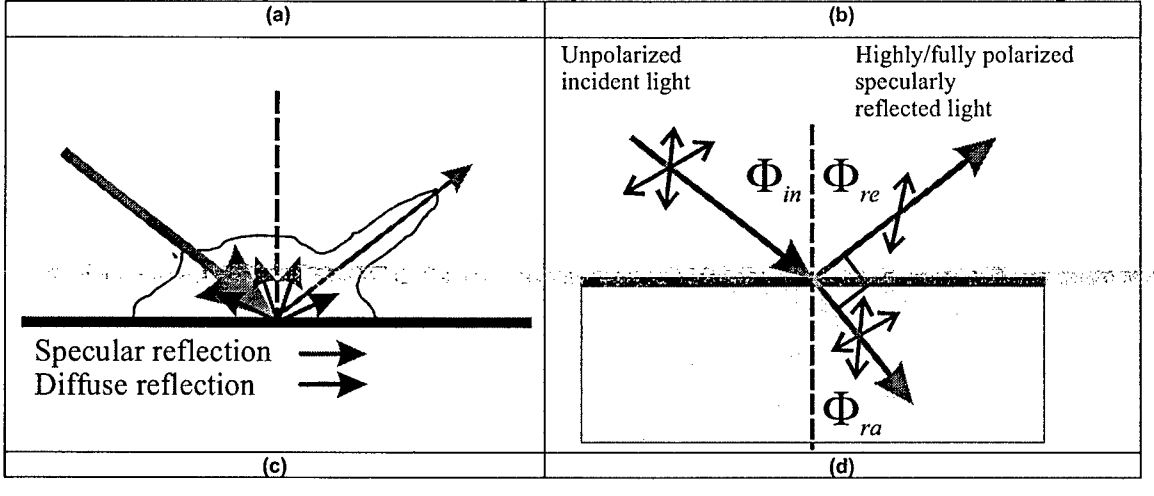

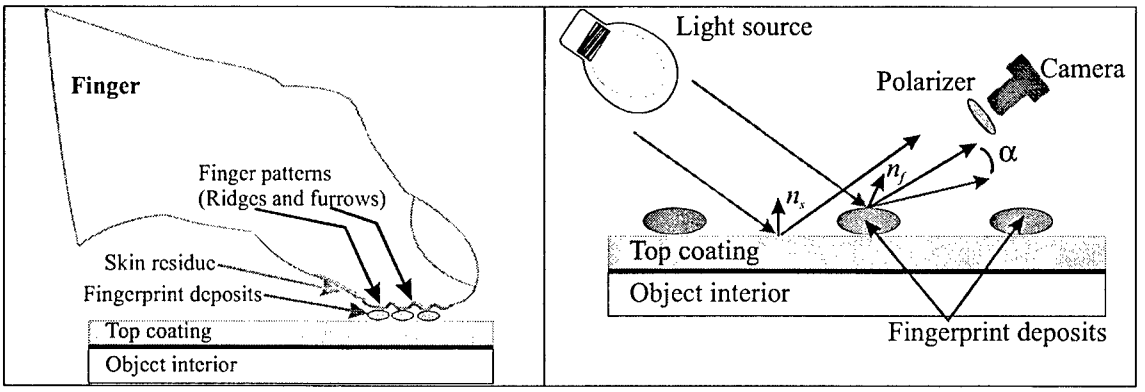

Fig. 11 Schematic of physical principles concerning non-contact latent fingerprint enhancement and lifting. (a) Macroscopic reflection from a surface consists of two distinct kinds, i.e. specular and diffuse. For specular reflection the angles of incidence and reflection are equal, while for the diffuse case the reflected intensity may approximately have an effectively uniform distribution over all directions in a hemisphere. Most surfaces exhibit both types of reflections, but one type may be stronger than the other. (b) Partial polarization of specularly reflected light from a semi-transparent dielectric surface. It is known that the light reflected from the smooth surface is partially polarized with the polarization being perpendicular to the plane of reflection. (c) Live human skin is kept soft and pliable by the constant oily secretion of hypodermic glands. The ridge area of the skin pattern tends to leave a dielectric residue on a surface touched by a finger. (d) The residue left in (c) forms the latent fingerprint. Using a method that generates a sufficient contrast difference between the latent fingerprint and the rest of the surface in the camera image, a successful detection and extraction can be achieved without applying physical or chemical treatments to the surface. Note that the camera position in (d) is oriented in such a way that it captures the specular component of reflected light from the clean surface only while the specular reflection component of the residue is not captured. Additionally, when a finger touches a pliable dielectric surface it could cause a plastic print on the surface. In this case the difference in the surface normal caused by the plastic print ridges will serve the same purpose of creating contrast in intensity and polarization under proper lighting.

We start with the principal physical and physiological basis of our non-contact optical latent fingerprint enhancement and lifting in this section. The more detailed formulas used in our computation will follow later. The physics underlying the method is illustrated in Fig. 11. When a finger touches the object surface, a dielectric residue mark bearing the fingerprint pattern is imprinted on it. The residue on the surface induces differences in optical polarization or reflection or both between the clean part of the surface and that bearing the print. The optical information is captured and enhanced by our unique optical setup and stored as digital images. Further digital processing of the captured images enables us to "develop" or "lift" the latent fingerprint pattern without applying any powder or other chemicals to the object. Our optical setup is designed on the basis of the well known Fresnel reflection theory for orthogonal polarizations and the theories for macroscopic surface reflectance developed for computer vision and graphics. As an aside, it is interesting to note that biologists and zoologists have found that certain animal species have visual systems that sense and utilize (in or near) visible light's polarization in the natural environment. e.g. backswimmer *Notonecta glauca* can detect the polarization of light reflected from smooth water surfaces and use it to land and plunge safely on the water surface[24,25]. Indeed, our original step to design our optical setup for latent fingerprint detection was inspired from this ability of *Notonecta glauca* in detecting the surface of the water.

In Fig. 11(c), we illustrate a cross section view of the fingerprint on a surface. The ridge area corresponds to a small amount of residue on the surface, while the furrow area does not. All existing enhancement methods take advantage of this situation by applying materials that selectively attach to or interact with only the residue area and produce a colored or fluorescent pattern of the residue area. Our non-contact method exploits this situation in a different way (Fig. 11(d)), with a common household light source (incandescent or fluorescent, does not really matters here), a camera and the surface being inspected arranged in such a way that the geometry conforms approximately to the law of (specular) reflection. Thus, the incident angle of light from the source approximately equals the viewing (reflection) angle of the camera, so that the camera will capture the light reflected specularly from the non-residue area, and also only the light reflected diffusely from the residue laden area. The reason is that the residue stain area is likely to have different surface normal directions and indices of refraction as compared with the uniform or smoothly varying surface normal direction of the unstained surface area. The highly localized nature of specular reflection energy distribution makes it very sensitive to even minute changes in the direction of the surface normal. Since the specular reflection component is, in general, much stronger than the diffuse reflection component[26] (see Fig. 11(a)), one potentially finds an enhanced contrast between the residue laden ridge mark and the clean surface furrow 'negative-mark'. Another often encountered case is a plastic fingerprint left on a pliable dielectric surface. There may or may not be biological residue left on the surface but the ridge and furrow patterns formed by the pliable dielectric material itself create differences in surface normal compared to the undisturbed surface area and will serve the same purpose.

In some cases this contrast enhancement from the specular reflection effect alone is insufficient. The object itself may have a complicated high contrast pattern under the top coating of the surface (see Fig. 11 (c) and (d)) that interferes with fingerprint pattern even after the enhancement. This problem has been recognized by many practitioners[27,28]. Discrete Fourier transform analysis has been shown to be able to remove regular patterns that vary periodically, but cannot deal with a general background that is not periodic. An additional characteristic of the specular reflection is that it tends to be partially polarized in a plane perpendicular to the plane of reflection, see Fig. 11(b). One or more polarization analyzers collecting polarization components at different angles can provide complete information about the polarization state of the reflected light. Based on the polarization information we can further extract only the specular component of this reflection and get a much cleaner fingerprint image because for the most part the light coming from the pattern beneath the top coating of the object surface is due mostly to unpolarized, diffuse reflection. We have also found that in some cases some of the polarization images simply show higher contrast between the fingerprint and its background than the fingerprint images recovered using specular reflection alone.

The general expression for the observed intensity of partially polarized light I as a function of the angle φ of orientation of a polarization analyzer can be written as follows:

$$I(\varphi) = I_U + I_A \cos\left[2(\theta - \varphi)\right] = I_U \left\{1 + p\cos\left[2(\theta - \varphi)\right]\right\} \tag{6}$$

where θ is the orientation angle of the major axis of the polarization ellipse, I_U is a half

of the total pixel intensity, and $p \equiv I_A / I_U$ is the degree of linear polarization at a given pixel in a digitized image. The reference axis for φ and θ can be arbitrarily chosen. Since the exact index of refraction of the surface in our study is considered unknown, putting one polarizer at a given orientation angle in front of the camera and taking a picture cannot provide complete information about the polarization state of the received light. By taking three pictures with the polarizer oriented at three different angles, for example φ=0, 45 and 90 degrees, we can recover I_U, I_A, and θ for each pixel of the image using the following expressions:

$$\begin{aligned} I_U &= (I_0 + I_{90})/2 \\ I_A &= \sqrt{(I_{45} - I_U)^2 + (I_{90} - I_U)^2} \\ \theta &= \arctan\left[(I_{45} - I_U)/(I_{90} - I_U)\right]/2 \end{aligned} \tag{7}$$

Here indices 0, 45, and 90 indicate the orientation of the polarizer in degrees when the image was taken. Because θ and $\theta+\pi$ are indistinguishable for phase-blind visual sensors in most conventional cameras, the meaningful range of θ is restricted to $(0 \sim \pi)$. We usually use θ in the range from 0 to π. Polarization camera systems able to rapidly take the required pictures have been developed by Wolff and his colleagues[29-31]. The formulation and symbols used here follows from our previous work[32,33] and are slightly different from those used by Wolff. Since the background object pattern is most likely caused by pigments beneath the transparent substrate that is used to hold them, the object pattern intensity signals are mostly due to diffuse reflection, which is nearly unpolarized and thus I_A and sometimes p are close to zero. Thus, with our polarization technique we can extract the purely specular reflection component from the top surface by computing images of I_A or p for every image point. Such images often carry a substantial contrast between the fingerprint residue pattern and the clean area in between. Note that if only 0 and 90 orientation images are taken, the fingerprint may still be enhanced in the polarization-difference image[34-38], but the 0 or 90 direction must be nearly parallel to either the object surface or the fingerprint ridge surface, which can be challenging to arrange when the surface is not flat.

Experiments

A step-by-step application of the new optical method is presented in Fig. 12~Fig. 19. Fig. 12 gives an overview of the experimental setup when the specially arranged light is on and the ordinary room light is turned off. The surface being inspected is the metal casing of an electric air pump (with brand name sticker "Linicon") which is painted orange. Fig. 13 shows how the surface looks like with the specially arranged lighting turned off, and the ordinary diffuse fluorescent room light on. The image in Fig. 13 is shown with a common digital enhancement available in most image-processing software, setting the brightest pixels in the image to the maximum possible value allowed by the display, and the darkest pixels to the lowest display value and linearly rescaling the rest pixel intensity values. Fig. 14 presents the same image data as in Fig. 13, but enhanced instead by histogram equalization. This enhancement method remaps the pixel values according to

the histogram distribution of their magnitudes, distributing them more evenly over the dynamic range of the display (see[39]). These two images illustrate the 'latent' nature of the fingerprint: the natural contrast is so low that not only the unaided human eye cannot detect it, but even widely used digital image enhancements do not reveal its presence. Fig. 15 and Fig. 16 present images taken with only the specular illumination turned on, and digitally enhanced with the same methods as used to produce Fig. 13 and Fig. 14, respectively. Imaging the light specularly reflected from the surface yields a major enhancement not achievable with the digital enhancements alone, an enhancement traditionally achieved with powders and chemicals, but completely without destructive side effects. Fig. 17 and Fig. 18 are zoomed in view showing the detailed quality of the recovered fingerprint images. Fig. 19 is Fig. 17 digitally reprojected and rotated to a canonical "up right" view, as if the picture was taken with a camera looking at right angle from the surface with the fingertip pointing up for easier comparison with standard database and for display in a court.

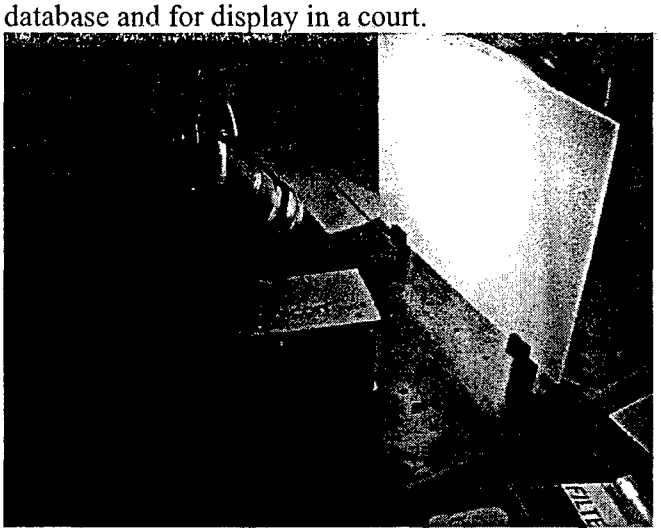

Fig. 12 Setup Overview for Fig. 13~Fig. 19.

Fig. 13 Ordinary lighting, linearly scaled.

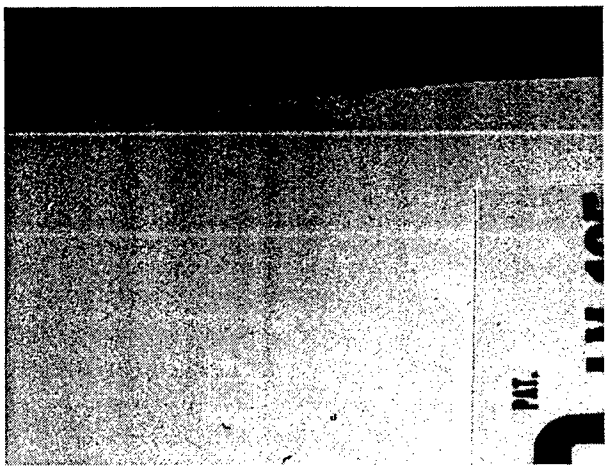

Fig. 14 Ordinary lighting, histogram equalized.

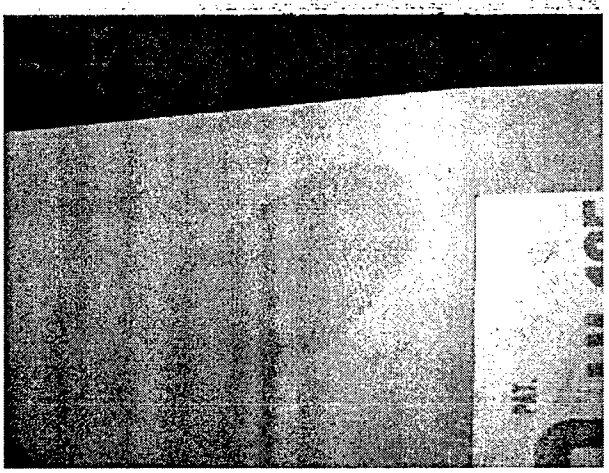

Fig. 15 Specular lighting, linearly rescaled.

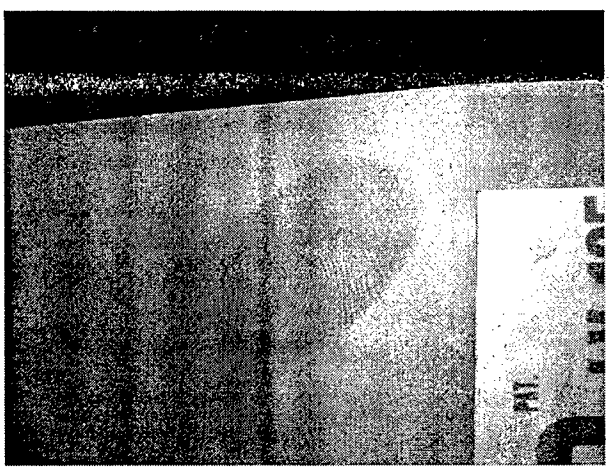

Fig. 16 Specular lighting, histogram equalized.

Fig. 17 Zoom in view of the fingerprint from Fig. 16.

Fig. 18 Further zoom in view from Fig. 17

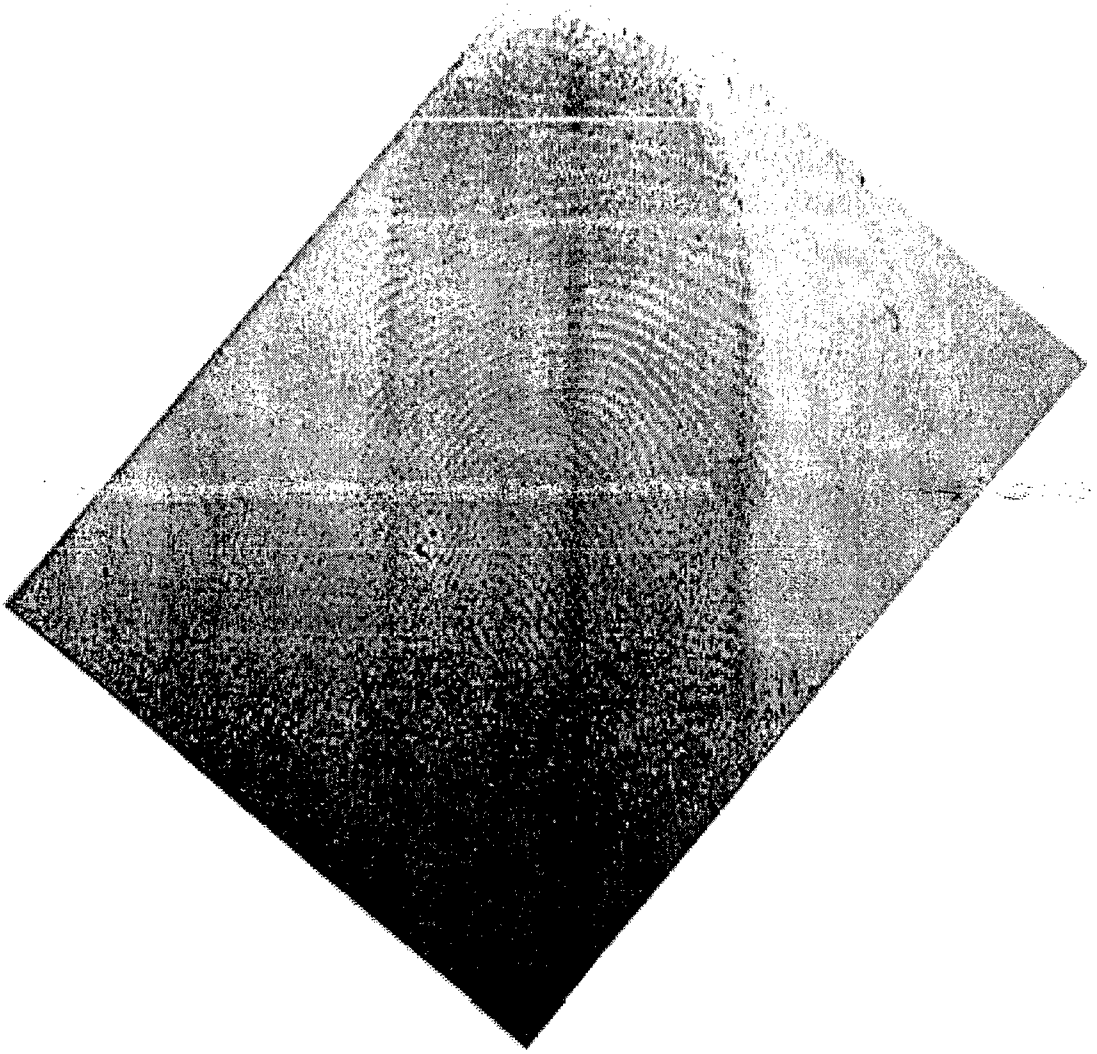

Fig. 19 Reprojected and rotated upright view of Fig. 17.

The results of another experiment employing our non-invasive optical method are illustrated in Fig. 20~Fig. 22. In this case, the surface with the latent fingerprint was the paper cover of an ordinary desk calendar (Fig. 20), and presented a greater challenge than the solid colored metallic surface. The paper surface contained a printed pattern whose light absorption interferes with the optical detection of the fingerprint. We used both specular reflection and polarization analysis to extract the latent fingerprint (Fig. 21). For the polarization analysis, images were taken with a linear polarization analyzer mounted in front of the camera, and oriented at three different angles. The picture displayed in Fig. 21 is the value image of the derived quantity I_A (see Eq. (7) in supporting material). We emphasize here that Fig. 21 is not an image of the ordinary intensity distribution, but rather a mapping of a certain physical quantity derived from the polarization distribution of the light comprising the image. The specular component of the surface reflection is now evident, and the background pattern is gone. Fig. 22 shows a cropped, close-up of the fingerprint area of the image seen in Fig. 21. These results lead to two additional conclusions: first, the non-invasive optical method can extract latent prints from some

paper surfaces as well as from smoother surfaces; and second, the processing of the polarization information in the image can further enhance the quality of the recovered latent fingerprint under certain conditions.

Sometimes the specular reflection component can be obscured by more intense diffuse reflection. We applied our methods to such a case, deliberately picking one of the strongest diffuse reflectors, a white cotton lining underneath a soft clear plastic CD sleeve (Fig. 23~Fig. 26). Fig. 23 shows an image taken without a polarizing filter in front of the camera. The diffuse white light is so strong that the specular reflection output can barely enhance the latent fingerprint on the plastic surface. However, the polarization-based analysis followed by the histogram equalization readily enhances the latent fingerprint (Fig. 24~Fig. 26).

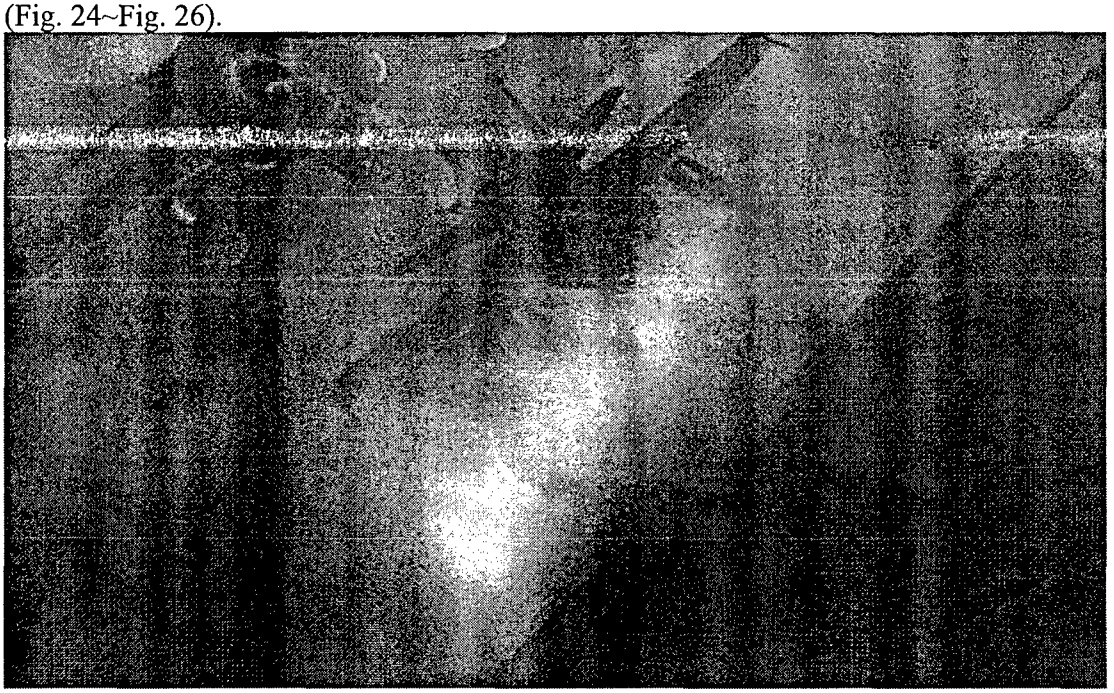

Fig. 20 Paper calendar cover with underlying picture. A fingerprint is revealed by specular lighting.

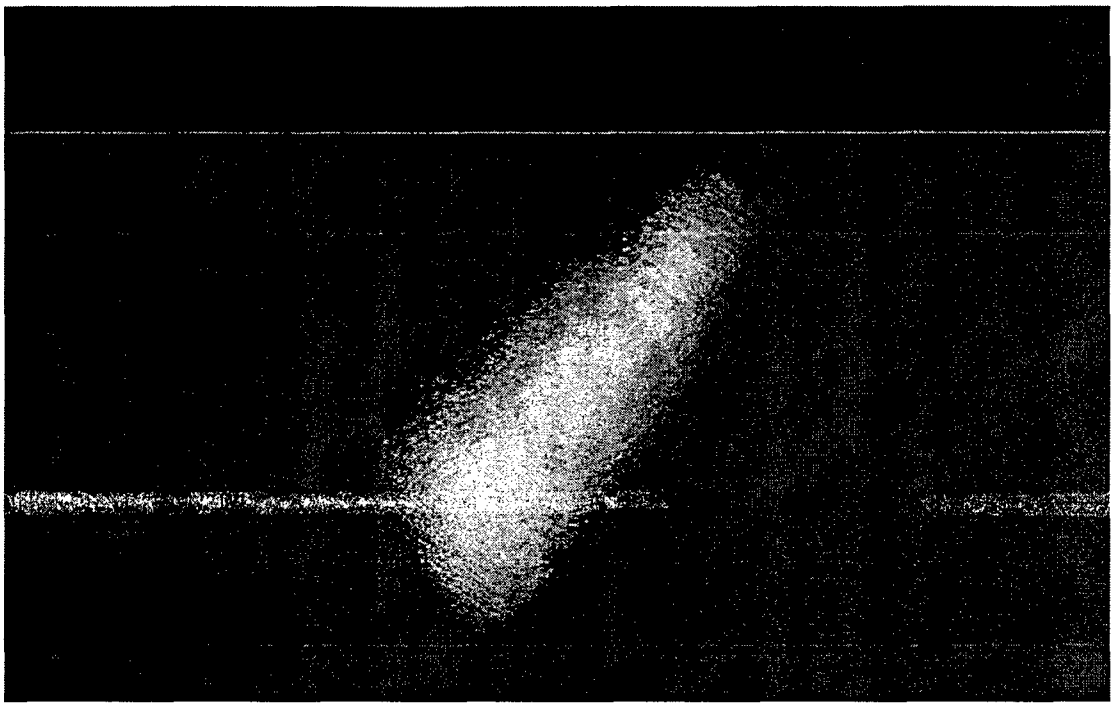

Fig. 21 Same item as Fig. 20 but with polarization processing. Background completely removed.

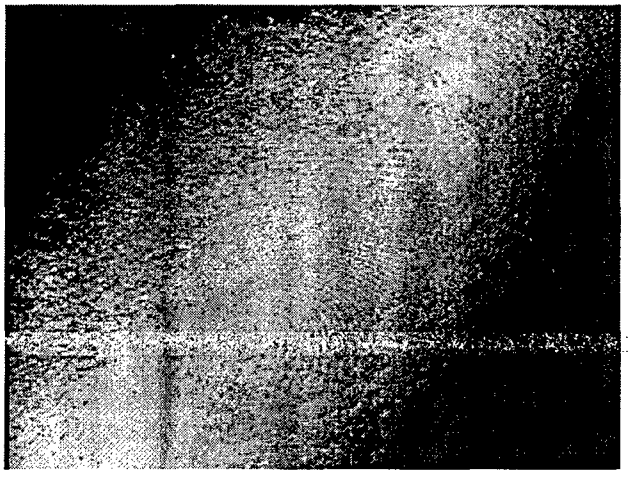

Fig. 22 Zoom in view of the fingerprint in Fig. 21.

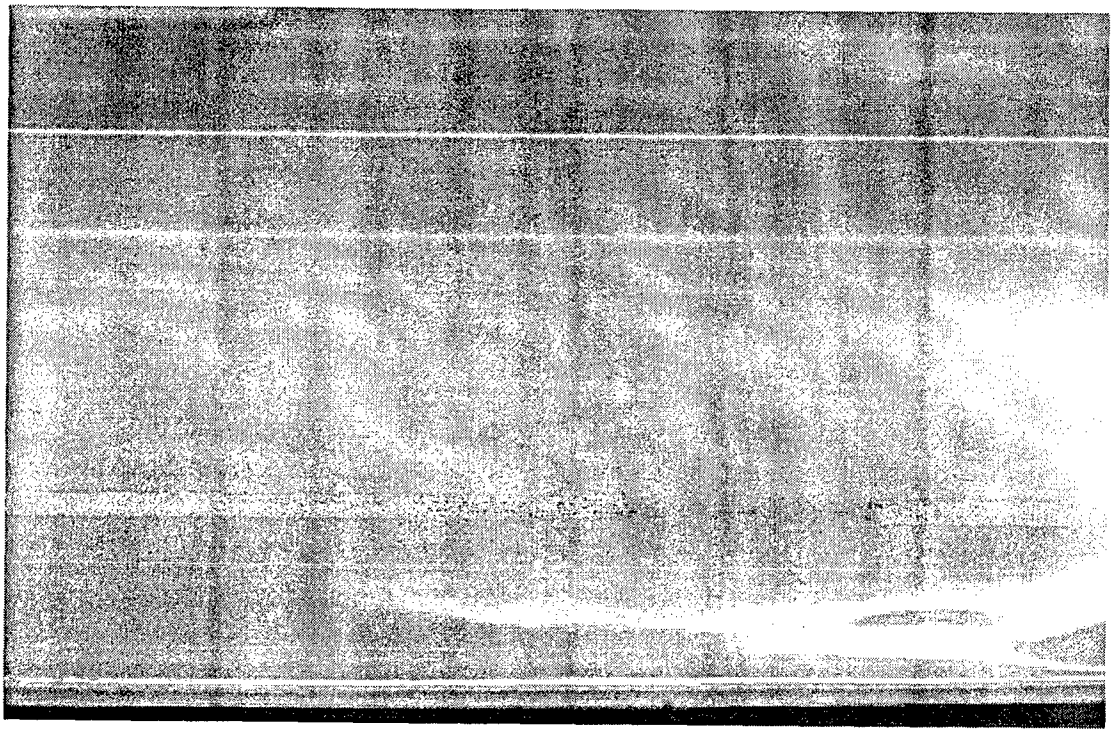

Fig. 23 A soft plastic CD sleeve with white cotton lining underneath, seen with ordinary lighting.

Fig. 24 Polarization I_A image. The latent fingerprint on the CD sleeve is exposed in high contrast.

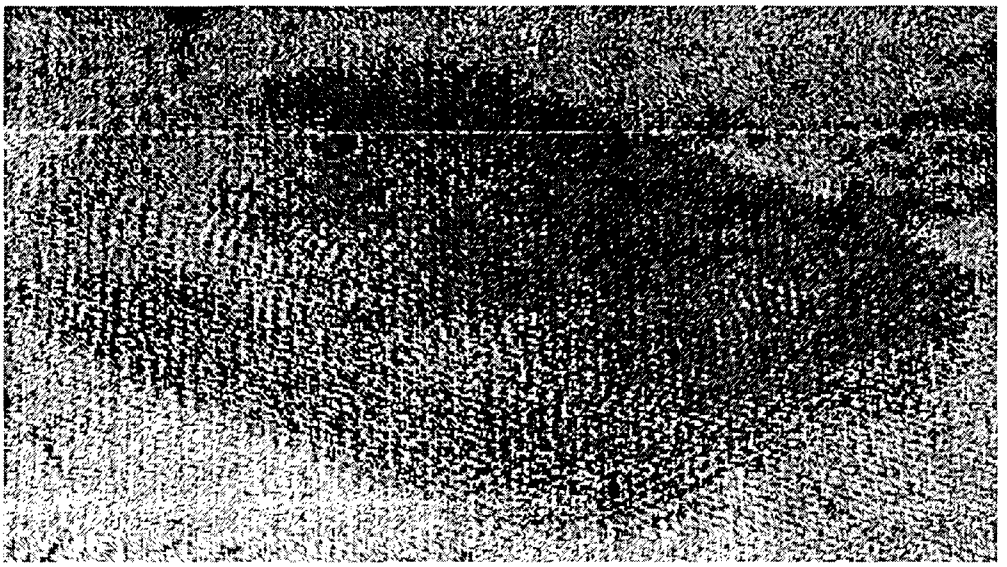

Fig. 25 Zoom in view of the fingerprint in Fig. 24.

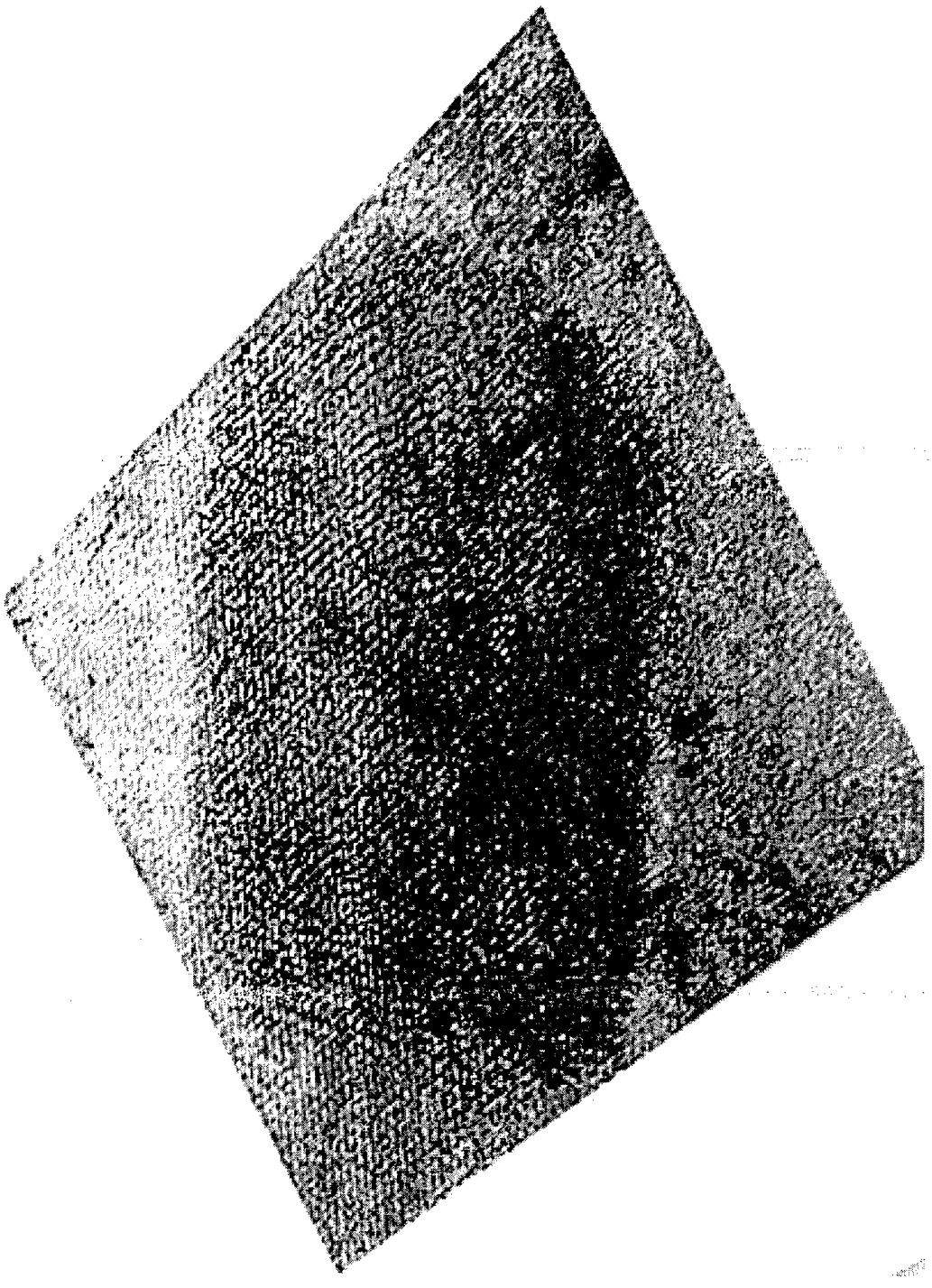

Fig. 26 Reprojected and rotated Fig. 25 to up right view.

The sticky side of a tape has traditionally caused trouble with invasive methods, especially methods that apply powder to the surface. Most powders and reagents can stick easily anywhere on the sticky surface, not just the fingerprint area. In contrast, sticky side of the tape is ideally suited to our method. The "sticky" material is a thin coat of pliable semi-transparent dielectric that fits our surface model perfectly. Whether the latent

fingerprint mark is formed by skin residue or by a plastic mark formed on the "sticky" surface, our surface model predicts that high contrast intensity or polarization images can be formed with proper lighting. We tested our method on a piece of transparent packing tape and the results are very good (Fig. 27). An example of plastic fingerprint mark detection using our method is shown in Fig. 28.

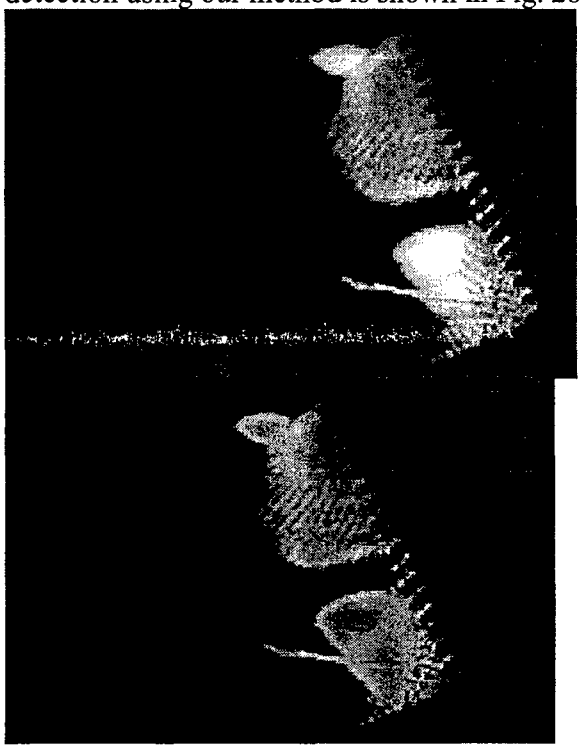

Fig. 27 Left: fingerprint found on the sticky side of the tape using specular reflection. Right: fingerprint found on the sticky side of the tape using polarization. The image is the I_A image. Note that no ordinary digital contrast enhancement is used on both images.

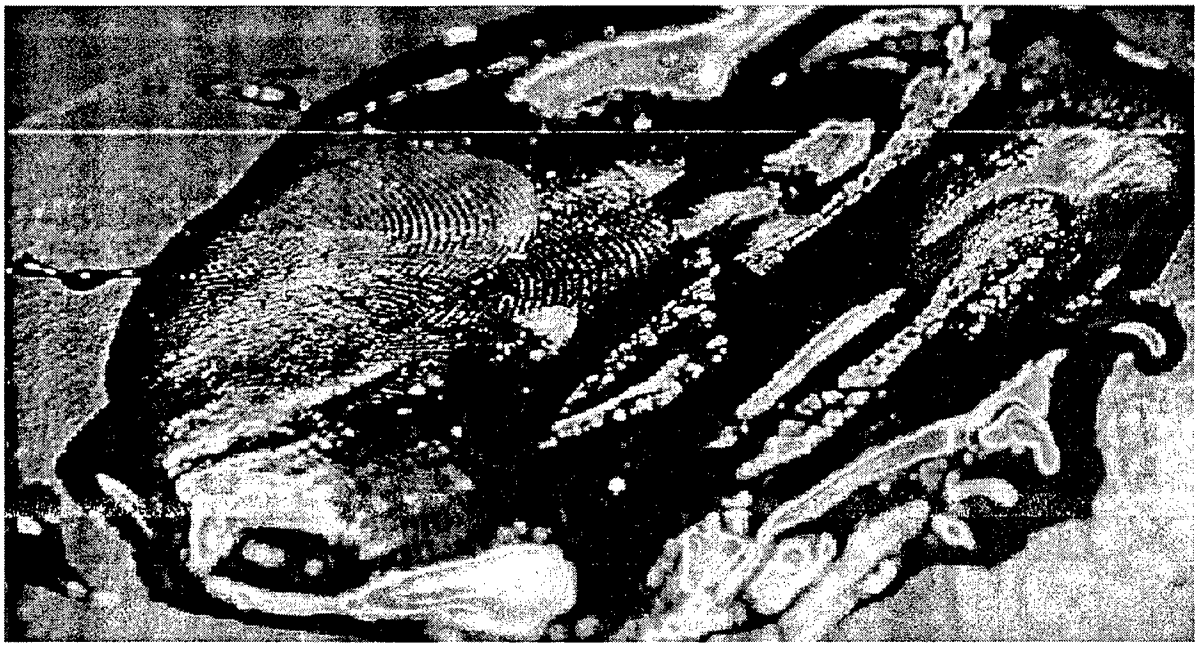

Fig. 28 Plastic fingerprint mark revealed on a piece of hardened epoxy resin in the degree of polarization (p) image. No ordinary digital contrast enhancement is used on this image.

Theory of the application of specular reflection to latent fingerprints

Modeling surface reflection on a microscopic scale is complicated and depends heavily on the detailed knowledge of the molecular material composition of the surface material. However, macroscopically, a more general model can be used that applies to a wider range of surfaces without the need for details about the surface with acceptable reduction in accuracy. This is desirable in many practical applications, notably in computer vision and graphics, where the details of the chemical and physical composition of surfaces are not known or are not of vital importance. Beginning with Refs[40,41], many surface reflection models based not on the exact chemical composition but rather on a plausible statistical model of the surfaces were proposed, see e.g. Refs[42,43]. A review of various models can be found in Refs[44,45]. Because in our applications we intend to extract the fingerprint without using any chemical analysis, the possibility of knowing the properties of surface material beforehand is excluded. However, a simple model that describes a general trend is good enough, because the ultimate form required for a fingerprint image is that of binarized black and white regions separating the ridge and furrow areas. There is no need to recover or to predict the exact brightness differences in the gray-level images taken for the purpose of recovering fingerprint marks. The simple Phong model[43] and Lambertian model[40], both widely used in many computer vision and graphics algorithms, satisfy these purposes.

Macroscopically, two well known general types of reflection can be named. The Lambertian model describes a surface producing perfectly diffuse reflection as

$$I = I_p k_d \cos\theta = I_p k_d \left(\hat{n} \cdot \hat{l}\right) \tag{8}$$

where I is the intensity of the image point sensed by the camera, I_p is the point light source's intensity, k_d is the reflection coefficient (either for a particular wavelength or for a particular camera's spectral response), θ is the angle between the surface normal $\hat{n}$ and the unit vector $\hat{l}$ in the direction of the light source as viewed from the point of reflection (see[44]). Note that the diffusely reflected light has the same intensity for all viewing directions.

Another type of reflection is that of highlights, or mirror like reflection observed on many smooth surfaces. A more subdued version is usually called "sheen". The Phong model is given by

$$I_\lambda = I_{a\lambda} k_a O_{d\lambda} + f_{att} I_{p\lambda} [k_d O_{d\lambda} \cos\theta + W(\theta) \cos^n \alpha] \tag{9}$$

where λ is the wavelength of the light, subscript 'a' denotes ambient light source, subscript 'p' denotes point light source, subscript 'd' denotes a diffuse reflection component, the new symbol O denotes color components in human and digital color vision components, f_{att} is the inverse square of decay distance of a point light source intensity, $W(\theta)$ is the diffuse reflection coefficient of the surface with a point light source angle of incidence θ, α is the angle between the exact view direction predicted by the law of reflection and the actual view direction, as shown in Fig. 11(d). For the current study, the most important information derived from (9) is that the intensity depends on α as a $\cos^n \alpha$. This gives a simple way to model a rapid decay in intensity if the view angle is different from that predicted by the law of reflection. This term suggests that if the camera, the light source, and the surface being inspected are arranged in a way predicted by the reflection law (see Fig. 11(d)), the image point for the original smooth surface without skin residue will show intensity typical for specular reflection, while the area with skin residue will have much less specular reflection due to the slight change in the direction of surface normal caused by the skin residue. The more mirror-like a surface can be modeled, the larger power of cosine decay it exhibits, which means better contrast in our specular-reflection --based latent fingerprint detection and lifting technique.

Providing all other factors being equal, the intensity of the specular reflection component is in general much stronger than the diffuse reflection component. Although, this statement is not always true, it has been widely accepted as a good rule of thumb in the majority of practical situations[26]. Since specular reflection has a tendency of concentrating reflected energy in a small solid angle, as opposed to the diffuse reflection which spreads all the reflected energy into a full hemisphere, the same amount of reflected energy will result in a much greater flux density in specular reflection and thus in image brightness. The specular reflection tends to be reflected only once from the smooth surface, while the diffuse reflection gives light that experienced a multiple scattering inside the surface before re-emerging. Each scattering only weakens the intensity but seldom enhances it. Wolff[26] experimentally measured the ratio between specular and diffuse reflection intensities for several different surfaces and reported ratios varying from about 150:1 to 250:1. For many digital sensors with 8-bit brightness resolution, this is close to the maximum intensity ratio of 255:1. This gives a strong support to our main assumption, that the specular reflection component is in general

stronger than the diffuse one. Our experiment results so far also support the validity of such assumption.

In Ref[26] another important theoretical result relating to fingerprint detection issue was reported, i.e.: if the reflection coefficient of the diffuse component is about 1/33 more than the reflection coefficient of the specular component, the diffuse component can be stronger or at least comparable to the specular component. If the underlying surface consists of complicated patterns similar in strength and spatial frequency to the latent fingerprint pattern on top of it, the method based on a purely specular reflection is not satisfactory. This is the point where the polarizer should be used.

The behavior of specular component is governed by the well-known Fresnel reflection coefficients formula[46]:

$$r_{\perp} \equiv \left(\frac{E_{0r}}{E_{0i}}\right)_{\perp} = \frac{n_i \cos\theta_i - n_t \cos\theta_t}{n_i \cos\theta_i + n_t \cos\theta_t} = \frac{\sin(\theta_i - \theta_t)}{\sin(\theta_i + \theta_t)}$$
$$r_{\parallel} \equiv \left(\frac{E_{0r}}{E_{0i}}\right)_{\parallel} = \frac{n_t \cos\theta_i - n_i \cos\theta_t}{n_i \cos\theta_t + n_t \cos\theta_i} = \frac{\tan(\theta_i - \theta_t)}{\tan(\theta_i + \theta_t)} \quad (10)$$

where subscripts 'i', 't', and 'r' stand for incident, transmitted, and reflected component. The subscripts '$\perp$' and '$\parallel$' are related to the plane of incidence. In Fig. 11(b) the plane of this paper is the plane of incidence. In case of the specular reflection it contains both the incident and reflected light wave vectors. It is well known (see e.g.,[46]) that $r_{\parallel}$ can be exactly zero at the Brewster's angle θ_B, which is given as

$$\tan\theta_B = \frac{n_t}{n_i}. \quad (11)$$

If light is incident from the air, $n_i \approx 1$, while n_t varies from 1.4 to 2.0 for most of dielectrics in the visible band (wavelength of about 400~700 nm)[46]. Eq. (11) shows that the corresponding Brewster's angles vary from 55 to 74 degrees, respectively. Although, there are certain materials with higher refractive index[46], we confine our discussion to the above-mentioned range of n_t. Therefore, when we consider the angle of incidence between 55 and 74 degrees, the reflected light is highly partially polarized with the plane of polarization perpendicular to the plane of incidence. This case is referred to as "horizontal polarization" with respect to the surface being inspected. So far we have only discussed dielectric surfaces which are adequate in most cases since "pure" metallic surfaces are rather rare in everyday life. Pure metal surfaces are oxidized quickly and the actual layer "responsible" for specular reflection is often either the oxides on the surface or the protective painting layer which is also a dielectric material. In fact, a lot of metallic-looking merchandise today are actually coated with highly reflective dielectric paints. In cases when the underlying pure metal reflects more light than the upper dielectric coating, the proposed method may not work.

Discussion

The currently popular latent fingerprint detection and extraction methods used by law enforcement agencies include, but are not limited to, powdering, Sudan black staining, iodine fuming, ninhydrin (sometimes followed by further enhancement with zinc chloride) and DFO application, silver nitrate development, cyanoacrylate (glue) fuming, gentian violet staining, vacuum metal deposition, laser excited luminescence, and RUVIS (Reflected Ultra Violet Imaging System)[1-4]. While this list may seem long, there is still need for new methods, because every existing method tends to be unsuitable for some surfaces, due either to its inadequacy in lifting the print from, or to its damaging side effects to the surfaces. In particular, the chemical and physical processing directly applied to the fingerprint bearing surface in order to extract latent fingerprints can potentially inflict deleterious effects upon the fingerprint, the operator, and/or the object surface being examined [1-3,10,18]. For example, the iodine vapor in the iodine fuming method is highly corrosive and toxic[2]. Thus, in practice, often valuable and/or irreplaceable objects are not searched for fingerprint at all[2,3,7], except in a few major cases involving extremely serious crimes. Furthermore, the chemicals used to enhance fingerprint contrast or to induce luminescence may need long processing time, are sometimes toxic, environmentally unfriendly, or radioactive. The process to speed up the chemical reaction can be dangerous, e.g. sodium hydroxide used to speed up cyanoacrylate fuming can generate extreme heat if the two come into contact[4]. Samples are often baked to high temperature after many fuming procedure to speed up the print development. Chemicals used for fingerprint enhancement can often be harmful to the operator if not handled correctly using proper procedure and protective equipments because they are designed to react with or adhere to the fingerprint residues, which are the same material found on human skin[3]. Some chemicals require specific solvents that have undesirable side effects; e.g., the phenol in the solution for Gentian violet is highly caustic and poisonous[2].

Lasers induced fluorescence is one of the first optical methods for lifting latent prints, utilizing induced luminescence of the fingerprint material[1-3,10]. However, there are several factors limiting its use. The natural fluorescence signal (without the prior application of strongly fluorescent chemical or powder) is in general very weak. Thus the laser used must operate in a specific frequency, and must have a high enough power rating. Such a laser device is fairly expensive and bulky (due to power and cooling requirements), and thus it can be deployed only to a few large and well funded crime labs and not easily made portable outside a dedicated crime lab[18]. Less powerful laser or arc lamp with filter can be used as substitute but will produce much reduced effectiveness. As a result these alternative systems need chemical enhancements. The fact that many commonly encountered fingerprint laden objects found at a crime scene contain organic substances that also fluoresce when excited by a laser often causes significant background noise[1,2,10,13,17-19]. Thus, laser-excited luminescence, like other existing methods, cannot be applied to certain types of surfaces. It has also been found that the signal strength of the natural fluorescence of fingerprints varies greatly from person to person and even from time to time of the same person[10]. As a result, in real applications laser-excited luminescence techniques are more often used with the aid of applying fluorescence enhancing chemicals to get better and more consistent results[1,2,13,17-19]. However the use of chemical fluorescence enhancers negates the non-contact advantage and the combined method reverts back to an invasive method.

RUVIS is pioneered by the research at the National Police Agency of Japan and was

originally targeted for enhancing cyanoacrylate-developed latent prints. It is found that the cyanoacrylate-developed latent prints that are translucent under visible light become opaque under UV. Latent prints deposited in sebaceous matter or oily residue can sometimes be detected by RUVIS before the application of enhancing materials. The oil strongly absorbs UV and show up as dark patterns under UV light and detector. RUVIS can sometimes detect fingerprints up to a year old in purely non-contact style[1]. The drawback is the need of expensive specialized UV light source and sensors. UV light can be harmful to both human eyes and skin so proper precaution and protective gear is necessary. Bramble *et al.*[47] proposed using laser in UV band to induce luminescence that is also in UV band. Although UV laser is not considered invasive, they find that the luminescence property of the fingerprint material decrease significantly after being exposed to UV laser for extended period of time[47].

The "Episcopic Coaxil Illumination" method proposed by Pfister[20] use the intensity difference between specular and diffuse reflection to enhance the visibility of latent fingerprint. The design always looks at the surface from the right angle. The advantage is that the picture will always appear in frontal view suitable for archiving. However with the advent of digital image processing, oblique view can be easily reprojected back to frontal view (see Fig. 19 and Fig. 26) so it is not that crucial. We have shown that by varying observation angles we can get better contrast in some cases. We have also shown that the partially polarized nature of oblique specular reflection can significantly enhance the contrast of latent fingerprint and at the same time suppress the interfering background pattern. Viewing the surfaces only at the right angle preclude the use of polarization because specular reflection at the right angle is not partially polarized by the surface.

There is a commercial product called "fingerprint camera" that has existed for a long time[4]. Some may confuse it as yet another non-contact optical method for the detection of latent fingerprints. However, this device is in fact an ordinary camera customized to record non-exemplar fingerprints that have been enhanced by other methods or for "patent fingerprints" that is already visible. The customization include dedicated lighting to reduce uneven lighting, shadow, and glare; a fixed object distance and fixed focus, aperture, exposure time, ...etc. These preset camera settings enable law enforcement officers who may not be photographic experts to be able to take good fingerprint pictures consistently for court use. Such a "fingerprint camera" does not have any "contrast enhancement" or "detection" capability for hidden latent fingerprints.

The novel optical method we propose here is capable of recovering high quality digital images of hidden latent fingerprints without the application of any chemicals or physical contacts with the examined object. Like any other existing latent fingerprint enhancement technologies, our method has its limitations. Our method is designed to take advantage of the intensity and polarization differences between specular and diffuse reflections so it will work best on a relatively smooth and non-porous surface. The chance of detecting fingerprints on a highly porous and absorbing surface like certain kinds of paper using our method is fairly low. However our method possesses unique advantages over existing methods on smooth surfaces in that complex patterns on the surface can be easily suppressed optically using our polarization method. Note that while the most common use of photographic polarization filter is to remove glare, our use of the polarizer is quite the opposite. Our polarization method, in a sense, extracts only the specular "glare" that was usually treated as a mere nuisance. Specifically we discovered that inside the

specular "glare" under certain conditions a high contrast clean latent fingerprint image is present.

Menzel[22] briefly mentioned the possibility of using polarization to detect fingerprint on glass. We have shown that polarization can be used to enhance fingerprint visibility on a wide variety of surfaces, not just on glass. We also show that polarization can be used to remove interfering background pattern that has not been mentioned before. Another advantage of our method is that our method is less affected by the degradation of latent fingerprint over time compared to methods that relies on chemical reactions with the organic residues or water in the latent fingerprint marks. Over time an exposed latent fingerprint mark will lose its water contents via evaporation, and the amino acid components will degrade and its chemical properties change[1-4]. Since our method does not rely on water or detailed chemical composition of the fingerprint mark, our method is less likely to be affected by chemical decomposition. As long as the geometric difference in the surface remains, our method can be used effectively. The example pictures shown were taken up to several weeks after the fingerprint is made (and kept in our lab/office environment undisturbed) and they show little degradation of quality.

Because of a great variety of the latent fingerprints that can potentially be found in very different crime scene all over the world, no single latent fingerprint enhancement method can handle all possible cases. Since every method targets different physical and chemical properties of different kinds of fingerprints, it is often found that applying more than one method on the same surface will unveil different fingerprints for different method, e.g. [18]. Thus the introduction of a new latent fingerprint detection method that uses different physical principles than those used by existing methods and one that will not interfere with other methods should always be beneficial to law enforcement efforts.

Conclusion

We have introduced a novel optical method to detect, enhance and lift the latent fingerprints that are otherwise difficult to see. Such method is non-invasive and so will not interfere with other forensic examinations and will not inflict deleterious side effects on the surface. The equipment required is much cheaper than most other non-contact methods proposed so far. The new method is not applicable to highly porous and absorbing surfaces but works well on most other surfaces. The new method also works on the sticky side of the tape, which is a particularly tricky surface for many invasive methods. The recovered latent fingerprint image has very good quality compared to other existing method. Since it does not interfere with other methods it is advisable to try this method before other methods.

REFERENCES

1. 1. *Advances in Fingerprint Technology, 1 ed.* (CRC Press, Boca Raton, FL, 1994).

2. 2. *Advances in Fingerprint Technology, 2 ed.* (CRC Press LLC, Boca Raton, FL, 2001).

3. 3. C. A. Coppock, *Contrast: An Investigator's Basic Reference Guide to Fingerprint Identification Concepts*(Charles C Thomas Publisher, Ltd., Springfield, IL, 2001).

4. 4. *The Science of Fingerprints: Classification and Uses*(Federal Bureau of Investigation, U.S. Government Printing Office, Washington, D.C., 1984).

5. 5. S. G. Demos and R. R. Alfano, "Optical fingerprinting using polarisation contrast improvement," Electronics Letters **33,** 582-584 (1997).

6. 6. K. H. Fielding, J. L. Horner, and C. K. Makekau, "Optical fingerprint identification by binary joint transform correlation," Optical Engineering **30,** 1958-1961 (1991).

7. 7. W. R. Scott, *Fingerprint Mechanics, a handbook; fingerprints from crime scene to courtroom, 1 ed.* (Charles C Thomas Publisher, Ltd, Springfield, IL USA, 1951).

8. 8. R. D. SR. Olsen, *Scott's Fingerprint Mechanics*(Charles C Thomas Publisher, Ltd, 1978).

9. 9. P. Margot and C. Lennard, *Fingerprint Detection Techniques, 6 ed.* (Institut de police scientifique et de criminologie, Univerite de Lausanne, Lausanne, Switzerland, 1994).

10. 10. B. E. Dalrymple, J. M. Duff, and E. R. Menzel, "Inherent fingerprint luminescence---detection by laser," J. Forensic Sci. **22,** 106-115 (1977).

11. 11. E. R. German, "Computer image enhancement of latent prints and hard copy output devices," in *Proceedings of the international forensic symposium on latent prints,* (Laboratory and Identification Divisions, Federal Bureau of Investigation, Quantico, VA, 1987), pp. 151-152.

12. 12. M. C. Cubuk and S. Saygi, "A rising value in evidence detection: Ultraviolet light," Forensic Sci. Int. **136,** 128 (2003).

13. 13. E. R. Menzel and J. M. Duff, "Laser detection of latent fingerprints-Treatment with fluorescers," J. Forensic Sci. **24,** 96-100 (1979).

14. 14. E. R. Menzel, "Laser detection of latent fingerprints-Treatment with phosphorescers," J. Forensic Sci. **24,** 582-585 (1979).

15. 15. E. R. Menzel and K. E. Fox, "Laser detection of latent fingerprints: Preparation of fluorescent dusting powders and the feasibility of a portable system," J. Forensic Sci. **25,** 150-153 (1980).

16. 16. D. W. Herod and E. R. Menzel, "Laser detection of latent fingerprints: Ninhydrin," J. Forensic Sci. **27,** 200-204 (1982).

17. 17. D. W. Herod and E. R. Menzel, "Laser detection of latent fingerprints: Ninhydrin followed by zinc chloride," J. Forensic Sci. **27,** 513-518 (1982).

18. 18. K. E. Creer, "Operational experience in the detection and photography of latent fingerprints by argon-ion laser," Forensic Sci. Int. **3,** 149 (1983).

19. 19. E. R. Menzel, J. A. Burt, and T. W. Sinor, "Laser detection of latent

fingerprints: treatment with glue containing cyanoacrylate ester," J. Forensic Sci. **28,** 307-317 (1983).

20. 20. R. Pfister, "The optical revelation of latent fingerprints," Fingerprint Whorld **10,** 64-70 (1985).

21. 21. C. J. Lennard and P. A. Margot, "Sequencing of reagents for the improved visualisation of latent fingerprints," Journal of Forensic Identification **38,** 197-210 (1988).

22. 22. E. R. Menzel, *Fingerprint detection with lasers, 2 ed.* (Marcel Dekker, Inc., New York, NY, 1999).

23. 23. D. Maltoni, D. Maio, A. K. Jain, and S. Prabhakar, *Handbook of Fingerprint Recognition*(Springer-Verlag, New York, NY, 2003).

24. 24. R. Schwind, "Zonation of the optical environment and zonation in the rhabdom structure within the eye of the backswimmer, *Notenecta glauca*," Cell and Tissue Research **232,** 53-63 (1983).

25. 25. G. Horváth, "Reflection polarization patterns at flat water surfaces and their relevance for insect polarization vision," Journal of Theoretical Biology **175,** 27-37 (1995).

26. 26. L. B. Wolff, "Relative brightness of specular and diffuse reflection," Optical Engineering **33,** 285-293 (1994).

27. 27. B. E. Dalrymple and T. Menzies, "Computer Enhancement of Evidence Through Background Noise Suppression," J. Forensic Sci. **39,** 537-546 (1994).

28. 28. T. Ko, "Fingerprint enhancement by spectral analysis techniques," in *Proc. of the 31st Applied Imagery Pattern Recognition Workshop*, (IEEE, Washington, D.C., 2002), pp. 133-139.

29. 29. L. B. Wolff, "Polarization camera for computer vision with a beam splitter," J. Opt. Soc. Am. A **11,** 2935-2945 (1994).

30. 30. L. B. Wolff and A. G. Andreou, "Polarization camera sensors," Image and Vision Computing **13,** 497-510 (1995).

31. 31. L. B. Wolff, T. A. Mancini, P. Pouliquen, and A. G. Andreou, "Liquid Crystal Polarization Camera," IEEE Transactions on Robotics and Automation **13,** 195-203 (1997).

32. 32. S.-S. Lin, K. M. Yemelyanov, E. N. Jr. Pugh, and N. Engheta, "Polarization Enhanced Visual Surveillance Techniques," in *Proceedings of IEEE International Conference on Networking, Sensing and Control*, (IEEE Systems, Man and Cybernetics Society, Taipei, Taiwan, 2004),

33. 33. K. M. Yemelyanov, S.-S. Lin, W. Q. Luis, E. N. Jr. Pugh, and N. Engheta, "Bio-inspired display of polarization information using selected visual cues," in *Proceedings of SPIE*, (SPIE-The International Society for Optical Engineering, San Diego, CA, 2003), pp. 71-84.

34. 34. M. P. Rowe, E. N. Jr. Pugh, and N. Engheta, "Polarization-difference imaging: a biologically inspired technique for observation through scattering media," Optics Letters **20,** 608-610 (1995).

35. 35. J. S. Tyo, M. P. Rowe, E. N. Jr. Pugh, and N. Engheta, "Target detection in optically scatter media by polarization-difference imaging," Applied Optics **35,** 1855-1870 (1996).

36. 36. J. S. Tyo, E. N. Jr. Pugh, and N. Engheta, "Colorimetric representation for use with polarization-difference imaging of objects in scattering media," J. Opt. Soc. Am. A **15,** 367-374 (1998).

37. 37. J. S. Tyo, "Optimum linear combination strategy for an N-channel polarization-sensitive imaging or vision system," J. Opt. Soc. Am. A **15,** 359-366 (1998).

38. 38. K. M. Yemelyanov, M. A. Lo, E. N. Jr. Pugh, and N. Engheta, "Display of polarization information by coherently moving dots," Opt. Express **11,** 1577-1584 (2003).

39. 39. R. C. Gonzalez and R. E. Woods, *Digital Image Processing, 2 ed.* (Prentice Hall, Inc., Upper Saddle River, NJ, 2001).

40. 40. J. H. Lambert, *Photometria sive de mensura et gradibus luminus, colorum et umbrae*(Eberhard Klett, Augsburg, Germany, 1760).

41. 41. K. E. Torrance and E. M. Sparrow, "Theory for off-specular reflection from roughened surfaces," J. Opt. Soc. Am. **57,** 1105-1114 (1967).

42. 42. R. L. Cook and K. E. Torrance, "A reflectance model for computer graphics," Computer Graphics **15,** 307-316 (1981).

43. 43. B.-T. Phong, "Illumination for computer generated pictures," Communications of the ACM **18,** 311-317 (1975).

44. 44. J. D. Foley, A. vanDam, S. K. Feiner, and J. F. Hughes, *Computer Graphics: Principles and Practice, 2 ed.* (Addison-Wesley Publishing Company Inc., Reading, MA, 1990).

45. 45. S. K. Nayar, K. Ikeuchi, and T. Kanade, "Surface Reflection: Physical and Geometrical Perspectives," IEEE Transactions on Pattern Analysis and Machine Intelligence **13,** 611-634 (1991).

46. 46. E. Hecht, *Optics, 3 ed.* (Addison Wesley Longman, Inc., Reading, MA, USA, 1998).

47. 47. S. K. Bramble, K. E. Creer, W. G. Qiang, and B. Sheard, "Ultraviolet luminescence from latent fingerprints," Forensic Sci. Int. **59,** 3-14 (1993).

Manuscript Entitled:

"Bio-Inspired, Adaptive Algorithms for 2- Channel Polarization Sensing under Various Polarization Statistics with Non-Uniform Distributions"

Konstantin M. Yemelyanov, Shih-Schön Lin, Edward N. Pugh Jr., Nader Engheta

In preparation for submission to Applied Optics

Bio-Inspired, Adaptive Algorithms for 2- Channel Polarization Sensing under Various Polarization Statistics with Non-Uniform Distributions

Konstantin M. Yemelyanov[1], Shih-Schön Lin[1], Edward N. Pugh Jr.[1,2,3], Nader Engheta[1,3]

[1]Department of Electrical and Systems Engineering, School of Engineering and Applied Science,

[2]F. M. Kirby Center for Molecular Ophthalmology, [3]Institute for Neurological Sciences,

University of Pennsylvania, Philadelphia, Pennsylvania 19104, U.S.A.

Abstract: Polarization of light carries much useful information about the environment. Several biological studies show evidences of certain animal species using polarization information for navigation and other purposes. It has been shown that bio-inspired Polarization Difference Imaging technique can be used to facilitate target detection and feature extraction in scattering media. It has been proven that "Polarization Sum" and "Polarization Difference" signals are the optimum linear combination for a scene with a uniform probability distribution of polarization directions. However in many real environments the scene has non-uniform probability distribution of polarization directions. Using principal component analysis on statistical scene data we developed a method to adaptively determine the two optimum information channels that can be formed as a linear combination of the signals of two original polarization channels. We also determined the optimal orientations of polarization filters that best achieve separation of a target from the background, where the target is defined as an area with distinct polarization characteristics as compared to the background. Experimental results and simulations confirm that adaptive polarization difference imaging outperforms the polarization difference imaging with fixed channels in most situations.

OCIS codes: 260.5430 Polarization, 330.1880 Detection, 330.7320 Vision adaptation, 110.2970 Image detection system, 100.2960 Image analysis

Introduction

Polarization is an intrinsic feature of light that provides valuable information about a scene beyond that provided by the scene's spectral (color) and intensity distributions. Polarized light has been studied extensively since Fresnel's works on the wave theory and the polarization important issue in many areas of modern technology. There are many books about polarized light (see, e.g., [48, 49]). Polarization information has proven useful in several fields, including computer vision, robotics, target recognition, and material classification (see, e.g., [50, 51, 52, 53, 54, and 55]). Polarization parameters, e.g., Stokes parameters, are in general more sensitive to the nature of a scattering surface than the total intensity is [56]. In such case, polarization imaging techniques offer the possibility of producing images having higher inherent visual contrast than conventional image processing of the intensity distribution [50]. Much of work has been devoted to target (particularly, small target) detection utilizing polarimetric properties of media has been done (see, e.g., [56, 57, 58]).

The polarization of light is not discernible to the unaided human eyes [59], but the polarization has been shown to provide valuable information to other species. In 1949, Nobel laureate Karl von Frisch established that honeybees through their perception of polarized light use the sun as a compass through their perception of the polarization pattern of light scattered from the sky [60, 61]. After this von Frisch's primary invent other researchers began to investigate polarization vision and found it in many different species, including fish, amphibians, arthropods, desert ants, and octopuses (see i.e. [63, 64, 65, and 66]). These animals use polarization information in many different ways, e.g. navigation, detecting water surfaces, enhancing visibility (similar to colors), and maybe even for mutual communications [67, 68, 69, 70].

The pattern of polarization in an image of a scene is a potentially rich source of information. While the human eye is "polarization-blind", man-made imaging systems have been developed to collect polarization information from scene. An important issue in polarization imaging is how best to process the polarization information after it is collected by the imaging system. In earlier investigations, we introduced the "Polarization-Difference Imaging" processing, inspired by polarization vision of certain animal species [71, 57]. We demonstrated that optical imaging systems utilizing PDI techniques may facilitate the detection of targets in scattering media even when the polarization signal is rather weak, and that such enhancement can increase by 3-fold the distance over which targets can be detected [71, 57, 72]. We have also investigated the issue of optimal representation of the polarization information to the "polar-blind" human [73, 74].

The idea of an adaptational mechanism in polarization vision is bio-inspired as well. Insects employ a retinal filter consisting of an array of ommatidia (polarization sensitive photoreceptors) that is matched to the polarization pattern of the sky [75]. This filter works as follows: The summed output from all polarization analyzers of the polarization sensitive area reaches a maximum at an optimal match between the receptor array and the celestial pattern. This provides the insect with the information of how to align its longitudinal body axis with the symmetry plane of the sky. In order to find a proper direction, the insect has to change its orientation and perform a "check" of polarization pattern for the each angle of orientation.

Using "matched filter" concepts, we develop here a polarization imaging technique based on the PDI, but "adaptable" to the environmental conditions, i.e., the

polarization "background" of a scene. The proposed polarization-based system adaptively adjusts its parameters to obtain the best possible segregation of targets from the background in a manner dependant on the polarization statistics of the scene.

The paper is organized as follows. In Section 2, we give a brief overview of polarization vision and define the polarization parameters used in the paper. In Section 3, we describe the Adaptive Polarization-Difference Imaging (APDI) algorithm. Section 4 is devoted to validation of the proposed technique, employing both experiments and simulations. In Section 4, we illustrate the performance of the algorithm in target-against-background detection using the experimental data obtained in a natural environment. Finally in Section 5, we propose an APDI based method that may be used in surveillance systems.

Physics of polarization imaging

The polarization of a local field of coherent light source can be represented as a superposition of two mutually orthogonal wave components. A phase difference between these components produce linearly, elliptically, or circularly polarized wave with its polarization direction determined by the relative strengths of the components. Non-coherent light contains large numbers of differently polarized light packets. Since human eyes and most normal camera sensors can only detect the total amount of light energy collected during an exposure time, when the light energy is uniformly distributed over all polarization directions, the detected signal will be the same for any polarization direction. Such light is called "unpolarized" and emitted by most common light sources, including the Sun or man-made incandescent light sources. The local polarization signal at the surface of a sensor (that cannot detect phase information) can in general be described as a combination of unpolarized and completely linearly polarized components.

Assume that we put a perfect linear polarizer in front of a normal polarization-insensitive device, such as a CCD or film camera. Let φ represent the angle that the polarization analyzer makes with reference direction, and the polarization angle $\theta(x,y)$ represents the orientation angle of the major axis of the local polarization ellipse at the image pixel position (x,y). Everywhere in this paper, we use a right hand side direction of the horizon as the reference direction and angles increase counter-clockwise. The observed pixel intensity $I(x,y)$ can be described as:

$$I(x,y,\varphi) = I_U(x,y)\left\{1 + p(x,y)\cos\left[2\left(\theta(x,y) - \varphi\right)\right]\right\}, \tag{12}$$

where I_U is the intensity of the unpolarized component, and p is the degree of linear polarization. The parameter p, the "degree of linear polarization", is defined as a ratio of the linearly polarized component I_p to the unpolarized component I_U: p varies between 0 and 1, where $p = 0$ corresponds to unpolarized light, and $p = 1$ corresponds to completely linearly polarized light. These three parameters, i.e., I_U, p, and θ, extracted for each pixel (x,y) of the image, provide a complete set of parameters that enable reconstruction of the scene image intensity distribution when view through at any given angle φ of orientation of the polarizer.

At each pixel of the scene the polarization (and intensity) of the impinging light is characterized by three independent parameters: thus, in order to provide the viewer with complete information about the polarization features of the object, at least three measurements of light intensity at different angles φ are required. These measurements can be made either simultaneously by three light intensity sensors (e.g., specially designed three CCD cameras) when each sensor has its polarizer set at a different angle, or sequentially by one single light intensity sensor changing the orientation of the single polarizer between the measurements. It is not our main goal to perform a detailed comparison of both methods in this paper. However, it is worth mentioning that our computational algorithm can be used with either measurement method after proper calibration.

Consider having three images of the scene, i.e., I_0, I_{45}, I_{90}, corresponding to three angles of orientation of the linear polarizer, namely, $\varphi = 0^\circ$, 45° and 90° with respect to the reference direction, we can calculate I_U, p, and θ at each image point as follows:

$$
\begin{aligned}
I_U(x,y) &= \left[I_0(x,y) + I_{90}(x,y)\right]/2 \\
p(x,y) &= \left[\left(1 - \frac{I_{45}(x,y)}{I_U(x,y)}\right)^2 + \left(1 - \frac{I_{90}(x,y)}{I_U(x,y)}\right)^2\right]^{1/2} \\
\theta(x,y) &= \arctan\left[\frac{I_U(x,y) - I_0(x,y)}{I_U(x,y) - I_{45}(x,y)}\right]
\end{aligned}
\tag{13}
$$

Once the parameters I_U, p, and θ are computed at each pixel of the scene image, we can reconstruct the image intensity for any angle φ using Eq. (12), even though no actual pictures are taken with a polarizer oriented at φ [51].

The concept of Adaptive Polarization-Difference Imaging (APDI)

Inspired by abilities of visual systems of certain animal species to sense polarization information, in the earlier works of our research group we introduced [57, 71, 72] and developed [73, 74] the concept of Polarization-Difference Imaging (PDI). The proposed PDI system [71] captures images of a scene at two orthogonal linear polarizations. For each pixel, located at (x,y), one gets a pair of image intensities, i.e., $I_0(x,y)$ and $I_{90}(x,y)$ taken at 0° and 90° orientation of the polarizer, respectively. The "Polarization Sum" (PS) and "Polarization Difference" (PD) signals can then be computed by the following way:

$$
\begin{aligned}
{}_{PS}I(x,y) &= I_{90}(x,y) + I_0(x,y) \\
{}_{PD}I(x,y) &= I_{90}(x,y) - I_0(x,y),
\end{aligned}
\tag{14}
$$

For an ideal linear polarization analyzer the PS image is equivalent to a conventional intensity image. Equations (14) can be more conveniently presented in matrix form:

$$\begin{bmatrix} {}_{PS}I \\ {}_{PD}I \end{bmatrix} = T \begin{bmatrix} I_{90} \\ I_0 \end{bmatrix}, \tag{15}$$

where the transformation matrix

$$T = \begin{bmatrix} 1 & 1 \\ 1 & -1 \end{bmatrix} \tag{16}$$

has the eigenvectors of the covariance matrix for the uniform polarization distribution as rows [76].

Using Principal Component Analysis (PCA) [80], Tyo has shown (see Ref. [76]) that PS and PD signals produce the optimum linear combination: thus the principal components (PCs) for a scene in which the polarization angle has a uniform distribution are two independent (orthogonal) channels, e.g., $I_0(x,y)$ and $I_{90}(x,y)$. The analysis and conclusion in [76] were made based on the analogy with the biology of color vision in the human visual system and related principle component analysis done by Buchsbaum and Gottschalk [78]. In their scenario the PS and PD channels were optimum in the information theory sense, i.e., their contents were statistically uncorrelated, thus requiring minimum bandwidth [78]. However, the situation may differ when the polarization angle of the pixels of a scene has a non-uniform distribution. What would then be the optimum linear combination for polarization channels in this case? Which criterion of "optimality" is applicable in this case? Answering these questions is the goal of or study.

Consider the general case such that the probability density function of polarization angle distribution is arbitrary one. Assume that a pair of images each with $M \times N$ pixels have been taken with two different orientations (not necessarily orthogonal) of the polarization analyzer, i.e., $I_1 = I(\varphi = \varphi_1)$, and $I_2 = I(\varphi = \varphi_2)$. We are interested in choosing the "optimal" pair of orientation angles of the two channels as well as the "optimal" weighting coefficients of the two channels to form a "Polarization-Opponent" image. The criterion of the "optimality" will be discussed below. We call the new computed pair of images "principal component" (PC) images.

The covariance matrix $\mathbf{C}$ of the two images is defined as follows

$$\mathbf{C} = \begin{bmatrix} E[I_1 I_1] - E^2[I_1] & E[I_1 I_2] - E[I_1]E[I_2] \\ E[I_1 I_2] - E[I_1]E[I_2] & E[I_2 I_2] - E^2[I_2] \end{bmatrix}, \tag{17}$$

where:

$$E[W] = \frac{1}{MN} \sum_{m=1}^{M} \sum_{n=1}^{N} W(x_m, y_n) \tag{18}$$

is the mean value taken over the ensemble of pixels in the polarization images. Parameter W is equal to $I_1 = I(\varphi = \varphi_1)$, $I_2 = I(\varphi = \varphi_2)$, or a product of thereof. Once eigenvalues (λ_1, λ_2) and the eigenvectors (v_1, v_2) of the covariance matrix $\mathbf{C}$ (17) are determined, the

transformation matrix which has eigenvectors as rows can be formed as follows:

$$T_A(\varphi_1,\varphi_2)=\begin{bmatrix}-\beta & \alpha\\ \alpha & \beta\end{bmatrix} \tag{19}$$

Here α and β are the components of the eigenvectors. The signs of α and β may be either positive or negative. The transformation matrix is formed in such a way that the first eigenvector corresponds to the largest eigenvalue. With the "adaptive" transformation matrix (19) thus determined, the corresponding "PC" images are computed as follows:

$$\begin{bmatrix}PC_1\\ PC_2\end{bmatrix}=T_A(\varphi_1,\varphi_2)\begin{bmatrix}I_1\\ I_2\end{bmatrix}. \tag{20}$$

Thus using Equations (20) we compute a pair of "adaptive" images, PC_1 and PC_2, based on any pair of real images taken at two orientations (may be identical) of the polarization analyzer, I_1 and I_2. The transformation matrix T_A is a function of the two polarizer angles and the correlation between the two real scene images taken at these two polarizer angles. In other words, T_A is "adapted" to the polarization distribution in the scene. In the previous "non-adaptive" PDI [76], [77], the transformation matrix was fixed (see [76]), as in (16) and not a function of the scene. By analogy with the transformation matrix of Tyo's "conventional" PDI system, we consider that the first PC (PC_1) the "adaptive" analog of the PS signal, and the second PC (PC_2) the "adaptive" analog of the PD signal. Our surmise was that by analyzing the second PCs of the given scene, certain important features, e.g. presence of target on a complex background, will be revealed.

In course of simulations we have synthesized the images for all the combinations of the two polarizer orientations where the angular orientation of the polarizer is within the range from 0 to 180 degrees with 5 degrees step (φ and φ+180° are indistinguishable cases since normal cameras cannot detect the phase information of light waves). For each pair of "non-target" images corresponding to the two different orientations of polarization analyzers (φ_1,φ_2) we obtained a full set of polarization parameters, i.e., $\alpha=\alpha(\varphi_1,\varphi_2)$, $\beta=\beta(\varphi_1,\varphi_2)$, $\lambda_1=\lambda_1(\varphi_1,\varphi_2)$, and $\lambda_2=\lambda_2(\varphi_1,\varphi_2)$. It should be noted that $\alpha=\alpha(\varphi_1,\varphi_2)$ and $\beta=\beta(\varphi_1,\varphi_2)$ always have the same shape and have theirs maximum and minimum values for the same pair of angles (φ_1,φ_2). In addition, maximum value of α and minimum value of β being taken by absolute value are equal (the same is true for minimum value of α and maximum value of β), i.e. $|\alpha_{\max}|=|\beta_{\min}|$ and $|\alpha_{\min}|=|\beta_{\max}|$.

It is reasonable to assume that the optimal pair of angles will be those with corresponding extreme eigenvalues or adaptive coefficients. Thus, we have the following three cases to consider, i.e., the pairs of polarizers' orientations:

1. The pair that maximize/minimize the adaptive coefficients α or β,

2. The pair that maximize/minimize the eigenvalues,
3. The pair of angles which has a preferential angle of the background polarization as a bisector.

The last case is solely intended for comparison between the conventional PD algorithm and our new adaptive algorithm.

For the target-detection purposes, the ideal choice of optimal angles should yield a PC image such that the variance in background pixel intensities are as low as possible while the variances in the target pixel intensities are either at their original value or at a higher value. A known trivial solution to achieve such condition is to subtract images corresponding to angles obtained by adding and subtracting 45 degrees to the preferential angle of the background's polarization. As the previous study indicates [57], selecting a pair of angles that are $\pm 45^{\circ}$ from the angle of the preferential polarization of the background eliminates the latter and reveals the target against it. It has been also proven [76] that for a case of a uniformly polarized background, this pair of angles is the optimal one with the corresponding adaptive coefficients $\alpha = -\beta = 1/\sqrt{2}$, and the images they yield (i.e., PS and PD) are the principal components of the scene. In the case of a non-uniformly polarized background, however, such a simple solution does not produce the desired result. Our extensive simulations on various computer-generated targets have shown that if the standard deviations of the polarization parameters are high enough, the optimal set of coefficients is different from those corresponding to the uniform case, and the background was not cancelled. Thus, there is a need for a more general tool which can be used for scenes with non-uniform polarization distributions. Our study proves that more sophisticated and time consuming calculations than a simple subtraction (case #3) are necessary to detect target in a non-uniformly polarized environment.

The eigenvalues λ_1 and λ_2 as functions of φ_1 and φ_2 are symmetric with respect to bisector line $\varphi_1 = \varphi_2$. Both the maximum and the minimum values of λ_1 are located on this line as well. This presents a degenerate case when both polarizers' angles of the two source images have the same orientation and is obviously not useful. Therefore, case #2 is reducing to analysis of behavior of only smallest eigenvalue, i.e. λ_2. The value of λ_2 presents the variance in the PC_2 image and that could imply that more interesting information can be obtained from the PC_2 image. We focused our study on cases #1 and #2, and the results were compared with those obtained for case #3, which represents the conventional PDI technique.

Validations of the APDI Algorithm and the Selection the Optimal Set of Parameters

For the verification of the APDI algorithm we conducted several sets of experiments and simulations. The first set of images was taking in our laboratory – a controlled environment with the illumination conditions maintained unchanged. This enabled an accurate calculation of sensitivity index in the context of target detection. The target was a specially designed object with known distinct polarization properties, and the background was kept simple though still exhibited non-uniform polarization statistics. The second set of images was taken with real-life targets under natural (sun light) illumination.

Experimental setup in the laboratory

The laboratory experimental setup and a specially manufactured target are shown in

Figure 1. Incandescent 150 W lamp was illuminating the cylindrical Plexiglas tank (12" height and 16" in diameter) from a side. The tank was filled with a solution of a 10 mL of whole milk diluted in approximately 27 L of water. The height of the water level in the tank was 21 cm. This created a model of dispersive media (such a method of simulation of scattering media was originally used by Tyo [57]). In order to produce Lambertian type illumination, an opal glass diffuser was placed between the tank and the light source. The target was an aluminum disk with 5.1 cm in diameter. The target surface was sandblasted and there were seven 1-cm^2 square patches attached to it (see Figure 1b). The six outer patches were abraded with emory paper in such a way, that they formed three orthogonally oriented pairs, i.e., 0° and 90°, 30° and 120°, 60° and 150° (with respect to the vertical axis). Patches with orthogonal directions in the scratches are located symmetrically with respect to the vertical axis. The surface of the center patch was sandblasted the same way as the base plate surface. The patches were raised a few mils from the base plate surface. The target was attached to the Plexiglas plate and facing up. The distance between the surface of the water ant the plane of the aluminum disk was 55 mm. The target was observed by Olympus E-10 SLR digital camera with Sunpack® 62 mm diameter circular glass polarizer attached in front of it. The images were taken sequentially for three different orientations of the polarizer, i.e., 0°, 45°, and 90° degrees by rotating the polarizer between shots. The time required to capture all three images was less than 10 seconds. The same Olympus digital camera and polarizer were used in our experiments in the natural (uncontrolled) environment.

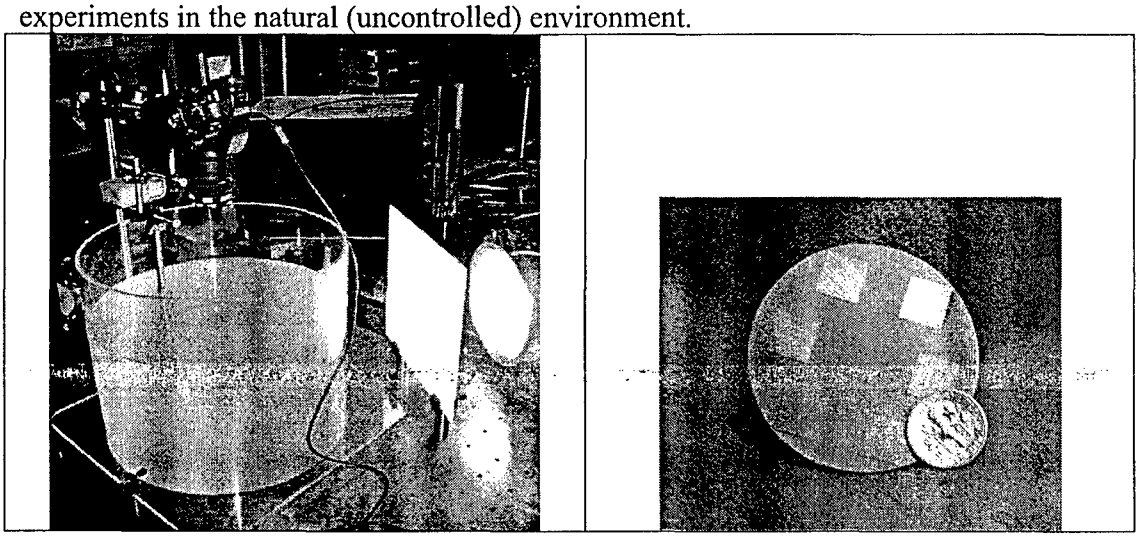

a) *b)*

Figure 1. Layout of the experimental setup: *a)* Photograph of the setup, *b)* 7-patch target together with a US 10 cent, "dime", coin.

All computer simulations in this study have been done using "The MathWorks MATLAB®" software package with its "Image Processing Toolbox". The captured images were stored in Olympus Raw Format (ORF), which gave us "raw" images of the scene, without any enhancements and modifications that most commercial digital cameras perform internally to make pictures "look better". The Olympus E-10 has a single chip color CCD with RGGB Bayer primary color filter. For our computations, we extracted the R, G, and B components of RGB (red-green-blue) output directly from the

RGGB Bayer filter pattern response, so that the image had only ¼ the total number of active pixels of the CCD chip (the G image is an average value of the two G filter responses). This transformation has been done by a specially written MATLAB® code. The "adaptive" algorithm may be applied to a pair of images representing one of the components (either R, G, B or V). The V (luminance) component of the HSV (hue-saturation-value) was computed by the MATLAB® Image Processing Toolbox and was, in fact, the maximum value of the R, G, or B channel at every pixel. In this paper we present results which were obtained based on the V component of the images.

The camera zoom was adjusted in such a way that the area occupied by the aluminum disk was only a portion of the target scene. In order to obtain of the "background" scene, we simply removed the aluminum disk from the scene while keeping all other experimental conditions including focusing distance of the camera intact. The original image was cropped to 800 by 600 pixels size to decrease the memory consumption. The polarization statistics of the background scene are shown in Figure 2. The histograms of the polarization parameters reveal an essentially non-uniform distribution of the polarization statistics of the scene with the average degree of linear polarization of about 25%.

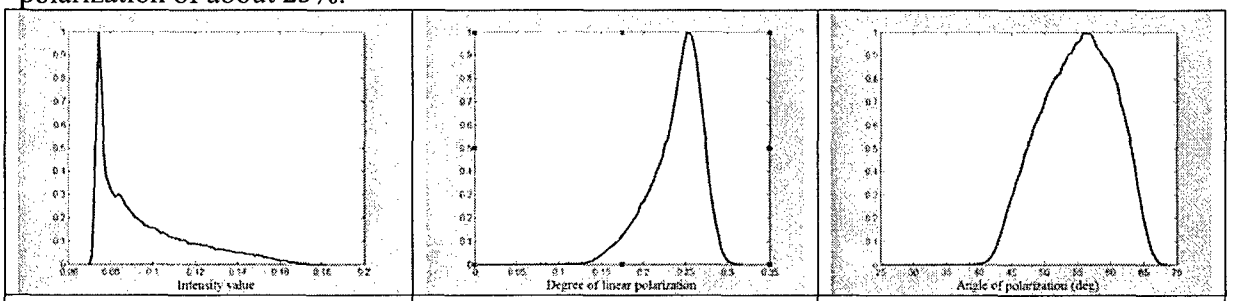

a) *b)* *c)*

Figure 2. Normalized histograms of polarization parameters of the background: A) Unpolarized pixel intensity, I_U ; B) Degree of linear polarization, p ; C) Angle of polarization, θ .

The APDI algorithm was applied to each "target-background" pair, and PC_1 and PC_2 images for all three cases described above were computed. The adaptive parameters corresponding to the cases under consideration are shown in Table 1.

Table 1 Adaptive parameters corresponding to the cases considered for the benchmark target

	θ_1, deg	θ_2, deg	α	β	$\lambda_1 \times 10^{-3}$	$\lambda_2 \times 10^{-5}$
Case #1	145	55	0.895	–0.446	1.116	0.611
Case #2	95	5	0.680	–0.733	1.005	3.447
Case #3	100	10	0.707	–0.707	1.004	3.327

The images of first and second principal components for all three cases are presented in Figure 3. Images of PC_1 for all selected cases look very similar and non-uniform illumination of the scene is clearly visible. Images of PC_2 in panels *b*) and *c*) of Figure 3 are similar because the pairs of angles for cases #2 and #3 are close to each other as well as adaptive parameters (see Table 1). While PC_2 image corresponding to case #1 (Figure 3*a*) is significantly different: fringes of the disk are clearly outlined and direction of

scratches in all patches are distinguishable. This is achieved due to intrinsic properties of the APDI algorithm, i.e., decreasing variance in the background of the scene. All images in Figure 3 are stretched to cover 8-bit display. In order to better represent relative difference in intensity levels between target region ant the background, we treated each PC image as a 3-dimentional surface, where the pixels' coordinates were given by x and y, and the level of intensity in each pixel was counted along z axis. The relative difference in intensity levels could be shown better if those surfaces were projected to xz plane with the observation point being located in the same plane. Such surfaces of PCs for all three cases are shown in Figure 4, where horizontal axis is the largest dimension of the image and the vertical axis gives raw values of pixels' intensities. Comparing pictures in the right column in Figure 4, one may notice that in panel *a*) variance in the background of PC_2 image is much smaller (from two to three times) than those in other panels. The region where the disk is located is noticeably segregated from the surrounding part of the image in panel *a*, while having the same range of variation in background and target regions for panels *b* and *c*. Thus, the case #1 may be a candidate to provide an "optimal" set of adaptive parameters. Pictures of PC_1 (left column in Figure 4) are very similar and no easily noticeable changes between different cases takes place. This is in agreement with the images of PC1 shown in left column of Figure 3.

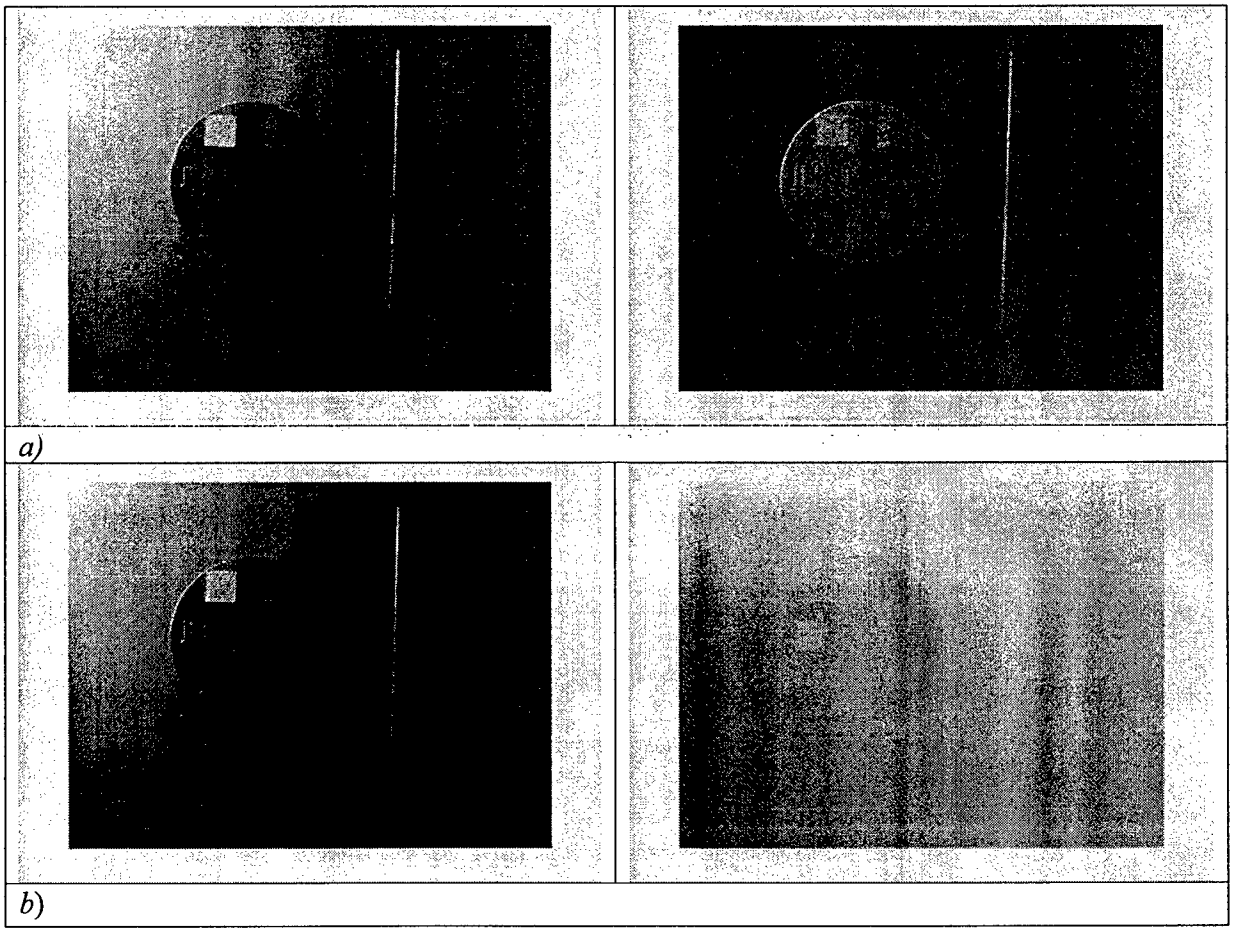

a)

b)

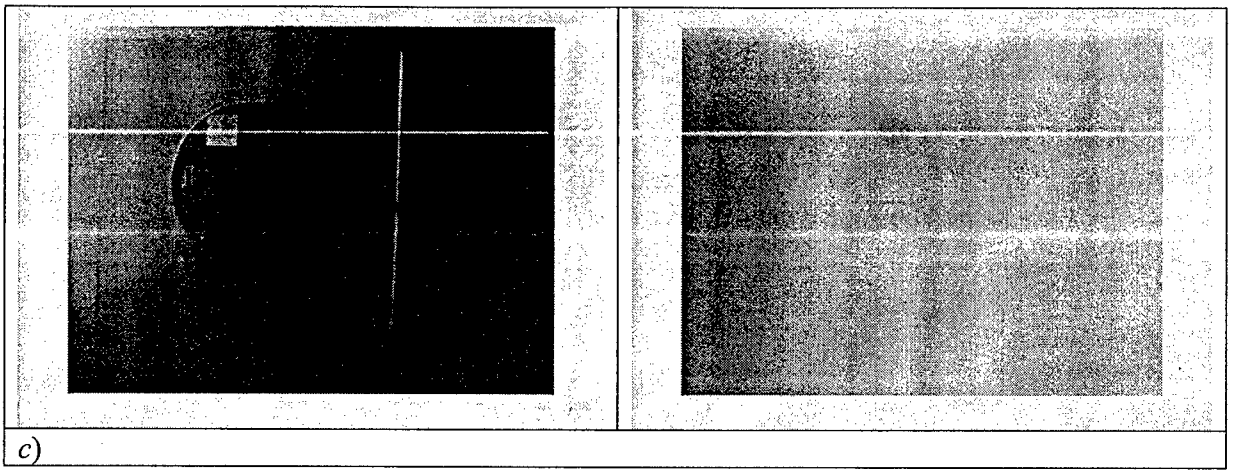

c)

Figure 3. Principal components of the scene corresponding to three cases of interest. Left column show PC_1, and right column PC_2 images, respectively. Panels *a*), *b*) and *c*) correspond to cases ## 1, 2, and 3, respectively. All images are linearly rescaled to exploit all the 8-bit displayable range.

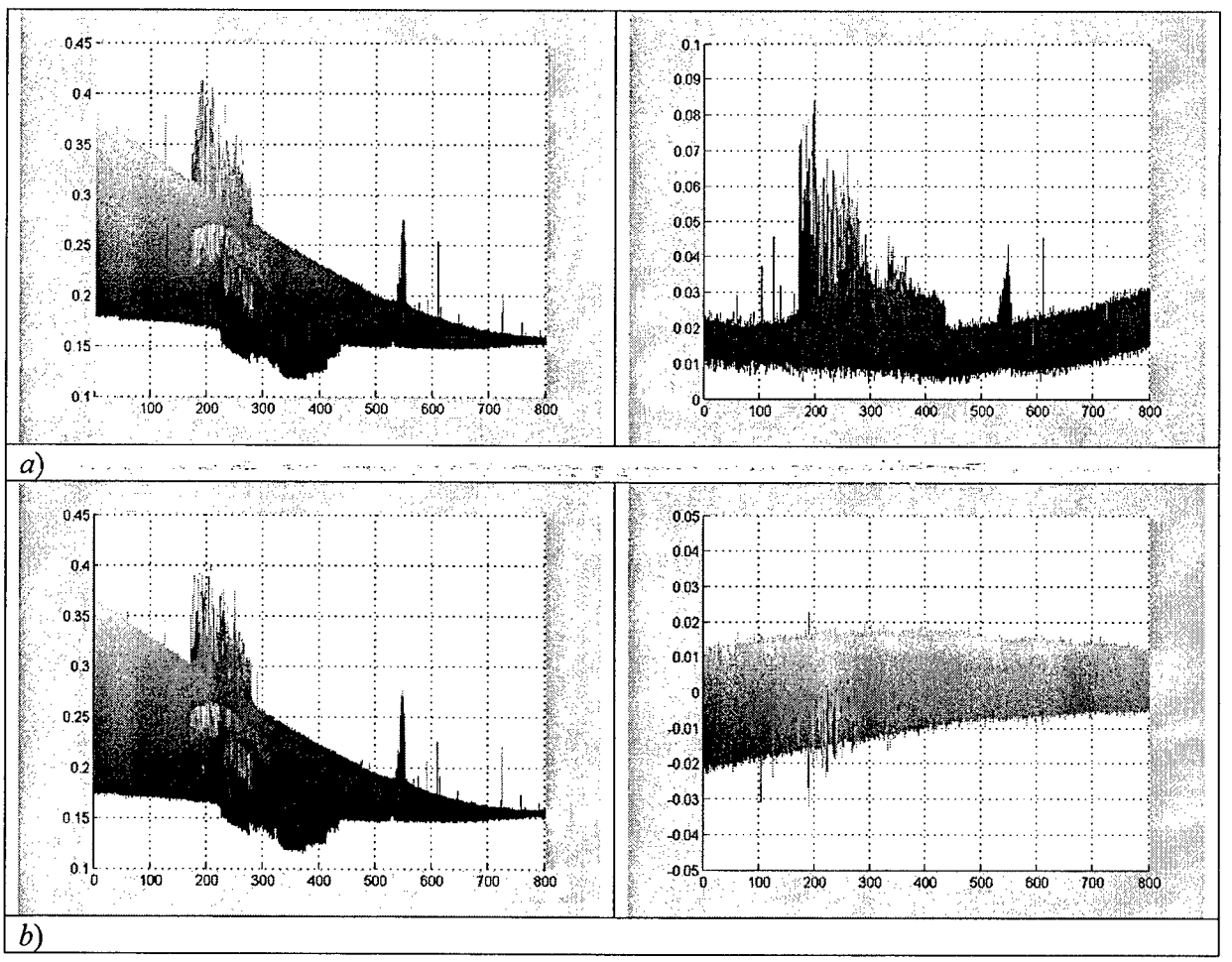

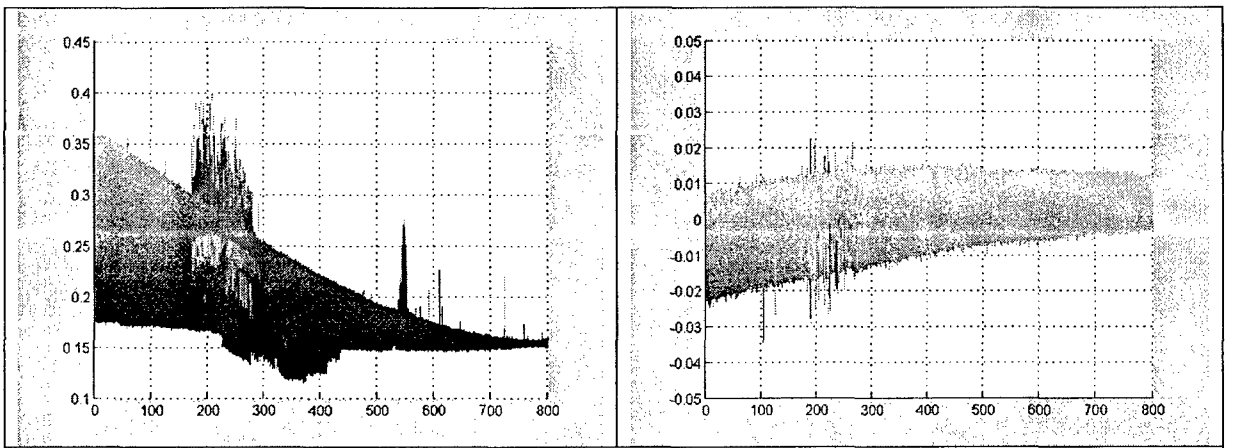

c)

Figure 4. Left panels show PC_1, and right – PC_2, respectively (shown as images in Figure 3). Each image presented as 3-D surface with pixels' intensities along z axis is projected on xz plane.

Performance evaluation: Sensitivity index

A consistent evaluation of the effectiveness of the target detection is important for this study. In addition to the subjective evaluation of the resulting images by human viewers, we also employ a more objective numerical evaluation. In this section, we present a concise description of the numerical evaluation method we use: the sensitivity index calculation. The sensitivity index is an instrument of Signal-Detection Theory (SDT), which is a measure of an observer's ability to discriminate a target from a background [79]. When the "signal-and-noise distribution" is detectably different from "noise-alone-distribution", the mean values of the two distributions are separated by a certain distance d_a, called the sensitivity index. The mean values are calculated over a series of sequential responses (separated in time) of the observer on the visual stimuli to be detected against the noise. With the increase of d_a, the number of correct decisions is expected to increase for any given decision process since the amount of overlap between the distributions is expected to increase. In our study as the "signal-and-noise distribution" we consider the scene distribution including both the target and the background area, and the "noise-alone distribution" as the scene distribution without the target area.

For the sensitivity index calculations, we have done a sequence of scene intensity measurements with temporal separation 3 minutes between the sets. The experimental setup was described in the previous subsection. We have taken 20 sets of images (each consisting of three images for different polarizer's orientations) of the background and 20 sets of images of target scenes.

The evaluation of the sensitivity index was made on the arbitrary chosen two square regions of 5 by 5 pixels each located on the target surface as shown in Figure 5. For each pair of the background and the target scenes, the average intensities inside the referenced regions in PC_1 and PC_2 images were calculated. As a result, we ended up with the two arrays of 20 points each corresponding to the cases we have considered. For each set of 20 points we have calculated the mean value and the standard deviation and

obtained a value of sensitivity index as:

$$d_a = \frac{\mu_T - \mu_B}{\sqrt{\left(\sigma_T^2 + \sigma_B^2\right)/2}}, \qquad (21)$$

where μ_B and σ_B^2 are the mean and the variance of the background scene, μ_T and σ_T^2 are the mean and the variance of the "target" scene (which contains both the background and the "target" object) [79].

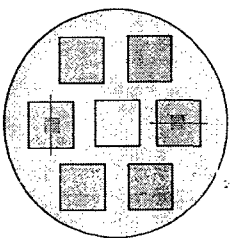

Figure 5. The scheme of the specially created target with regions used for the sensitivity index calculation marked in blue color. Red lines identify the direction of scratches in the specific patch. The left side region is referred to as "region one", and the right side region is referred to as "region two", respectively.

Thus the values of the sensitivity index for PC_2 images corresponding to the three cases considered were the following: $d_a = 1.703$ and $d_a = 1.687$, $d_a = 0.772$ and $d_a = -1.371$, $d_a = 1.419$ and $d_a = -0.908$, respectively. Here the first value of d_a in a pair corresponds to the left-hand side region (see Figure 5) and the second value to the right-hand side region, respectively. Estimations of the sensitivity indices for different cases show that the APDI algorithm provides the higher rate of target-against-background distinction then conventional PDI technique. A significantly larger value of sensitivity index for the principal component generated using the maximum adaptive coefficients gives an idea that such coefficients might be corresponding to the *optimal* pair of angles.

The sensitivity of the APDI algorithm to the rotation of the optimal pair of angles

The APDI algorithm may be used as an effective tool in a visual surveillance system. An important issue in this application is: "how sensitive are the adaptive pairs to rotation of the polarization channels?"

Assume that using the APDI technique an optimal set of adaptive parameters was found. Consider then the optimum pair was rotated by certain angle clockwise or counter-clockwise. Would it be possible to obtain the PC_2 image of the same quality? The simulation on the sensitivity of the adaptive algorithm use the same set of experiment data as described in the previous section. The adaptive coefficients were applied to the pair of images corresponding to angles rotated by 5 and 10 degrees counter-clockwise from the optimal pair (case #1). In Figure 6 we present both the images of PC_2 and their corresponding surface plots projections. Panel *a*) is the same image as those in Figure 4*a*, panels *b*) and *c*) show PCs obtained by rotating the optimal pair of angles by 5 and 10 degrees, respectively. Comparison between panels in Figure 6 reveals that by rotating the

optimal angle pair, both the background level and its variance are increasing while the intensity level of the target is staying on approximately the same level. This can be shown in the histograms of the PC2 images (see Figure 7).

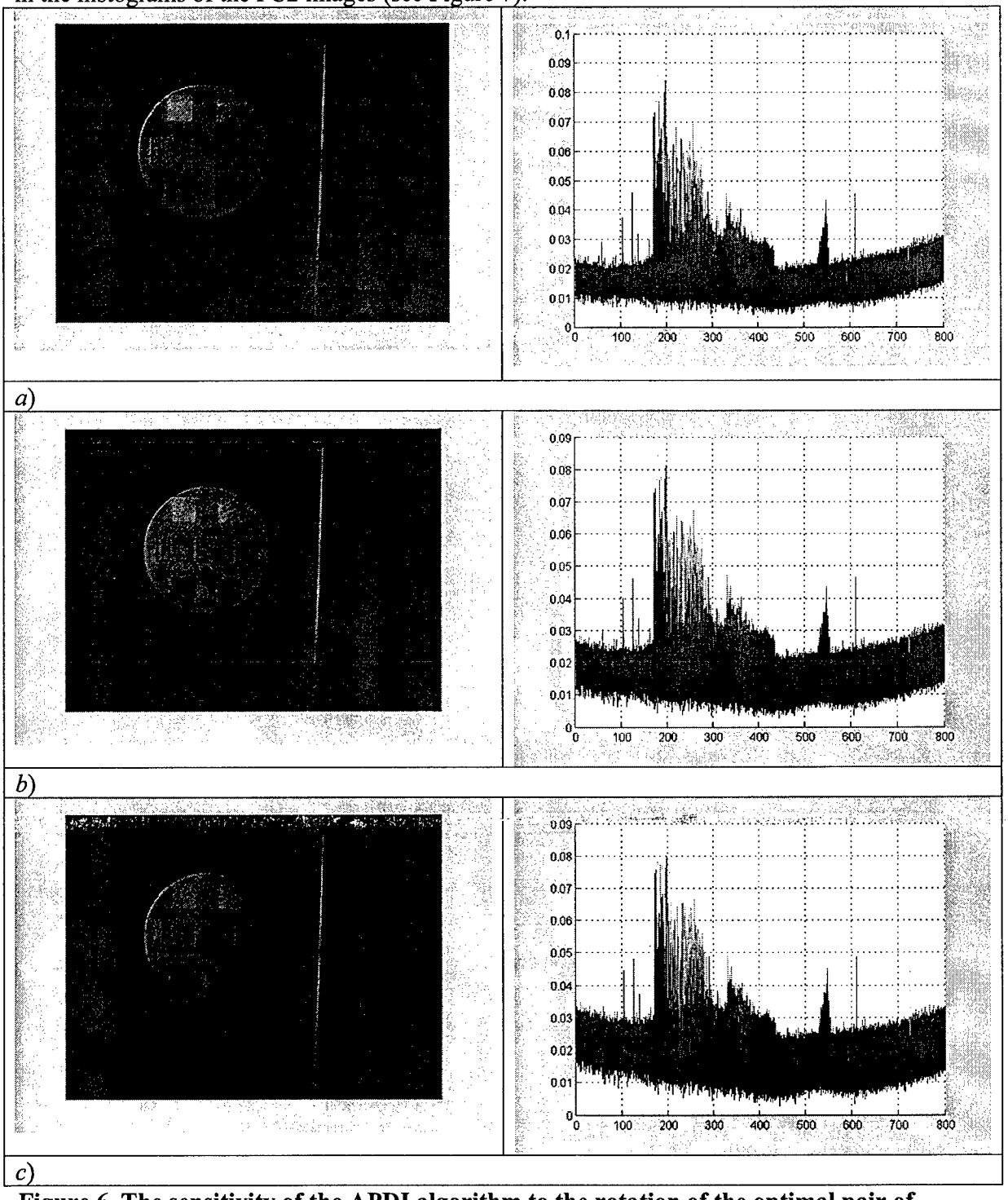

Figure 6. The sensitivity of the APDI algorithm to the rotation of the optimal pair of angles by 5 and 10 degrees counter-clockwise. Panels a) shows same PC_2 image as in Figure 3a; Panels b) and c) show images obtained by rotating the optimal pair by 5

and 10 degrees counter-clockwise, respectively. Left column shows PC_2 images stretched to cover 8-bit display range. Right column shows PC_2 images as 3-D surfaces projected to xz plane, where z axis gives pixels' intensity value.

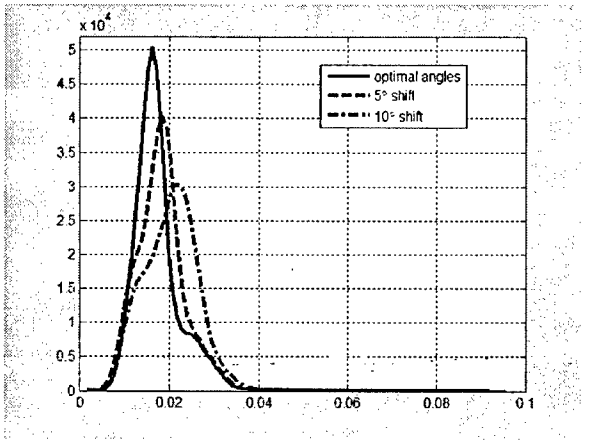

Figure 7. Histograms of the PC_2 images shown in Figure 6. Increasing of variance in the PC_2 with rotation of the optimal pair of angles is shown.

Target Detection against a Non-Uniformly Polarized Background under Natural Illumination Conditions

In addition to the experiments in the lab, we performed several experiments under the natural illumination conditions. Every experiment session include capturing three images of both the background scene and the target scene. Unlike the lab experiments, where the background is mostly a uniform scene, here the background is a relatively complex one, and contains several different objects.

The first experiment presented here was done inside the Levine Hall of the University of Pennsylvania. The images for this experiment show the stone floor surface of the hall. The scene consisted of the shadow region formed on the floor by the combined shadows of an upright standing person and the window frame. The rest of the scene was illuminated by the sunlight passing through the window glass. The camera was located opposite to the window and elevated above the floor, thus the scene was illuminated by sunlight in such a way that the light beam coming from the sun and a beam reflected from the scene formed the same plane. The floor was of mainly dark grey color with a broad pattern. The "target" object was a translucent plastic CD case. We took three images of the background and the target scenes. The camera settings were kept the same for both the background only image sets and the image sets with the target in the scene. Figure 8 shows three polarization components (I_U, p, and θ) for both the background and the target scenes placed side-by-side for easier comparison. Figure 8 shows that the target object has lower degree of polarization than surrounding background.

Using our adaptive algorithm, the optimal pair of angles are found to be $\varphi_1 = 140^\circ$ and $\varphi_2 = 50^\circ$, and the adaptive coefficients are $\alpha = 0.9965$ and $\beta = -0.0834$. The histogram of the background angle of polarization shows that the preferential angle of

polarization of the background is approximately $\theta_B = 140^\circ$, which means that the optimal angle pair is the angle of preferential polarization and the angle orthogonal to it. Both the maximum and the minimum angles corresponding to the largest eigenvalue are found in the bisector line of eigenvalue surface, where λ_1^{max} is located at the point $\varphi_1 = \varphi_2 = \theta_B$, and λ_1^{min} is located at the point $\varphi_1 = \varphi_2 = \theta_B \pm 90^\circ$. This information is very useful: if the preferential polarization angle is known a priori then the optimal angle pairs can be found directly without time-consuming computation. On the other hand this can be an effective way to recover the preferred polarization direction in a scene.

Comparing the principal component images of the scene (see panels *b*) and *d*) in Figure 9) one may see a significant improvement in the target/background contrast of the second principal component image over the conventional PD image. In order to have a complete comparison, we included also images that correspond to the pair of angles bringing the smallest eigenvalue to the maximum (case #2), i.e., consider images with the minimum variance in intensity. For this experiment, the maximum value of λ_2 are found at $\varphi_1 = 105^\circ$, $\varphi_2 = 15^\circ$ and the corresponding coefficients are $\alpha = 0.5016$, $\beta = -0.8650$. Principal component images created in this case are also presented in Figure 9 (panels *g*) and *h*)). Although an improvement over the conventional PD image is noticeable (comparing panels *d*) and *h*) in Figure 9), the *optimal* pair of angles yields better results.

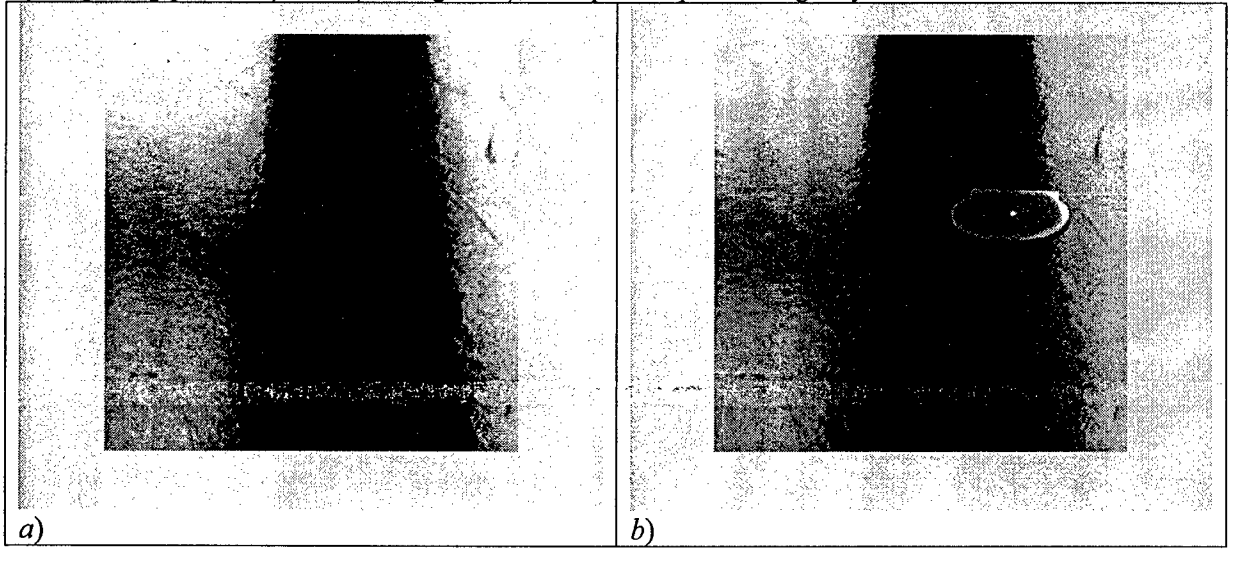

a) *b*)

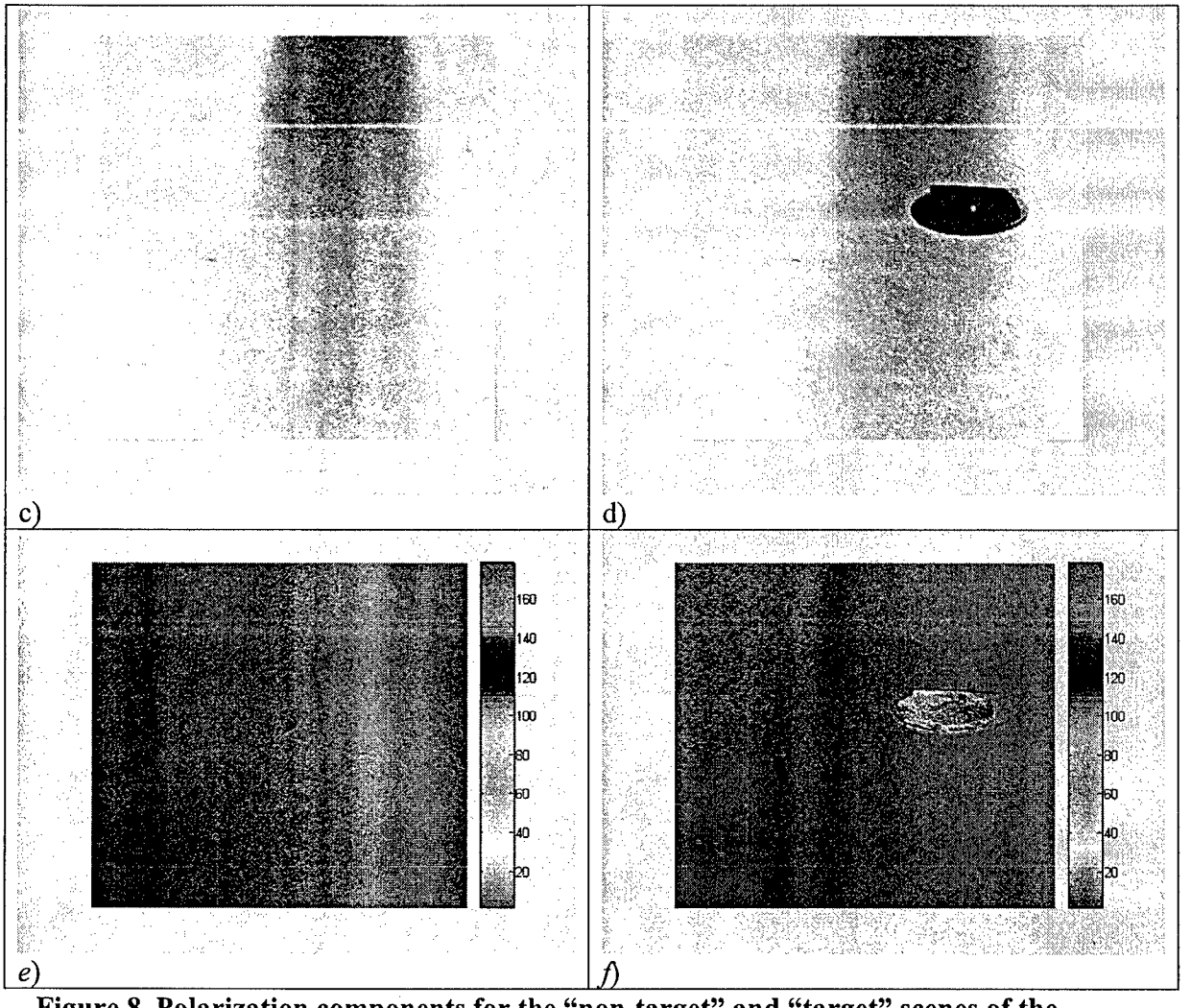

Figure 8. Polarization components for the "non-target" and "target" scenes of the experiments under natural lighting. The left panel shows I_U, p, and θ (top to bottom) image of the "non-target" scene, and the right panel shows those for the "target" scene. The I_U plots in both cases are linearly rescaled to use the full 8-bit grayscale display range.

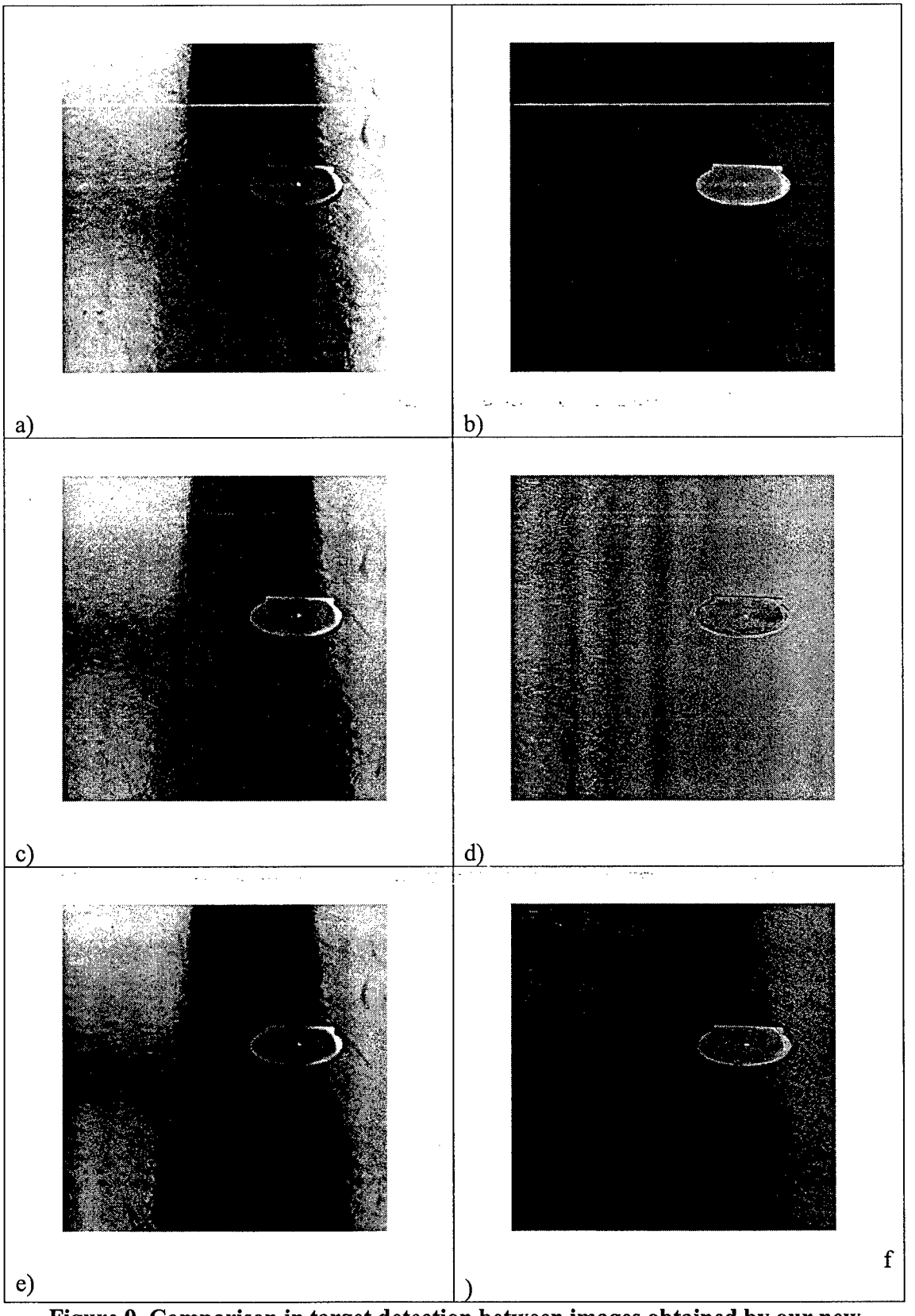

Figure 9. Comparison in target detection between images obtained by our new

adaptive algorithm and by the conventional PDI algorithm. They are the principal components images obtained from the images shown in Figure 8. Panels a) and b) are PC_1 and PC_2 of the scene. Panels c) and d) are conventional PS and PD images. Panels e) and f) are PC_1 and PC_2 corresponding to the maximum value of the smallest eigenvalue. All images were linearly rescaled to cover 8-bit gray level display range.

A few additional notes should be added. Since APDI algorithm deals with the statistics of the observing scene, if the target occupies only a small portion of the scene adaptive coefficients and optimal pair of angles obtained from statistics of the "background scene" differs from those obtained from the statistics of "target scene" only at higher digits after coma. Thus APDI algorithm may be applied to the target scene directly without gathering additional information from the background. If the size of the target object is larger than a certain threshold level, the complete set of measurements required to segregate the target object from the background. Although in our study we dealt with the scenes which had a non-uniform distribution in polarization parameters, the polarization angle of the background had only one preferential direction of polarization. If the scene has two or more regions of significant area which have different angle of preferential polarization certain improvement may be required, such as segmentation of the scene based on its polarization statistics. These results will be reported in our next paper.

Using the APDI in Polarization Assisted Surveillance System

Based on the computer simulations and experiments presented above we propose our new algorithm to be used for target-detection purposes. The initial optimal angles may be selected such that one of the angles is equal to the preferential polarization angle of the background and the other angle chosen to be orthogonal to the preferential angle. In order to make sure that the selected optimal pair is the right one, the calculations of adaptive coefficients in a few points (maybe two or three) around the selected point should be performed. The pair with the maximum values of the coefficients are then used as the optical angle pair. This way we avoid the most costly computational process and significantly decrease the computational time which is very important for real-time applications.

In previous works of our research group we already mentioned a polarization-assisted panoramic surveillance system utilizing the omni-directional mirror [81]. That system processed the polarization information of the scene and used our novel mapping techniques [74] for presenting the information to the human observer. The new APDI algorithm proposed in this work will be combined with the omni-directional system to function as a powerful polarization based omni-directional surveillance system.

The surveillance system will operate by the following scheme. First the camera system will gather information about the scene assuming that all objects in the observation field belong to the background. This set of images, will be stored to form a database. The adaptive coefficients are computed based on the information stored in the database. The next series of images, e.g., 20 more images, will be considered as the "target" images and have adaptive coefficients applied to them. At the same time these images will substitute the initial set of background images and will be used for calculating the next set of adaptive coefficients if it is found that there is no target in them. This process will be repeated. The number of images used in the set may vary

depending on the need of specific applications and may be adjusted by an operator. Such a system will provide the operator with an enhanced view of the scene and helps him to track the appearance of the new "target" objects.

Conclusions

We have developed a new set of techniques to adaptively form an optimum linear combination for the polarization channels. Utilizing the technique of principle component analysis for non-uniform distributions of the polarization state in an scene, we can determine the optimum linear combination of polarization channels to produce the best PC images that distinguishes the target out of the background. These coefficients depend on the polarization statistics of the scene, and can be adaptively adjusted as the imaging system observes different environments. The optimum combinations for polarization channels with unequal weighting coefficients so obtained are suitable for environments with preferential polarization distribution (such as under water or in foggy media). This new discovery may point to an interesting research direction in the polarization vision in certain aquatic species. It may also be used to produce images with higher contrast between targets and a polarized background to facilitate target detection of an imaging system.

Acknowledgements

This work was supported by the U.S. Air Force Office of Scientific Research (AFOSR), through grants F49620-01-1-0470, F49620-02-1-0140, and the DURIP grant F49620-02-1-0241.

References and notes

48. W. A. Shurcliff, Polarized light, production and use, Harvard University Press, Cambridge, 1962.
49. D. Goldstein, Polarized light, Marcel Dekker, Inc., 2003.
50. J. E. Solomon, "Polarization imaging," Applied Optics **20**, 1537–1544 (1981).
51. L. B. Wolff, "Polarization camera for computer vision with a beam splitter," J. Opt. Soc. Am. A **11**, 2935–2945 (1994).
52. L. B. Wolff, T. A. Mancini, P. Pouliquen, and A. G. Andreou, "Liquid crystal polarization camera," IEEE Trans. on Robotics and Automation, **13**, 195–203 (1997).
53. L. B. Wolff, "Polarization-based material classification from specular reflection," IEEE Trans. on Pattern Analysis and Machine Intelligence **12**, 1059–1071 (1990).
54. W. G. Egan, W. R. Johnson, and V. S. Whitehead, "Terrestrial polarization imagery obtained from the Space Shuttle: characterization and interpretation," Appl. Opt. **30**, 435–442 (1991).
55. H. Chen, L. B. Wolff, "Polarization phase-based method for material classification and object recognition in computer vision," Proc. of IEEE Computer Society Conference on Computer Vision and Pattern Recognition, 128–135 (1996).
56. F. Goudail, P. Terrier, Y. Takakura, L. Bigue, F. Galland, V. DeVlaminck, "Target detection with a liquid-crystal-based passive Stokes polarimeter," Appl. Opt. **43**, 274–282 (2004).
57. J. S. Tyo, M. P. Rowe, E. N. Pugh, Jr., and N. Engheta, "Target detection in optically scattered media by polarization-difference imaging", Appl. Opt. **35**, 1855–1870 (1996).
58. F. Goudail and Ph. Réfrégier, "Statistical algorithms for target detection in coherent active polarimetric images," J. Opt. Soc. Am. A **18**, 3049–3060 (2001).

59. Although, human visual system does not have an ability to sense polarized light, the polarization is still might be perceptible in the form of Haidinger's brush.
60. K. von Frisch, "Die polarisation des himmelslichtes als orientierender faktor bei den tanzen der bienen", Experientia **5**, 142–148 (1949).
61. K. von Frisch, Tanzsprache und Orientierung der Bienen. Berlin: Springer (1965)
62. R. Wehner, G. D. Bernard, "Photoreceptor twist: a solution to the false colour problem," Proc. Natl. Acad. Sci. USA **90**, 4132-4135. (1993)
63. T. Labhart, "Polarization opponent interneurones in the insect visual system," Nature **331**, 435–437 (1988).
64. R. Wehner, "Polarized-light navigation by insects," Scientific American **235**, 106–114 (1976).
65. N. Shashar, T. W. Cronin, "Polarization contrast vision in octopus," The Journal of Experimental Biology **199**, 999-1004 (1996).
66. I. Pomozi, G. Horváth, R. Wehner, "How the clear-sky angle of polarization pattern continues underneath clouds: full-sky measurements and implications for animal orientation," The Journal of Experimental Biology 204, 2933–2942 (2001).
67. N. Shashar, P. S. Rutledge, and T. W. Cronin, "Polarization vision in cuttlefish - A concealed communication channel?," The Journal of Experimental Biology **199**, 2077-2084 (1996).
68. K. von Frisch, "Nobel Lecture," http://www.nobel.se/medicine/laureates/1973/frisch-lecture.pdf
69. R. Wehner, "Neurobiology of polarization vision," Trends in Neurosciences **12**, 353-359 (1989).
70. G. Horváth, J. Gál, T. Labhart, R Wehner, "Does reflection polarization by plants influence colour perception in insects? Polarimetric measurements applied to a polarization-sensitive model retina of Papilio butterflies," The Journal of Experimental Biology 205, 3281–3298 (2002).
71. M. P. Rowe, E. N. Pugh, Jr., J. S. Tyo, and N. Engheta, "Polarization-difference imaging: a biologically inspired technique for observation through scattering media", Opt. Lett. **20**, 608–610 (1995).
72. J. S. Tyo, E. N. Pugh, Jr., and N. Engheta, "Colorimetric representation for use with polarization-difference imaging of objects in scattering media", J. Opt. Soc. Am. A **15**, 367–374 (1998).
73. K. M. Yemelyanov, M. A. Lo, E. N. Pugh, Jr., and N. Engheta, "Display of polarization information by coherently moving dots," Opt. Express **11**, 1577-1584 (2003), http://www.opticsexpress.org/abstract.cfm?URI=OPEX-11-13-1577
74. K. M. Yemelyanov, S.-S. Lin, W. Q. Luis, E. N. Pugh, Jr., and N. Engheta, "Bio-inspired display of polarization information using certain visual cues," to be appeared in Proceedings of SPIE – The International Society for Optical Engineering **5158** (2003).
75. R. Wehner, "'Matched filters' – neural models of the external world," Journal of Comparative Physiology A **161**, 511-531 (1987).
76. J. S. Tyo, "Optimum linear combination strategy for an N-channel polarization-sensitive imaging or vision system," J. Opt. Soc. Am. A. **15**, 359–366 (1998).
77. As "regular" or "conventional" PDI we always in this paper understand the technique introduced in [71].

78. G. Buchsbaum, A. Gottschalk, "Trichromacy, opponent colours coding and optimum colour information transmission in the retina," Proc. R. Soc. London, Ser. B **220**, 89–113 (1983).
79. N. A. Macmillan, C. D. Creelman, Detection Theory: A User's guide, Cambridge University Press, London (1991).
80. I. T. Jolliffe, Principal Component Analysis, Springer-Verlag, New-York (1986).
81. S.-S. Lin, K. M. Yemelyanov, E. N. Pugh, Jr., and N. Engheta, "Polarization Enhanced Visual Surveillance Techniques," Proc. IEEE International Conference on Networking, Sensing, and Control, Taipei, Taiwan, pp. 216-221 (2004).

List of Figure Captions

Manuscript Entitled:

"Separation of overlapping cast shadow components using polarization"

Shih-Schön Lin, Konstantin M. Yemelyanov, Edward N. Pugh Jr., Nader Engheta

In preparation for submission to Optics Express

Separation of overlapping cast shadow components using polarization

Shih-Schön Lin, Konstantin M. Yemelyanov

Electrical and Systems Engineering Department, University of Pennsylvania, 220 South 33rd Street Moore 203 Philadelphia, PA 19104-6390, USA
shschon@seas.upenn.edu, kostya@ee.upenn.edu.

Edward N. Pugh, Jr.

F. M. Kirby Center for Molecular Ophthalmology and Institute of Neurological Sciences, University of Pennsylvania 422 Curie Boulevard, Philadelphia, PA 19104-6390, USA
pugh@mail.med.upenn.edu

Nader Engheta

Electrical and Systems Engineering Department and Institute of Neurological Sciences, University of Pennsylvania, Philadelphia, PA 19104, USA
engheta@ee.upenn.edu

Abstract: Shadow is an inseparable part of all natural scenes. When there are multiple light sources or multiple reflections several different shadows may overlap on the same location and create complicate patterns. Shadows are potentially good source of scene information if the shadow regions can be properly identified and segmented. However, shadow region identification and segmentation is a difficult task and shadows not properly identified often interfere with machine vision tasks like object recognition and tracking. We propose here a new shadow separation method based on the polarization of light. Polarization information of the scene captured by our polarization-sensitive camera is shown to separate shadows from different light sources effectively. Such shadow separation is almost impossible to realize with traditional intensity only images.

OCIS Codes: (150.0150) Machine vision; (110.0100) Image processing; (260.5430) Polarization; (230.5440) Polarization-sensitive devices

References and Links

1. Introduction

Shadow is formed whenever there is a light source and an occlusion that blocks part of the light. With the exception of the ambient light, which is assumed to be omni directional, all light sources illuminate only from a specific direction. Shadows are further classified into "self" and "cast" shadow. "Self" shadow refers to the regions of an object that is not directly illuminated by a light source due to its surface orientation; "cast" shadow refers to a region that is not illuminated by a light source due to occlusion by other objects. Shadowed regions usually appear darker than the lit regions and their color properties (e.g., hue and saturation) also appear different than the lit regions. Such differences in intensity and color create additional patterns and boundaries/edges that often confuse human observers or machine vision algorithms that identify and segment objects using these cues. For this reason there have been many techniques developed to identify, segment, and remove shadows from an imageor a video sequence[1-19]. However, all existing works use only the intensity and/or color information of light, in some cases also combined with temporal and geometric information available. The third fundamental property of light, the polarization, is never used for the purpose of shadow segmentation. Furthermore, many existing methods assumes very simple shadow model: an area of a scene is classified either as shadow or non-shadow. In fact it is possible for an area to be both shadow and lit area for different light sources simultaneously, as explained below.

Since light reflected from a surface can itself act as another light source, in most real scenes shadow regions can overlap and create quite complicated situations. For example, a surface area may be inside

some shadow area for certain light sources but not for other light sources. There can also be "shadow within shadows", in which certain area of the shadow of one light source is also the shadow area of another light source. Most existing machine vision methods tries to remove shadows altogether and not much has been done to further separate complicated overlapping shadows. Part of the reason is that this is an even more difficult task than removing shadows altogether using traditional vision sensors that detect only intensity and color information of light.

Polarization is an integral property of light, but unaided human eyes and most machine vision cameras cannot detect this property. However it has been found that many animal species can "see" the polarization information and make good use of it to their advantages [20-23]. Inspired by biological polarization vision, our group has used polarization sensitive cameras, to enhance target delectability in scattering media and for enhanced surveillance [24-26]. We have also developed methods to display these polarization information to human observers[27,28]. Although one of the primary sources of light, the sun light, is not polarized in the visible band before entering the atmosphere of earth, the light reflected/scattered from object surface is often at least partially polarized. In this work we show that complex overlapping cast shadows that are almost impossible to distinguish in the intensity and color only images can be easily segmented from each other in polarization parameter images.

2. Relations between Polarization Parameters and Shadows

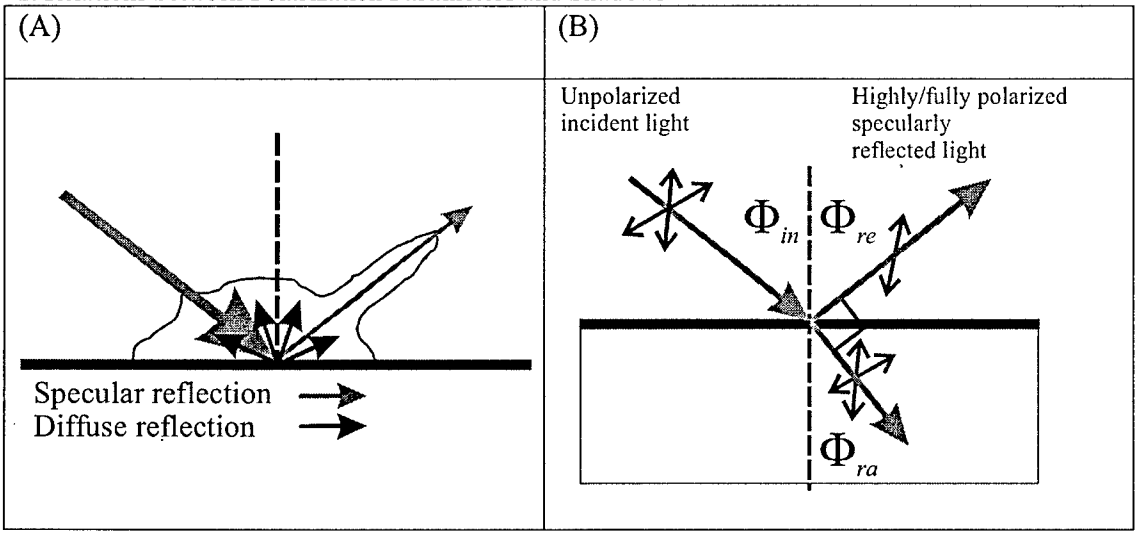

Fig. 29 (A) General macroscopic reflection model (B) Polarization of light resulting from specular reflection from a dielectric surface.

Light is an electro-magnetic wave which is by nature a transverse wave. This means that the electric field vector E of light oscillates along a direction perpendicular to the direction of travel of the light. This is the direction of polarization of light. Since most natural light is not coherent, when there is equal distribution of light energy polarized in all direction, the observed light intensities does not show any preference in polarization direction and the light is considered unpolarized. However, when light is scattered or reflected/refracted there will be selective filtering of light energy according to their polarization so the resulting light will have a preferential direction of polarization. See Fig. 29 (A), the generally accepted macroscopic reflection model is that light incident on a surface will be partially reflected specularly and partly reflected diffusely. The ratio of energy reflected diffusely and specular is surface dependent and also relates to the angle of incidence. The diffusely reflected components often considered undergone multiple random reflection microscopically so statistically can be considered unpolarized. However, the specular reflection component is usually at least partially polarized. This can be explained using the Fresnel reflection coefficients formula[29]:

$$r_{\perp} \equiv \left(\frac{E_{0re}}{E_{0in}}\right)_{\perp} = \frac{n_{in}\cos\Phi_{in} - n_{tr}\cos\Phi_{tr}}{n_{in}\cos\Phi_{in} + n_{tr}\cos\Phi_{tr}} = \frac{\sin(\Phi_{in} - \Phi_{tr})}{\sin(\Phi_{in} + \Phi_{tr})}$$
$$r_{\parallel} \equiv \left(\frac{E_{0re}}{E_{0in}}\right)_{\parallel} = \frac{n_{tr}\cos\Phi_{in} - n_{in}\cos\Phi_{tr}}{n_{in}\cos\Phi_{tr} + n_{tr}\cos\Phi_{in}} = \frac{\tan(\Phi_{in} - \Phi_{tr})}{\tan(\Phi_{in} + \Phi_{tr})} \quad (22)$$

where subscripts '*in*', '*tr*', and '*re*' stand for incident, transmitted, and reflected component; r the reflectance; E stands for the amplitude of the electric field; n the index of refraction of the media. . The subscripts '$\perp$' and '$\parallel$' are related to the plane of incidence. In Fig. 29(B) the plane of this paper is the plane of incidence. In case of the specular reflection it contains both the incident and reflected light wave vectors. It is clear that the reflectance of light that is parallel polarized and perpendicularly polarized is in general not the same. In particular, $r_{\parallel}$ can be exactly zero at the Brewster's angle θ_B, which is given as:

$$\tan\theta_B = \frac{n_t}{n_i}. \quad (23)$$

In this case the reflected light will be completely polarized along the direction perpendicular to the plane of incidence. In the visible band practically all observed light from most object surface is reflected light. If we compare the light observed in a cast shadow area to the light observed from area lit by the light source, it is clear from Eq. (22) that they will in general have different polarization properties.

Another important source of polarized light is the scattering of light by the atmosphere of the earth. The scattering of sun light by the air particles can be explained by the theory of *Rayleigh scattering*[29], which models the particles as an electric dipole and the scattered light as results of dipole radiation. Since the dipole radiation cannot radiate energy at directions along the direction of oscillation, the scattered light observed at a right angle from the incident light direction will be polarized parallel to the plane that is orthogonal to the direction of incident light. The scattering is also wavelength dependent:

$$P \propto (1/\lambda)^4 \quad (24)$$

where P stands for the radiance power and λ the wavelength of light. This is the reason we see a blue sky in the sunny day. What we do not perceive with our unaided human eyes is that the sky light is also polarized, the more so from directions 90 degrees from the position of the Sun. We show in this work that such natural phenomenon can be used to neatly separate complex shadows. For example, an area that is inside the shadow caused by the direct sun light but is lit by the polarized ambient sky light will show certain polarization, while the are that is in both the shadow area of the direct sun light and the sky light will show no polarization at all.

In addition to the linearly polarized case, there exist cases called circular and elliptical polarization that can result from two coherent but orthogonally polarized light components in the same frequency but with different phase lags[29]. However most imaging sensor can only sense the integration of light energy over time and the phase information is not recorded. The general expression for observed intensity of partially polarized light I as a function of the angle of orientation of polarization analyzer φ can be written as follows:

$$I(\varphi) = I_U + I_A\cos\left[2(\theta-\varphi)\right] = I_U\left\{1 + p\cos\left[2(\theta-\varphi)\right]\right\} \quad (25)$$

where θ is the orientation angle of the major axis of the polarization ellipse, I_U is a half of the total pixel intensity, and $p \equiv I_A / I_U$ is the degree of linear polarization at the pixel. The reference axis for φ and θ can be arbitrarily chosen. Since the exact index of refraction of the surface in our study is considered unknown, putting one polarizer at a given orientation angle in front of the camera and taking a picture can not provide the complete information about the polarization state of the received light. By taking three pictures with the polarizer oriented at three different angles, for example φ =0, 45 and 90 degrees, we can recover I_U, I_A, and θ for each pixel of the image using the following expressions:

$$I_U = (I_0 + I_{90})/2$$
$$I_A = \sqrt{(I_{45} - I_U)^2 + (I_{90} - I_U)^2} \quad (26)$$
$$\theta = \arctan\left[(I_{45} - I_U)/(I_{90} - I_U)\right]/2$$

Here indices 0, 45, and 90 indicate the orientation of the polarizer in degrees when the image was taken. Because θ and $\theta+\pi$ are indistinguishable for phase-blind visual sensors in most conventional cameras, the meaningful range of θ is restricted by π. We usually use θ range from 0 to π. A system of two cameras with a controllable polarizer and a beam splitter to rapidly take the required pictures has been developed in [30].

There are other natural processes that can produce polarized light, like dichroism (polarization produced via selective absorption), birefringence (different index of refraction for differently polarized light), ...etc. are less common in natural environment will not be considered here.

3. Experiments

The first example is an outdoor scene of a walkway in front of a building with all-glass walls. See Fig. 30, the Sun is illuminating from the right hand side of the picture with shadows cast by trees along the walkway. Most existing shadow handling algorithm will most likely just segment out the dark areas as shadow areas or remove/reduce the contrast in brightness caused by the shadow. However there is more complicated overlapping shadow patterns hidden inside the scene that are not detectable using only intensity, color, and even temporal and geometrical information used by existing shadow handling methods.

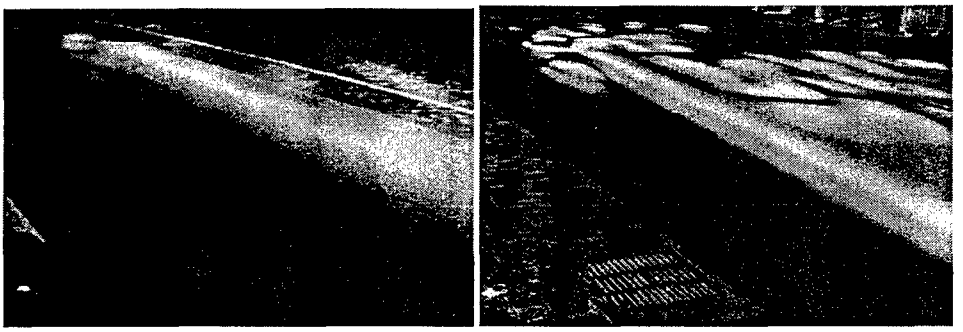

Fig. 30 Left: ordinary intensity image of an outdoor scene with light and shadow. Right: the same scene showing the degree of polarization image. Hidden patterns of shadows within shadows are clearly visible in high contrast.

In this scene the glass-wall building to the left hand side of the picture is reflecting the sun light from the glass part but not from the thin frame part around each piece of glass. The reflected light is polarized and the reflection pattern is cast on the scene overlapping with the easily visible shadow pattern caused by the direct sun light. The reflected light is weaker than the direct sun light and the pattern is essentially not visible in the intensity only image. However, when we use polarization sensitive camera and extract the degree of polarization image these hidden pattern of overlapping shadow is revealed, see Fig. 30 Right. The area that is neither lit by direct sun light nor by the reflected light from the glass is both dark and unpolarized. These are the cast pattern of the glass frames of the glass-wall building to the left of the picture. The area that is not lit by the direct sun light, thus appear as part of the shadow area in the intensity image, but is lit by the polarized reflected light from the glass pieces of the glass-wall building, exhibits strong polarization. The degree of polarization image normalize the polarization effects with respect to the total intensity as shown in Eq. (26), so these area will show up as bright area in the degree of polarization image in Fig. 30 Right. To show that these glass piece patterns revealed by the degree of polarization image is unique and not hidden in the intensity only images due to poor contrast in the shadow area, we conduct linear contrast enhancement and followed by gamma correction of 0.5 to both images shown in Fig. 30 and the results are shown in Fig. 31. It is clear that the hidden shadow patterns are only revealed in the degree of polarization image. Fig. 32 Left shows the glass-wall and frames of the building. Fig. 32 Right is the same walk way when the bright direct sun light is blocked. This shows that the patterns revealed in the degree of polarization image is indeed caused by the hidden shadow.

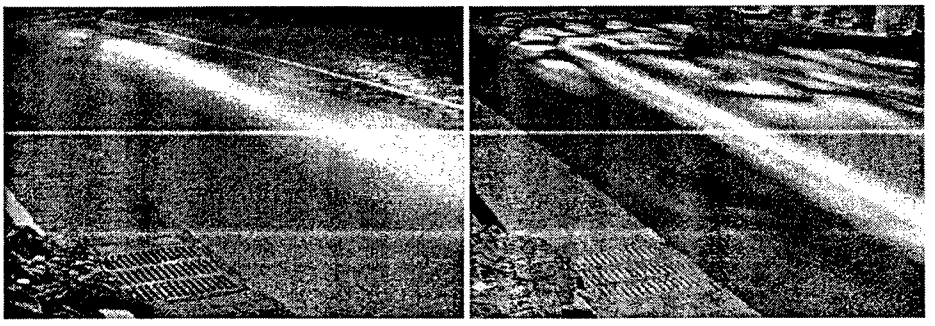

Fig. 31 Images in Fig. 30 contrast enhanced by linear intensity range stretch followed by gamma correction of 0.5 to show the details in the dark area. Left: intensity image. Right: degree of polarization image. It is clear that the pattern revealed in the polarization image is not present in the intensity image even after contrast enhancement.

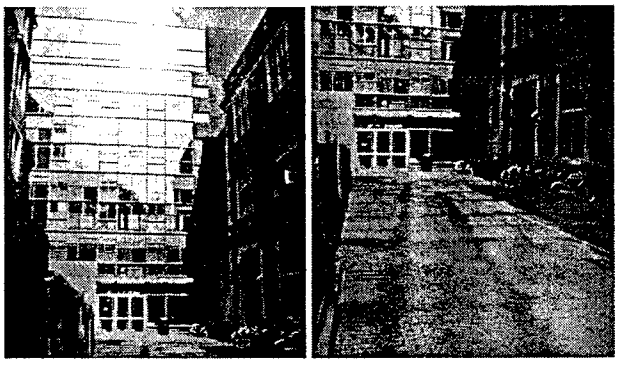

Fig. 32 Left: the glass-wall building showing big glass rectangles and frames. Right: A picture of the same walk way as in Fig. 30 and Fig. 31 taken another day when the direct sun light is blocked due to nearby construction scaffolding. The shadow pattern cast on the walk way by the glass-wall and frames is visible.

We performed a lab controlled experiment to further confirm our results obtained outdoors. The setup is a 150W incandescent light illuminating from the opposite side of the camera and a 15W fluorescent light illuminating from the right hand side of the picture.

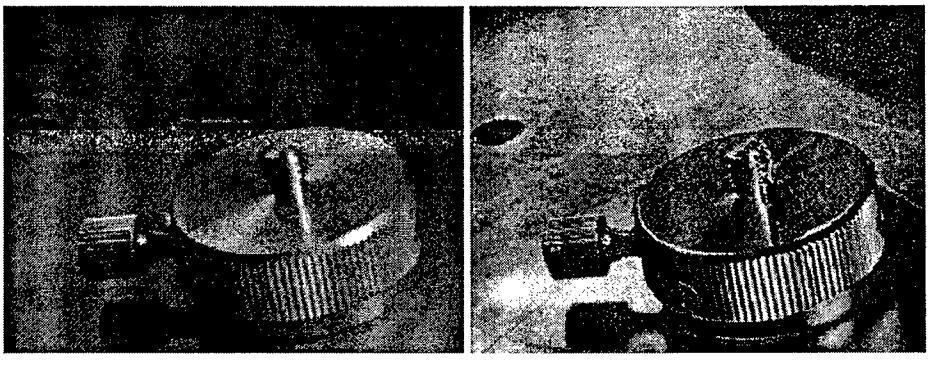

Fig. 33 A metal pillar on a optical table illuminated by a strong incandescent light from the side opposite to the camera, while another much weaker fluorescent light illuminating from the right hand side of the picture. Left: Intensity only image. Right: Degree of Polarization image.

See Fig. 33. In the intensity only image only the shadow of the dominating light source is visible. However, in the degree of polarization image, both shadows are visible and separated clearly in high contrast. The "shadow" of the much weaker light from the right hand side shows up as a bright area to the left of the metal pillar. The reason is that the strong light reflected from the table is polarized because the view geometry while the side illuminating light is very weakly polarized due to the view geometry. As a result, the area that is not lit by both light source is totally dark, and is least polarized and show up as the darkest area in the degree of polarization image. The area that is lit by both the strong light source and the weak light source is polarized but the degree of polarization is weakened by the unpolarized irradiance caused by the weak unpolarized light from the right hand side of the picture. The shadow area of the weak

light source is almost invisible in the intensity only image. However such area is the most highly polarized area because it is polarized due to reflecting the strong light source and its degree of polarization is not reduced by the unpolarized reflection of the weak light source from the right hand side. The contrast between the revealed shadow due to weak side illumination and the neighboring area is very good so it is very suitable for many well known segmentation method to extract this area. Fig. 34 left shows one example segmentation using region growing that starts with 2 by 2 regions. The side shadow area is cleanly separated from the image when 21 or more regions are segmented. Fig. 34 shows the result of extracting the side shadow area from the degree of polarization image.

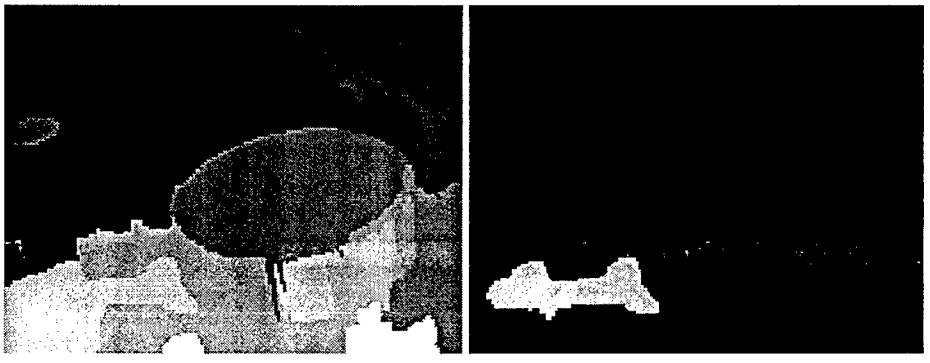

Fig. 34 Left: Segmentation results from region growing of Fig. 33 Right into 21 regions. Right: Hidden shadow area extracted from Fig. 33 Right.

4. Discussions

All existing shadow handling methods have limitations. Many methods are designed to handle specific applications like aerial photography or traffic monitoring, so that the lighting condition is simplified or can be known a priori. There may be requirements of known geometry of the scene or known precise pixel sensitivity calibration data of the camera. The polarization based shadow segmentation method suggested here also has limitations. While this method is not strictly tied to a specific application, it does require that not all light sources come from the back the camera when all light sources are not polarized. This is because that Eq. (22) works best with specular reflection which is seen most strongly when the light is reflected in front and toward the viewing camera. There are several methods available that can estimate the illumination directions of multiple light sources using information in the image[31-34]. Combining our polarization detection methods with such illumination direction estimation methods will be very promising and is our work in progress. This polarization shadow detection method will also be very useful when combined with other well known shadow cues like intensity, color, and geometry to achieve more accurate shadow segmentation and give more detailed information on the origin of each shadow components. As demonstrated in our experiments, the information found by polarization is unique is cannot be found by other shadow cues alone.

5. Conclusion

We have presented a novel shadow segmentation method using the natural polarization property of light. The polarization of light conveys important information about the scene. Polarization have been used in many other vision tasks like removing glare and removing glare but have not been used to aid the segmentation of complex shadows in a scene. Many existing shadow handling methods not using polarization can only handle simple shadow geometry caused by one light source. Our use of polarization enable us to deal with the complex situation of multiple light sources causing multiple overlapping shadows that is difficult to even detect in the traditional intensity only images. The proposed polarization shadow segmentation method also provides a new shadow verification criteria that can potentially be integrated into a shadow analysis algorithm together with other well known shadow cues to provide more accurate shadow segmentation.

References and links

1. M. Nagao, T. Matsutyama, and Y. Ikeda, "Region extraction and shape analysis in aerial photographs," Computer Vision, Graphics, and Image Processing 10, 195-223 (1979).

2. R. Gershon, A. D. Jepson, and J. K. Tsotsos, "Ambient illumination and the determination of material changes," J. Opt. Soc. Am. A 3, 1700-1707 (1986).

3. R. Irvin and D. Mckeown, "Methods for exploiting the relationship between buildings and their shadows in aerial imagery," IEEE Transactions on Systems Man and Cybernetics 19, 1564-1575 (1989).

4. J. M. Scanlan, D. M. Chabries, and R. W. Christiansen, "A Shadow Detection and Removal Algorithm for 2D Images," in *Proc. of Int'l Conf. on Acoustics, Speech, and Signal Processing*, 1990), pp. 2057-2060.

5. Y. Liow and T. Pavlidis, "Use of shadows for extracting buildings in aerial images," Computer Vision, Graphics, and Image Processing 49, 242-277 (1991).

6. C. Wang, L. Huang, and A. Rosenfeld. "Detecting clouds and cloud shadows on aerial photographs," Pattern Recognition Letters 12, 55-64 (1991).

7. D. Koller, K. Danilidis, and H.-H. Nagel, "Model-based object tracking in monocular image sequences of road traffic scenes," International Journal of Computer Vision 10, 257-281 (1993).

8. C. Jiang and M. O. Ward, "Shadow segmentation and classification in a constrained environment," CVGIP: Image Understanding 59, 213-225 (1994).

9. G. Funka-Lea and R. Bajcsy, "Combining color and geometry for the active visual recognition of shadows," in *Proc. Int. Conf. on Computer Vision*, 1995), pp. 203-209.

10. J. Stauder, R. Melch, and J. Ostermann, "Detection of moving cast shadows for object segmentation," IEEE Transactions of Multimedia 1, 65-77 (1999).

11. J. A. Marchant and C. M. Onyango, "Shadow-invariant classification for scenes illuminated by daylight," J. Opt. Soc. Am. A 17, 1952-1961 (2000).

12. G. Finlayson, S. Hordley, and M. S. Drew, "Removing shadows from images," in *ECCV*, 2002), pp. 823-836.

13. R. Cucchiara, C. Grana, M. Piccardi, and A. Prati, "Detecting Moving Objects, Ghosts, and Shadows in Video Streams," IEEE Transactions on Pattern Analysis and Machine Intelligence 25, 1337-1342 (2003).

14. T. Gevers and H. Stokman, "Classifying color edges in video into shadow-geometry, highlight, or material transitions," IEEE Transactions of Multimedia 5, 237-243 (2003).

15. A. Prati, I. Mikic, M. M. Trivedi, and R. Cucchiara, "Detecting Moving Shadows: Algorithms and Evaluation," IEEE Transactions on Pattern Analysis and Machine Intelligence 25, 918-923 (2003).

16. I. Sato, Y. Sato, and K. Ikeuchi, "Illumination from Shadows," IEEE Transactions on Pattern Analysis and Machine Intelligence 25, 290-300 (2003).

17. S. Nadimi and B. Bhanu, "Physical Models for Moving Shadow and Object Detection in Video," IEEE Transactions on Pattern Analysis and Machine Intelligence 26, 1079-1087 (2004).

18. E. Salvador, A. Cavallaro, and T. Ebrahimi, "Cast shadow segmentation using invariant color features," Computer Vision and Image Understanding 95, 238-259 (2004).

19. J. M. Wang, Y. C. Chung, C. L. Chang, and S. W. Chen, "Shadow Detection and Removal for Traffic Images," in *Proceedings of the 2004 IEEE International Conference on Networking, Sensing and Control*, (IEEE, Taipei, Taiwan, 2004), pp. 649-654.

20. K. Frisch, "Die polarisation des himmelslichtes als orientierender faktor bei den tanzen der bienen," Experientia 5, 142-148 (1949).

21. R. Wehner, "Polarized-light navigation by insects," Scientific American 235, 106-114 (1976).

22. R. Schwind, "Zonation of the optical environment and zonation in the rhabdom structure within the eye of the backswimmer, *Notenecta glauca*," Cell and Tissue Research 232, 53-63 (1983).

23. G. Horváth, "Reflection polarization patterns at flat water surfaces and their relevance for insect polarization vision," Journal of Theoretical Biology 175, 27-37 (1995).

24. M. P. Rowe, E. N. Jr. Pugh, and N. Engheta, "Polarization-difference imaging: a biologically inspired technique for observation through scattering media," Optics Letters 20, 608-610 (1995).

25. J. S. Tyo, M. P. Rowe, E. N. Jr. Pugh, and N. Engheta, "Target detection in optically scatter media by polarization-difference imaging," Applied Optics 35, 1855-1870 (1996).

26. S.-S. Lin, K. M. Yemelyanov, E. N. Jr. Pugh, and N. Engheta, "Polarization Enhanced Visual Surveillance Techniques," in *Proceedings of IEEE International Conference on Networking, Sensing and Control*, (IEEE Systems, Man and Cybernetics Society, Taipei, Taiwan, 2004),

27. J. S. Tyo, E. N. Jr. Pugh, and N. Engheta, "Colorimetric representation for use with polarization-difference imaging of objects in scattering media," J. Opt. Soc. Am. A 15, 367-374 (1998).

28. K. M. Yemelyanov, M. A. Lo, E. N. Jr. Pugh, and N. Engheta, "Display of polarization information by coherently moving dots," Opt. Express 11, 1577-1584 (2003).

29. E. Hecht, in *Optics , 3 ed.* (Addison Wesley Longman, Inc., Reading, MA, USA 1998).

30. L. B. Wolff, T. A. Mancini, P. Pouliquen, and A. G. Andreou, "Liquid Crystal Polarization Camera," IEEE Transactions on Robotics and Automation 13, 195-203 (1997).

31. A. P. Pentland, "Finding the illuminant direction," J. Opt. Soc. Am. 72, 448-455 (1982).

32. Y. Zhang and Y. Yang, "Illuminant direction determination for multiple light sources," in *Proc. IEEE Conf. on Computer Vision and Pattern Recognition*, 2000), pp. 269-276.

33. J. Pinel and H. Nicolas, "Estimation 2d illuminant direction and shadow segmentation in natural video sequences," in *Proceedings of VLBV*, 2001), pp. 197-202.

34. M. W. Powell, S. Sarkar, and D. Goldgof, "A simple strategy for calibrating the geometry of light sources," IEEE Transactions on Pattern Analysis and Machine Intelligence 23, 1022-1027 (2001).

AFRL-SR-AR-TR-05-

0304

REPORT DOCUMENTATION PAGE

1. AGENCY USE ONLY (Leave blank)	2. REPORT DATE	3. REPORT TYPE AND DATES COVERED
	July 17, 2005	Final Report, Mar 1, 2002 - Dec 31, 2004

4. TITLE AND SUBTITLE
Bio-Inspired Sensing and Display of Polarization Imagery

5. FUNDING NUMBERS
F49620-02-1-0140

6. AUTHOR(S)
Nader Engheta (PI)
Edward N. Pugh, Jr., (co-PI)

7. PERFORMING ORGANIZATION NAME(S) AND ADDRESS(ES)
University of Pennsylvania
Department of Electrical and Systems Eng
200 South 33rd Street
Philadelphia, PA 19104

8. PERFORMING ORGANIZATION REPORT NUMBER

9. SPONSORING / MONITORING AGENCY NAME(S) AND ADDRESS(ES)
AFOSR
4015 Wilson Blvd.
Arlington, VA 22203-1954

10. SPONSORING / MONITORING AGENCY REPORT NUMBER

11. SUPPLEMENTARY NOTES

12a. DISTRIBUTION / AVAILABILITY STATEMENT
Unlimited

DISTRIBUTION STATEMENT A
Approved for Public Release
Distribution Unlimited

12b. DISTRIBUTION CODE

13. ABSTRACT *(Maximum 200 Words)*

During our research efforts on this program, we have introduced, developed, and studied various imaging algorithms, sensing schemes and visualization and display methodologies inspired and informed by biological consideration, and have demonstrated that these bio-inspired polarization sensing and imaging techniques enable us to achieve better target detection, enhanced visibility in otherwise low-contrast conditions, longer detection range in optically scattering media, man-made polarization-sensing adaptation based on changing environments, surface deformation/variation detection (e.g., detection of finger prints on a smooth surface using polarization-based vision), "shadow removal" by displaying polarization information instead of conventional intensity information, and many more novel outcomes. These results have shown the numerous possibilities and potential applications of these bio-inspired methods in various sensing, imaging, and display technologies. We have also explored several ideas for mapping polarization information onto visual cues suitable for observers, including using pseudocolor mapping, static and dynamic textures with varying in orientations, flickering and modulating luminance and/or color contrast of scenes in terms of certain aspects of polarization values, and fusing polarization information into optical imagery. Our efforts have shown that the *polarization* can bring another "dimension" of information into the domain of imaging and sensing for detection, visibility enhancement, and display methodologies.

14. SUBJECT TERMS	15. NUMBER OF PAGES
Polarization imaging, Target detection, visibility, bio-inspired methods	116
	16. PRICE CODE

17. SECURITY CLASSIFICATION OF REPORT	18. SECURITY CLASSIFICATION OF THIS PAGE	19. SECURITY CLASSIFICATION OF ABSTRACT	20. LIMITATION OF ABSTRACT
Unclassified	Unclassified	Unclassified	None

7-25-05